Mechanical Properties of Metamaterials in Time Domain: Numerical Homogenisation Approach

Ismail Hamed Ali Abuzayed

A thesis is submitted towards the fulfilment requirements
for the degree of

Doctor of Philosophy in

The Department of Civil and Structural Engineering

At The University of Sheffield

August 2022

Abstract

The mechanical behaviour of metamaterials typically depends on their microstructural configuration and composition. The design of these materials requires extensive experiments or complex finite element models which tend to be numerically demanding. In order to understand, control and optimise the macroscopic mechanical behaviour, in this thesis numerical homogenisation is applied to a simple square unit cell with a single inclusion using a combination of elastic and viscoelastic responses on the micro level. Through a systematic analysis of unit cell behaviour with increasingly complex microstructural configurations, it is shown how certain macroscale constitutive laws can be obtained in a controlled and controllable manner. The effective properties obtained from quasi static tests were used to predict the homogenised dynamic response of periodic unit cells. Finally, the concept of *time homogenisation* is introduced as a method of obtaining the effective properties from the dynamic time history response of unit cells.

Acknowledgement

First and foremost I would like to thank my supervisors, Prof. Harm Askes and Dr. Zuhal Ozdemir for their intellectual support on personal, academic and professional levels. Throughout the last four years, you've magnificently supported me throughout all stages of my PhD, in which I have learned valuable knowledge and developed incredible skills. I will be forever grateful to you and I hope to continue to learn from each other and collaborate in the future. Furthermore, I would like to thank my colleagues Dr. Ibrahim Alzamzami, Dr. Nasser Alanzai, Dr (to be). Irem Yagmuroglu and all others in the department of Civil and Structural Engineering, for long hours discussions and the incredible memories we had together. Finally, I would like to thank my family, starting with my parents, you've always wanted me to pursue a PhD and have supported me in all regards. A special thank you to my sisters and brother Dr (to be). Ibrahim Abuzayed, who has helped and supported me throughout the years of my studies.

Contents

Abstract i

Acknowledgement iii

Table of Content viii

List of Figures xiv

List of Tables xv

Glossary xvii

1 Introduction 1

1.1 Aim and Motivation 1

1.2 Scope and Objectives 3

1.3 Thesis outline 4

2 Literature Review and Theoretical Background 7

2.1 Introduction 7

2.2 Metamaterials 9

2.3 Homogenisation methods 11

2.4 Representative volume element 15

2.5 Principles of Homogenisation 17

2.6 Review of Materials Constitutive Models 20

2.6.1 Linear elasticity 20

2.6.2 Linear viscoelasticity 22

2.6.3 The Maxwell form of the Standard Solid Model for Viscoelastic Material 24

3 Modelling methodology **27**

3.1 Introduction 27

3.2 Finite Element Modelling 28

3.2.1 Mesh criteria and convergence 30

3.2.2 Time step convergence 31

3.2.3 Element formulation 33

3.3 Boundary conditions 35

3.3.1 Boundary conditions under quasi-static loading 35

3.3.2 Boundary conditions under dynamic loading 37

3.4 Automated script 39

3.5 Parallel computing 42

4 Quasi-static loading conditions **43**

4.1 Introduction 43

4.2 Linear elastic RVE with void inclusion 44

4.3 Viscoelastic RVE with void inclusion 48

4.4 Composite RVE (linear elastic matrix with viscoelastic inclusion) 51

4.5 Summary, evaluation and applicability 59

5 Dynamic Loading conditions **61**

5.1 Introduction 61

5.2 Principles of dynamics 62

5.2.1 SDoF: Linear spring 63

5.2.2 SDoF: Linear spring and a dashpot in series 65

5.2.3 SDoF: Linear spring and a dashpot in series connected in parallel with another Linear spring 69
5.3 Loading conditions 75
5.4 Linear elastic unit cell 77
5.5 Viscoelastic unit cell 81
5.6 Composite unit cell 85
5.7 Unit cell response in dynamics and effective mechanical properties 91

6 Time Homogenisation 97

6.1 Introduction 97
6.2 Time homogenisation of linear elastic unit cells 98
6.3 Time homogenisation of viscoelastic unit cells 100
6.4 Time homogenisation of composite unit cells 103

7 Conclusion and Future Research 109

7.1 Summary and evaluation 109
7.2 Potential Future Work 110

Bibliography 113

A Script samples 129

A.1 Periodic boundary conditions function 129
A.2 Abaqus python script 131
A.3 LS-DYNA input file 135
A.4 Parallel computing script 139
A.5 Analytical solution of dynamic problem (spring) 140
A.6 Analytical solution of dynamic problem (Maxwell) 140
A.7 Analytical solution of dynamic problem (SSM) 141

B Homogenised properties equations constants 143

C Normalised results **147**

C.1 Linear Elastic 147

C.2 Maxwell viscoelastic 148

C.3 Composite 149

D Further Dynamics Results **151**

D.1 Linear elastic RVE with viscoelastic inclusion inclined at $\theta = 0°$. 151

D.2 Linear elastic RVE with viscoelastic inclusion inclined at $\theta = 90°$ 153

D.3 Maxwell viscoelastic RVE, space homogenised stress and strain . . 155

List of Figures

2.1 Representative volume element of a periodic metamaterial. 17

2.2 (a) Maxwell viscoelastic model (b) Maxwell form of the Standard Solid model 22

3.1 Representative volume element (1 mm × 1 mm) 28

3.2 Mesh partitioning criteria 30

3.3 Convergence of elastic modulus 32

3.4 Convergence of dynamic viscosity 32

3.5 Hourglass in viscoelastic RVE (displacements are magnified 5 times) 34

3.6 Periodic boundary conditions: (a) Relaxation (b)Creep 37

3.7 Proposed boundary conditions for dynamic excitation 39

3.8 Flowchart for the analysis code 41

3.9 Parallel computing architecture 42

4.1 Variation of homogenised elastic modulus $\bar{E}$ with inclusion's inclination angle θ for different aspect ratios and constant inclusion's area A_r=0.175 mm^2 45

4.2 Variation of homogenised Poisson's ratio $\bar{v}$ with inclusion's inclination angle θ for different aspect ratios and constant inclusion's area A_r=0.175 mm^2 46

4.3 Comparison between the FE homogenised elastic modulus $\bar{E}$ and its prediction along different inclination angles θ (A_r=0.175 mm^2 and AsR=3) 47

4.4 Variation of homogenised elastic modulus $\bar{E}$ with inclination angle θ using creep and relaxation tests (A_r=0.175 mm^2 and AsR=3) . 49

4.5 Variation of homogenised dynamic viscosity $\bar{\eta}$ with inclination angle θ using creep and relaxation tests (A_r=0.175 mm^2 and AsR=3) 50

4.6 Composite unit cell with viscoelastic inclusion 52

4.7 Relaxation: Micro behaviours of matrix (a) and inclusion (b), Macro behaviour of a composite unit cell (c) 53

4.8 Creep: Micro behaviours of matrix (a) and inclusion (b), Macro behaviour of a composite unit cell (c) 54

4.9 Variation of homogenised initial elastic modulus $\bar{E}_0$ with the inclination angle θ for the composite unit cells 1 to 3 given in Table 4.2 (A_r=0.175 mm^2) 55

4.10 Variation of homogenised infinite elastic modulus $\bar{E}_\infty$ with the inclination angle θ for composite unit cells 1 to 3 given in Table 4.2 (A_r=0.175 mm^2) 55

4.11 Variation of homogenised dynamic viscosity $\bar{\eta}$ with the inclination angle θ for composite unit cells 1 to 3 given in Table 4.2 (A_r=0.175 mm^2) 56

4.12 Variation of homogenised dynamic viscosity $\bar{\eta}$ with the inclination angle θ for composite unit cells 4 to 6 given in Table 4.2 (A_r=0.175 mm^2) 56

4.13 Variation of homogenised initial elastic modulus $\bar{E}_0$ with the inclination angle θ for composite unit cell 5 given in Table 4.2 (A_r=0.175 mm^2 and AsR=3) 57

4.14 Variation of homogenised infinite elastic modulus $\bar{E}_{\infty}$ with the inclination angle θ for composite unit cell 5 given in Table 4.2 (A_r=0.175 mm^2 and AsR=3) 58

4.15 Variation of homogenised dynamic viscosity $\bar{\eta}$ with the inclination angle θ for composite unit cell 5 given in Table 4.2 (A_r=0.175 mm^2 and AsR=3) 58

5.1 Linear spring-mass model 63

5.2 Linear spring-dashpot in series model 65

5.3 Linear spring-dashpot (in series) connected in parallel with a linear spring 69

5.4 Impulse loading 75

5.5 Displacement vs time due to a sudden constant load applied on a linear elastic unit cell 78

5.6 Velocity vs time due to a sudden constant load applied on a linear elastic unit cell 79

5.7 Displacement vs time due to an impulsive load applied on a linear elastic unit cell 80

5.8 Velocity vs time due to an impulsive load applied on a linear elastic unit cell 81

5.9 Displacement vs time due to a sudden constant load applied on a viscoelastic unit cell 82

5.10 Velocity vs time due to a sudden constant load applied on a viscoelastic unit cell 83

5.11 Displacement vs time due to an impulsive load applied on a viscoelastic unit cell 84

5.12 Velocity vs time due to an impulsive load applied on a viscoelastic unit cell 85

5.13 Displacement vs time due to a sudden constant load applied on an elastic unit cell 86
5.14 Velocity vs time due to a sudden constant load applied on an elastic unit cell 87
5.15 Displacement vs time due to an impulsive load applied on an elastic unit cell 89
5.16 Velocity vs time due to an impulsive load applied on an elastic unit cell 90
5.17 Single unit cell with void inclusion (A_r=0.175 mm^2, ASP=3 and $\theta = 45°$) (dimensions 1 mm × 1 mm) 91
5.18 Macro models of 2×2 unit cells (a) and 4×4 unit cells 92
5.19 Displacement vs time due to a sudden load applied on an elastic 2 × 2 unit cell macro model with void inclusion (A_r=0.175 mm^2, ASP=3 and $\theta = 45°$) 93
5.20 Velocity vs time due to a sudden load applied on an elastic 2 × 2 unit cell macro model with void inclusion (A_r=0.175 mm^2, ASP=3 and $\theta = 45°$) 93
5.21 Displacement vs time due to a sudden load applied on an elastic 4 × 4 unit cell macro model with void inclusion (A_r=0.175 mm^2, ASP=3 and $\theta = 45°$) 94
5.22 Velocity vs time due to a sudden load applied on an elastic 4 × 4 unit cell macro model with void inclusion (A_r=0.175 mm^2, ASP=3 and $\theta = 45°$) 94

6.1 Space homogenised stress (a) and strain (b) 99
6.2 Homogenised elastic modulus vs time due to different loading conditions. 100
6.3 Ratio of time homogenised stress and strain vs time due to quasi static and dynamic loading. 102

6.4 Ratio of time homogenised stress and strain vs time due to quasi static and dynamic constant displacements. 103

6.5 Ratio of time homogenised stress and strain vs time due to quasi static and dynamic loading. 106

6.6 Ratio of time homogenised stress and strain vs time due to quasi static and dynamic constant displacements. 106

C.1 Variation of homogenised elastic modulus $\bar{E}$ with the inclination angle θ for elastic unit cell(A_r=0.175 mm^2) 147

C.2 Variation of homogenised elastic modulus $\bar{E}$ with the inclination angle θ for elastic unit cell (A_r=0.175 mm^2 and AsR=3) 148

C.3 Variation of homogenised elastic modulus $\bar{E}$ with the inclination angle θ for viscoelastic unit cell (A_r=0.175 mm^2 and AsR=3) . . 148

C.4 Variation of homogenised dynamic viscosity $\bar{\eta}$ with the inclination angle θ for viscoelastic unit cell (A_r=0.175 mm^2 and AsR=3) . . 149

C.5 Variation of infinite homogenised elastic modulus $\bar{E}$ with the inclination angle θ for a composite unit cell (A_r=0.175 mm^2 and AsR=3) 149

C.6 Variation of homogenised dynamic viscosity $\bar{\eta}$ with the inclination angle θ for a composite unit cell (A_r=0.175 mm^2 and AsR=3) . . 150

D.1 Displacement vs time due to a sudden constant load applied on an elastic RVE with viscoelastic inclusion (A_r=0.175 mm^2, ASP=3 and $\theta = 0°$). 151

D.2 Velocity vs time due to a sudden constant load applied on an elastic RVE with viscoelastic inclusion (A_r=0.175 mm^2, ASP=3 and $\theta = 0°$) 152

D.3 Displacement vs time due to an impulsive load applied on an elastic RVE with viscoelastic inclusion (A_r=0.175 mm^2, ASP=3 and $\theta = 0°$) 152

D.4 Velocity vs time due to an impulsive load applied on an elastic RVE with viscoelastic inclusion (A_r=0.175 mm^2, ASP=3 and $\theta = 0°$) . 153

D.5 Displacement vs time due to a sudden constant load applied on an elastic RVE with viscoelastic inclusion (A_r=0.175 mm^2, ASP=3 and $\theta = 90°$). 153

D.6 Velocity vs time due to a sudden constant load applied on an elastic RVE with viscoelastic inclusion (A_r=0.175 mm^2, ASP=3 and $\theta = 90°$) 154

D.7 Displacement vs time due to an impulsive load applied on an elastic RVE with viscoelastic inclusion (A_r=0.175 mm^2, ASP=3 and $\theta = 90°$) 154

D.8 Velocity vs time due to an impulsive load applied on an elastic RVE with viscoelastic inclusion (A_r=0.175 mm^2, ASP=3 and $\theta = 90°$) 155

D.9 Space homogenised stress 155

D.10 Space homogenised strain 156

List of Tables

2.1 Mechanical metamaterials micro structures [114] 8

4.1 Linear viscoelastic material model parameters 48
4.2 Material Properties of the composite unit cells 52

B.1 Elastic modulus equation constant (x_0) values for different Aspect ratio and area combinations for all types of RVEs 143
B.2 Elastic modulus equation constant (C) values for different Aspect ratio and area combinations for all types of RVEs 144
B.3 Dynamic viscosity equation constant (x_0) values for different Aspect ratio and area combinations for RVEs with viscoelastic matrix and void inclusion 144
B.4 Dynamic viscosity equation constant (C) values for different Aspect ratio and area combinations for RVEs with viscoelastic matrix and void inclusion 144
B.5 Dynamic viscosity equation constant (x_0) values for different Aspect ratio and area combinations for RVEs with elastic matrix and viscoelastic inclusion 145
B.6 Dynamic viscosity equation constant (C) values for different Aspect ratio and area combinations for RVEs with elastic matrix and viscoelastic inclusion 145

Glossary

RVE: The smallest volume at which it can yield the effective properties of the macro behaviour when analysed. It should be large enough to contain sufficient information about the microstructure [41, 47].

Unit cell: The smallest building block that a metamaterial is built by, or the smallest microstructure that a metamaterial is built by its duplicates.

Metamaterials: meta means "beyond" in Greek, and metamaterials are materials that explicit unusual properties which cannot be found in natural materials [61]; examples of such unusual properties include negative Poisson's ratio and negative compressiblity.

Static: response of material that has no time dependence, such as a linear elastic RVE under constant load.

Quasi static: response of material that has time dependence, but neglected inertial effect, such as viscoelastic RVE under constant loading.

Dynamic: response of a material where inertial effects are high and cannot be ignored such as an RVE modeled under an impulsive loading.

Plane stress: If the stress across one plane is very small or null, that plane can treated as a plane stress and the problem can be simplified to 2D.

Plane strain: If the strain across one plane is very small or null, that plane can treated as a plane strain and the problem can be simplified to 2D.

Chapter 1

Introduction

1.1 Aim and Motivation

Materials were key factors in humanity's development over history, such that ages were named after them e.g. the stone, the bronze and the iron ages. The growth of human activities has increased the demand for innovative materials. The initial innovation in materials was in their composition and fabrication method; for instance, the use of steel reinforcement bars in concrete structures to overcome the weakness of concrete in resisting tension loads. Another basic example is carbon steel, in which adding carbon to iron improves the overall strength. Modern industries, e.g. the aerospace industry, increased the demand for high-performance materials with relatively low weight. A well known example that can fulfil such requirements are composite materials e.g. carbon fibre and glass fibre, which tend to have a very high strength-to-weight ratio.

With the presence of nanotechnology, the factors that influence material overall properties at small length scales can be studied. At the same time, the development of additive manufacturing technologies made it more feasible to manipulate relevant properties, at small length scales, that influence the material properties.

The state of the art metamaterials allow us to alter the micro structural configuration and composition. Therefore, we can achieve materials with properties that are challenging or impossible to achive in conventional materials [97,112]. Examples of these properties include negative Poisson's ratio[1] metamaterials [13, 46], which can be implemented in many engineering applications such as foams with acoustic properties [89]. Another remarkable example is negative compressibility[2] metamaterials [36, 77], which can be applied to develop actuators and protective mechanical devices, subwavelength lenses and acoustic shielding [36, 77]. Furthermore, strain rate dependent metamaterials, such as negative viscoelastic[3] behaviour [56], can be utilised to develop special medical devices and soft robotics [56]. Design and optimisation of metamaterials can be achieved using experimental and numerical approaches. Experimental approaches tend to give a reliable understanding of the performance of a metamaterial. However, using experimental programs to optimise a metamaterial often leads to material wastage and high costs. Thus numerical approaches is more suitable for optimisation as they allow us to study and optimise different factors that influence metamaterials properties. Metamaterials macroscopic properties are highly dependent on the microstructural configuration, and parent materials; therefore, developing an understanding of these effects, microstructural configuration, and parent material, for a certain type of metamaterials can be used towards optimization.

The recent fast growing and inspiring applications of metamaterials have motivated this present study aiming to develop a parametric study tool to understand the influence of microstructural configuration and material composition on the overall behaviour of metamaterials. In this thesis, the focus is on elastic and viscoelastic behaviour of metamaterials.

---

[1] Negative Poisson's ratio: behaviour of materials that contract transversely when compressed and expand transversely when stretched [13].

[2] Negative compressibility: behaviour of materials that expand in at least one direction while they are compressed in all directions [36].

[3] Negative viscoelasticity: materials that show less instantaneous stiffness when loaded with higher strain rates [56].

1.2 Scope and Objectives

In this section, a summary of the scope and objectives of this thesis is presented. First, a review of metamaterials design and optimisation methodologies will be carried out, with a focus on the most generic methodologies that are not restricted to a single microstructure or material behaviour; followed by obtaining a methodology to model metamaterials with relatively low computational cost. In this study all analysis has been made to 2D unit cells to simplify the problem, where extension of this work to 3D is possible and kept for future work. Furthermore, loading scenarios were uniaxial all through this thesis; this has been considered such hat more time is given to studying different material properties and inclusions. This methodology has then be used to develop a numerical analysis code to study the influence of micro structure aspects and material composition on the overall performance, leading to formulation of closed form expressions of the effective elastic and viscoelastic properties of periodic metamaterials under quasi static loading conditions. The effective properties from quasi static tests were then used, along with analytical solutions, to predict the behaviour under dynamic loading. Finally, an attempt is carried out to obtain effective properties of periodic metamaterials from the dynamic response. The novel contributions of this thesis, in terms of theoretical work, are the development of homogenisation in space as well as in time and the homogenisation of transient mechanical behaviour. Furthermore, in terms of implementation, a novel contribution of this thesis is the development of the script described in Section 3.4 that allows for large-scale automated parameter studies.

The objectives of this study are:

- To develop a homogenisation tool that is capable of carrying out parametric studies of 2D unit cells.
- To study the macrostructural properties and how they are influenced by inclusion's size and orientation on simple metamaterials with elastic and viscoelastic unit cells.
- To implement the concept of numerical homogenisation in time domain dynamics and test if the response of single unit cell is enough to obtain macro material properties from dynamic behaviour.
- To introduce the concept of time averaging to obtain effective properties of periodic metamaterials from the dynamic response.

1.3 Thesis outline

Chapter 1: A summary of the motivation and objectives of this thesis.

Chapter 2: A literature review on the evaluation of mechanical properties of metamaterials with an emphasis on homogenisation methods. A summary of principles of numerical homogenisation was included along with constitutive models of materials used in this thesis.

Chapter 3: Discussion of all the numerical work and methodology used in this study, furthermore a discussion of challenges and limitations. The chapter starts by presenting aspects of fine element modelling such as element types, mesh criteria and time step convergence. In addition, a discussion of boundary conditions is presented for cases of quasi static and dynamic loading conditions. Finally, a script is presented that has been developed to perform parametric studies of a large number of RVEs (Representative Volume Element) in a fully automated manner.

Chapter 4: In this chapter, a parametric study was conducted under quasi static loading conditions for elastic, viscoelastic and composite RVEs with different inclusion's area, inclination angles and aspect ratios. Closed form expressions were found that describe the macroscale material properties in terms of the microscale constituents.

Chapter 5: This chapter starts with a derivation of an analytical solution, under dynamic loading, for single degree of freedom systems of Maxwell viscoelastic and the standard solid models including inertia. Furthermore, it presents the dynamic homogenised response of RVEs in the time domain, and compares it with analytical obtained from quasi-static tests.

Chapter 6: This chapter introduces the time homogenisation hypothesis as a method to obtain homogenised material properties from dynamic time domain response of elastic, viscoelastic and composite unit cells, in which time averaging was employed to lower the fluctuations of stress and strain and thus obtain homogenised material properties with increased confidence.

Chapter 7: This chapter highlights the main findings and conclusions. In addition, a discussion of limitations and possible improvements for future research is presented in detail.

Chapter 2

Literature Review and Theoretical Background

2.1 Introduction

Modern manufacturing technologies, such as additive manufacturing, have made it possible to specify and design microstructural properties to achieve desired macrostructural properties, which may be difficult to achieve with conventional or natural materials [8]. The concept of metamaterials refers to materials that are build with specified microstructure to gain desired properties on the macro level [97]. According to the literature, metamaterials applications in engineering roughly fall into three main fields, namely electromagnetic, acoustic and mechanical applications [4].

The macro level properties of metamaterials depend on the properties of the original material, relative density and the microstructural configuration of the unit cell, and they can be designed using different parent materials and manufacturing techniques. Typical examples of metamaterials geometries in the literature include lattice structures such as pyramids [62], octagons [24] and re-entrant cubes [80, 81], more metamaterials micro structures can be found in Table 2.1. Furthermore, parent materials vary from metals such as titanium [55, 64, 80, 81] and stainless steel [37, 62, 96, 107] to polymers [38] and porous ceramics [15]. In this thesis, the focus will be on mechanical metamaterials with particular emphasis on elastic and viscoelastic properties.

Table 2.1: Mechanical metamaterials micro structures [114]

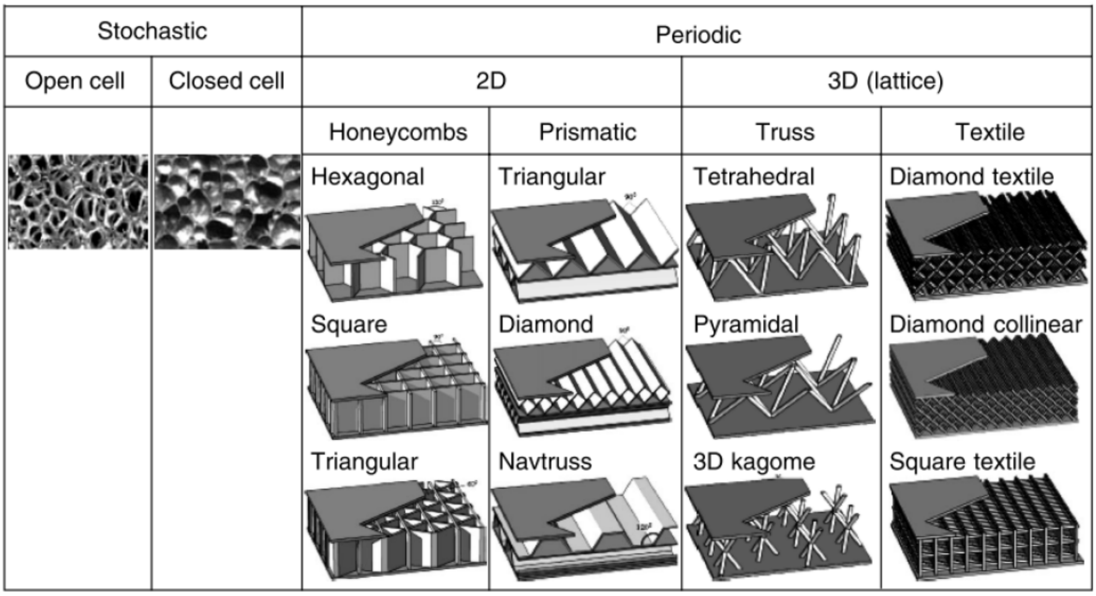

Stochastic		Periodic			
Open cell	Closed cell	2D		3D (lattice)	
		Honeycombs	Prismatic	Truss	Textile
		Hexagonal	Triangular	Tetrahedral	Diamond textile
		Square	Diamond	Pyramidal	Diamond collinear
		Triangular	Navtruss	3D kagome	Square textile

In this chapter, a review of metamaterials mechanical properties evaluation methods with emphasis on homogenisation methods is presented in Sections 2.2 and 2.3. A discussion about the size of the representative volume element (RVE) is presented in Section 2.4; a background review of the basic principles of homogenisation is summarised in Section 2.5. Finally, Section 2.6 presents a review of the relevant constitutive models.

2.2 Metamaterials

According to the literature, the analysis of metamaterials can be summarised into main three main methodologies, which are experimental, analytical and numerical approaches. In this section, relevant examples of each approach are presented, along with a discussion of each approach's advantages and limitations. Several studies have addressed the mechanical performance of metamaterials experimentally, e.g. [15, 71]. Sypeck and Wadley have used an experimental procedure to compare open-cell periodic lattice metamaterials with stochastic cellular structures; they concluded that open-cell periodic lattice metamaterials provide higher mechanical properties (stiffness, energy absorption, and heat exchange) compared with stochastic cellular structures [98]. A remarkable experimental study that addressed the dynamic behaviour of crystals metamaterial can be found in the works of Liu *et al.*, where they developed sonic crystals metamaterial for the purpose of localising resonant [68]. The authors have reported that the overall behaviour of the material shows an effective negative elastic constitutive matrix constants under *low sonic* frequencies [68]. Experimental approaches can be particularly useful to identify failure modes [80]. However, experimental approaches are not conclusive for optimisation of the metamaterial microstructure, since they are often costly, dependent on trial and error, and subject to limitations of the experimental set-up [58].

To overcome the limitations of experimental procedures, analytical approaches can be utilised to design or determine the properties of metamaterials, for instance by using structural mechanics theories based on trusses, beams [58] or plates [99]. These methods can be used to identify the initial failure properties such as the yield strength, but they are feasible for relatively simple microstructural geometries and simple material models [58]. To assess more general structural and material properties, analytical approaches can be combined with numerical simulations such as finite element (FE) computations. Bruno and coworkers studied the relationship between micro and macro properties on porous ceramic, closed cell stochastic cellular materials under uniaxial loading [15]. Their results show a linear dependency between average micro stress and applied macro stress through the porosity, void distribution and ratio, of the ceramic sample. Furthermore, it was found that the average *micro strain* depends on the macro strain through the *morphology factor*, while the microscopic modulus does not depend on *morphology* and Poisson's ratio does not depend on porosity [15]. Furthermore, Maskery and coworkers investigated a surface-based lattice numerically in terms of cell type, orientation and volume fraction, resulting in general design parameters and design criteria. The unit cell geometry was found to play an important role in determining the elastic modulus, while the effect of orientation on the elastic modulus was found to be less pronounced [71]. In a related study, a Ti-6Al-4V titanium alloy lattice has been studied under cyclic and fatigue loading, which demonstrated the potential use of lattice metamaterials in dental fillings [55]. Indeed, it has been reported by several studies that numerical modeling of metamaterials is computationally demanding [2, 81]. Few studies have addressed optimisation of metamaterials for specific applications and loading scenarios. Relevant examples of such studies include *auxetic* metamaterials [113], *buckling induced* mechanical metamaterials for energy absorption applications [21], lattice structures [92], 3D fabricated multi layer metamaterials for energy absorption performance [50]. These optimization methods can be utilised to optimise a specific type of metamaterial for a specific application or loading conditions. However, these optimisation methods exhibit a limitation on the metamaterial geometry, loading conditions, and material models.

2.3 Homogenisation methods

Using conventional numerical modelling techniques, such as detailed FE models, to simulate the full metamaterial specimen usually requires high computational cost and time. A promising alternative is homogenisation methods, which depend on detailed modelling of a unit cell and using averaging techniques to homogenise the results to obtain the macro mechanical properties of metamaterial. This can lead to significant reductions in analysis time and computational cost. Furthermore, it allows researchers to study factors that influence the macro constitutive parameters of metamaterials such as micro material properties and microstructural configuration. Thus, a better understanding of the influence of micro properties on the macro level behaviour can be gained, in which this knowledge can be employed in optimising the microstructural configuration and material properties to achieve desired performance at macro level. Several homogenisation schemes have been utilised to determine homogenised material properties, see for instance the in-depth review of Kouznetsova and coworkers [60]. Another noteworthy review that addresses the implementations and challenges of computational homogenisation can be found in the work of Geers [30]. The first, and most basic approach of homogenisation focuses on homogenised moduli and follows the so-called rule of mixtures. This method is simple and straightforward and can provide upper and lower bounds of the relevant properties, however, it works only for linear material behaviour [60].

The second approach is analytical homogenisation [26,40,42,47]. In this method, the homogenised material properties of the macrostructure are obtained from the analytical or semi-analytical solution of a boundary problem of one inclusion in an infinite matrix material. Several studies in the literature have employed analytical approaches to obtain homogenised material problems. Examples of such studies include the work of Li *et al.* on honeycomb sandwich plates under bending [63], Wang's study on unidirectional composites [105], and Chen and Schuh study on periodic composites [22] using an analytical homogenisation approach. Indeed this method is self-consistent and it yields accurate results for regular geometries, however it cannot be used to model the behaviour of *cluster structures* nor high contrasts between phases [60].

A third method is asymptotic homogenisation theory [25, 28, 101]. Indeed, this method is an expansion of displacement and stress fields utilising natural length parameters, such as the ratio of size and distribution of heterogeneities between microstructure to macrostructure. Effective homogenised properties can be obtained using this method as well as local stress and strain values. An outstanding implementation of asymptotic homogenisation in analysing linear elastic periodic composite materials is presented in the studies of Pinho-da-Cruz *et al.* and Oliveira *et al.* [78, 85]. However, this method is typically restricted to simple microstructural geometries, small strains and simple material behaviour [60].

Fourthly, unit cell numerical methods rely on fitting the results of detailed modelling of a microscale Representative Volume Element (RVE) to the macrostructural homogenised properties. The concept of an RVE was introduced by Hill [47] and it is taken as a volume portion at micro-level such that the homogenised mechanical behaviour of the RVE is equivalent to the macrostructural mechanical behaviour. The RVE should typically be as small as possible, but large enough to contain sufficient details about the heterogeneities [103], further details and discussion about RVE existence and definition are included in Section 2.4. A fundamental assumption in any numerical homogenisation scheme is that random heterogeneous material is statistically homogeneous – that is, the macrostructure behaves similarly, within user-defined levels of acceptable error, to duplicates of a single RVE. To predict the behaviour of heterogeneous materials using numerical homogenisation, an RVE should be defined and analysed; the results should be subsequently fitted in a postulated constitutive relation between micro and macro levels. Numerical homogenisation has been utilised and developed for many applications such as polymers [103], ceramics [33] and concrete [90]. This method allows simulation of complex microstructural behaviour and, hence, the study of the microstructure configuration effect on the overall macroscale properties and response. The main challenge in numerical homogenisation is establishing a robust and versatile constitutive connection between micro and macro levels [60].

Fifthly, multiscale computational homogenisation methods have been developed [27, 60, 72, 95, 100]. This method does not yield a closed-form expression for the macrostructural material behaviour, but instead estimates the macrostructural stress-strain relationship by solving, numerically, boundary value problems for RVEs assigned to every integration point in the macrostructure. Computational homogenisation consists of three main steps, which employ two levels of simulations and have to be applied iteratively for every time step. First, an arbitrary homogenised specimen (representing the macro level) is solved using the FEM. Next, the strains obtained at each integration point are applied as loading to a unique RVE corresponding to a given integration point. The last step is to solve the RVE response and translate the obtained microscale reaction forces into macroscale stresses for the full specimen [60]. This method is suitable to model complex microstructures as it does not have a limitation on the number or configuration of RVEs. On the other hand, this method is less suitable for optimisation design purposes, and studying material behaviour due to microstructural effect, as it yields a phenomenological stress-strain behaviour for the macrostructure based on microstructural solution, rather than a closed-form constitutive law.

Indeed, the microstructural configuration of metamaterials also play an important role in the *dynamic* mechanical response [4, 8, 52, 75]. Several studies have employed different methods of homogenisation to study the dynamic behaviour of metamaterials. A state of the art multi scale computational homogenisation approach for metamaterials was introduced by Pham *et al.* and further developed by Liu and Reina where they formulated a second-order enriched homogenisation scheme to simulate linear elastic metamaterials [65, 84, 87]. This approach has been widely used in the literature, for instance, Liu and Reina have employed this approach to study resonant behaviour of elastic metamaterials and band gaps; they have reported that employing homogenisation in modeling leads to a fraction of the cost of modeling the macro model [66]. Other homogenisation approaches were suggested in the literature to model metamaterials in dynamics; for instance, Molinari and Mercier have employed the averaged velocity field and virtual work principle to obtain a relationship between macroscopic stress and strain rate of heterogeneous metamaterials [74]. On the other hand, Sieck *et al.* have obtained a non-local expression for the effective properties of infinite periodic acoustic metamaterials, where they have used the averaged stain and momentum fields to obtain expressions [93]. The methods discussed in this paragraph are powerful tools to analyse a well defined microstructure, however, the numerical homogenisation method is more suitable to formulate a closed form constitutive model of the macro material properties, based on microstructural configuration and properties. Obtaining a direct relation between macro and micro properties helps in developing knowledge about the influence of micro properties, and their importance, on macro behaviour, and yet optimisation of these micro properties can be carried out. in In this work, the numerical homogenisation approach will be applied to RVEs under static[1], quasi static[2] and dynamic[3] loading conditions.

2.4 Representative volume element

The concept of representative volume element (RVE) refers to the smallest portion of the volume that can be used to obtain the effective homogenised macro properties; however, the RVE should be large enough to contain sufficient details about the micro structure [41]. The spatial dimensions of the RVE differ from one material to another, due to the level of heterogeneity, micro material behaviour, and microstructural configuration of heterogeneities. In a general non-periodic heterogeneous material, a study to determine the correct RVE size is essential prior to applying any homogenisation or averaging. Analytical, statistical and experimental procedures have been suggested and used to determine the size of an RVE. For an overview of RVE existence and determination methodologies, the reader is referred to [32].

In the literature, several studies have addressed RVE size determination; for instance, Kanit *et al.* have suggested a methodology to determine the RVE size of random composites using statistical and numerical approaches [57]. Pelissou *et al.* have studied random composites, where they established a *correlation factor* between RVE size required to model elastic and fracture behaviours [83]. Furthermore, Mirkhalaf *et al.* studied the RVE size of heterogeneous polymers that undergo a softening behaviour; they concluded side lengths equal to 5 times the average grain size is sufficient to represent the macro behaviour [73]. Koohbor *et al.* have studied the RVE size of woven composites experimentally, where they concluded that the RVE size of woven composites is dependent on strain and loading orientation [59]. It is noted by several studies that setting a firm determination methodology of RVE size is challenging in modelling material behaviour that undergoes *localisation*, such as softening behaviour and fracture [73, 83].

---

[1] Static: response of material that has no time dependence, such as a linear elastic RVE under constant load.

[2] Quasi static: response of material that has time dependence, but neglected inertial effect, such as viscoelastic RVE under constant loading.

[3] Dynamic: response of a material where inertial effects are high and cannot be ignored such as an RVE modeled under an impulsive loading.

On the other hand, determining the RVE size of periodic metamaterials is relatively straightforward, since periodic metamaterials are made of duplicates of a specific unit cell. Several studies have demonstrated that the RVE of periodic materials can be taken as a single unit cell under quasi static loading conditions [34, 49, 103]; this consideration is valid in case the RVE is used to study homogenised effective properties. If the study aims to evaluate a phenomenon where *localisation* occurs such as fracture or stress softening, more than one unit cell might be required to obtain an RVE as shown in the following studies [76,109,110]. In this thesis, the aim of the study is to evaluate macro material parameters of periodic metamaterials; therefore, a simple periodic metamaterial RVE with single inclusion is considered as shown in Figure 2.1, where the effects of the inclusion's size, aspect ratio and inclination angle with respect to the loading will be studied in the following chapters. A verification has been carried out by a rudimentary convergence study, comparing the response of 1x1 unit cell with that of 2x2 and 4x4 unit cells, concluding that a single inclusion unit cell can be used as an effective RVE for various loading conditions.

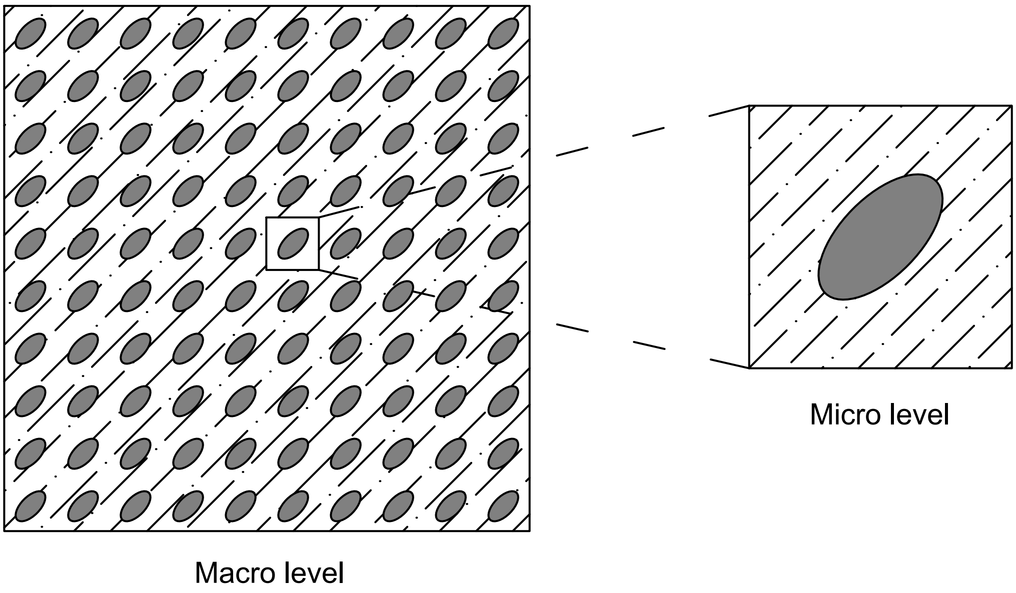

Figure 2.1: Representative volume element of a periodic metamaterial.

2.5 Principles of Homogenisation

In this section a brief explanation of the averaging concepts in homogenisation theories is presented, starting by a definition of the homogenised stress and strain, followed by the concepts of average stress and average strain theorems and finalising with the Hill-Mandel macrohomogeneity condition [31,47,48,60,103,111].

The volume average of a generic quantity $\bar{\psi}$ is defined as [47,48]

$$\bar{\psi} = \frac{1}{\Omega} \int_{\Omega} \psi(x, y)\, d\Omega \tag{2.1}$$

where $\bar{\psi}$ is the averaged, homogenised, quantity at the macro level, while $\psi(x, y)$ is the quantity at the micro level, x and y are the spatial coordinates. Ω is the volume domain of the integral, hence Ω becomes the volume of the RVE (V_R).

Next, the strain is written as $\varepsilon_{ij} = \frac{1}{2}(u_{i,j} + u_{j,i})$, where u is the displacement, the index before the comma indicates the displacement component, while the index following the comma indicates a partial derivative with respect to the local coordinate [47, 48].

$$\bar{\varepsilon}_{ij} = \frac{1}{V_R}\int\limits_{V_R} \varepsilon_{ij}(x,y)\,dV = \frac{1}{V_R}\int\limits_{V_R} \frac{1}{2}(u_{i,j}+u_{j,i})\,dV = \frac{1}{2V_R}\oint\limits_{\partial V_R} (u_i n_j + u_j n_i)\,dS \quad (2.2)$$

where the Gauss divergence theorem has been employed to change the volume integral to an associated boundary integral. Here n_i is the outward normal vector of the RVE boundary ∂V_R.

Substituting $u_i = x_j\bar{\varepsilon}_{ij}$ in Equation (2.2), where x_j is a vector of RVE dimensions and $\bar{\varepsilon}_{ij}$ is the averaged strain tensor, then yields

$$\frac{1}{2V_R}\oint\limits_{\partial V_R} (x_j\bar{\varepsilon}_{ij}n_j + x_j\bar{\varepsilon}_{ji}n_i)\,dS = \frac{1}{2V_R}\oint\limits_{\partial V_R} (\bar{\varepsilon}_{ik}x_k n_j + \bar{\varepsilon}_{jk}x_k n_i)\,dS \quad (2.3)$$

Equation (2.3) is turned to a volume integral as follows,

$$\frac{1}{2V_R}\int\limits_{V_R} (\bar{\varepsilon}_{ik}\delta_{kj} + \bar{\varepsilon}_{jk}\delta_{ki})\,dV = \bar{\varepsilon}_{ij} \quad (2.4)$$

This finding is called the average strain theorem which demonstrates that the avarage strain, obtained from displacement along the RVE boundary, is equal to the homogenised strain $\bar{\varepsilon}_{ij}$ [111].

In equilibrium, the stress field σ_{ij} in a complex microstructured RVE is not constant over the volume of the RVE; the stress field can be written as follows

$$\sigma_{ij} = \sigma_{ik}\delta_{jk} = \sigma_{ik}\frac{\partial x_j}{\partial x_k} = (\sigma_{ik}x_j)_{,k} - \sigma_{ik,k}x_j \tag{2.5}$$

In first order homogenisation an assumption of $\sigma_{ij,j} = 0$ is considered, which is valid for RVEs in equilibrium and with zero body forces [31, 60, 111]. Therefore Equation (2.5) is reduced to

$$\sigma_{ij} = (\sigma_{ik}x_j)_{,k} \tag{2.6}$$

Applying the averaging integral of Equation (2.1) and employing the Gauss divergence theorem yields

$$\bar{\sigma}_{ij} = \frac{1}{V_R}\int\limits_{V_R}(\sigma_{ik}x_j)_{,k}\,dV = \frac{1}{V_R}\oint\limits_{\partial V_R}\sigma_{ik}x_j n_k\,dS \tag{2.7}$$

Using the equality $t_i^0 = \sigma_{ik}n_k$, where t_i^0 is the traction, the homogenised stress can be written as

$$\bar{\sigma}_{ij} = \frac{1}{V_R}\oint\limits_{\partial V_R} t_i^0 x_j\,dS \tag{2.8}$$

The so called average stress theorem can be verified if Equation (2.7) holds, which states that the averaged stress over the entire RVE is equal to the stress obtained from the boundary of the RVE [111] as follows

$$\frac{1}{V_R}\int\limits_{V_R}(\sigma_{ik}x_j)_{,k}\,dV = \frac{1}{V_R}\oint\limits_{\partial V_R} t_i^0 x_j\,dS = \bar{\sigma}_{ij} \tag{2.9}$$

The transition between micro to macro properties should satisfy the Hill-Mandel macrohomogeneity condition [31, 47, 48, 60]. The condition states that the homogenised, averaged, strain energy density is equivalent to the strain energy density of the heterogeneous RVE; in other words the virtual work at macro and micro levels should be equal.

The strain energy density at macro level is defined as:

$$U = \frac{1}{2}\bar{\sigma}_{ij}\bar{\varepsilon}_{ij} \tag{2.10}$$

The following condition should be satisfied in order for the Hill-Mandel macrohomogeneity condition to hold:

$$\bar{\sigma}_{ij}\bar{\varepsilon}_{ij} = \frac{1}{V_R}\int\limits_{V_R} \sigma_{ij}\varepsilon_{ij}\, dV \tag{2.11}$$

It has been demonstrated that uniform traction, uniform displacement and periodic boundary conditions satisfy the Hill-Mandel macrohomogeneity condition [31,111]-see Section 3.3 for a detailed discussion of boundary conditions for RVEs.

2.6 Review of Materials Constitutive Models

This section summarises the relevant equations of linear elasticity [7, 70], linear viscoelasticity [12, 70, 104] and the Maxwell form of the Standard Solid Model [12, 70, 104] for viscoelastic material behaviour. These constitutive equations will be employed in the numerical parametric studies in the following chapters.

2.6.1 Linear elasticity

A 2D linear elastic plane stress constitutive equation can be written, as usual [7, 70], as:

$$\begin{bmatrix}\sigma_{xx}\\ \sigma_{yy}\\ \sigma_{xy}\end{bmatrix}=\begin{bmatrix}C_{11} & C_{12} & 0\\ C_{21} & C_{22} & 0\\ 0 & 0 & C_{23}\end{bmatrix}\begin{bmatrix}\varepsilon_{xx}\\ \varepsilon_{yy}\\ \gamma_{xy}\end{bmatrix}=\frac{E}{1-\upsilon^2}\begin{bmatrix}1 & \upsilon & 0\\ \upsilon & 1 & 0\\ 0 & 0 & \frac{1-\upsilon}{2}\end{bmatrix}\begin{bmatrix}\varepsilon_{xx}\\ \varepsilon_{yy}\\ \gamma_{xy}\end{bmatrix} \tag{2.12}$$

where $[\sigma_{xx}, \sigma_{yy}, \sigma_{xy}]^T$is the stress vector, $[\varepsilon_{xx}, \varepsilon_{yy}, \gamma_{xy}]^T$ is the strain vector, E represents elastic modulus and υ represents Poisson's ratio.

If uniaxial tension is applied to a 2D elastic model in the x direction (11) via an imposed strain vector of [ε_{xx}, 0, 0], the homogenised elastic constants $\bar{C}_{11}$ and $\bar{C}_{12}$ can be obtained from the following expressions; where by applying a strain vector of [1, 0, 0] $\bar{C}_{11}$ and $\bar{C}_{12}$ are equal to σ_{xx} and σ_{yy}:

$$\sigma_{xx} = C_{11}\varepsilon_{xx} = \frac{E}{1-\upsilon^2}\varepsilon_{xx} \tag{2.13}$$

$$\sigma_{yy} = C_{21}\varepsilon_{xx} = \frac{E\upsilon}{1-\upsilon^2}\varepsilon_{xx} \tag{2.14}$$

The macroscopic constitutive parameters C_{ij} can be evaluated by the following equation; while, the macroscopic stress $\bar{\sigma}_{ij}$ and strain $\bar{\varepsilon}_{ij}$ were computed using Equations (2.3) and (2.8).

$$\bar{C_{ij}} = \frac{\bar{\sigma}_{ij}}{\bar{\varepsilon}_{ij}} \tag{2.15}$$

From Equations (2.13) and (2.14), the macroscopic homogenised elastic modulus $\bar{E}$ and Poisson's ratio $\bar{\upsilon}$ can be expressed as

$$\bar{E} = \bar{E}_{11} = \bar{C}_{11}\left(1-\left(\frac{\bar{C}_{21}}{\bar{C}_{11}}\right)^2\right) \tag{2.16}$$

$$\bar{\upsilon} = \bar{\upsilon}_{12} = \left(\frac{\bar{C}_{21}}{\bar{C}_{11}}\right) \tag{2.17}$$

The other constitutive constants can similarly be found via appropriately defined alternative imposed strain vectors.

2.6.2 Linear viscoelasticity

Certain types of materials exhibit changes in their behaviour over time, e.g. stress relaxation, creep or more general strain rate dependence. Among the several models that have been developed to represent the viscoelastic behaviour of materials, we mention Maxwell, Kelvin-Voigt, the standard linear solid model, Burgers model and the generalized Maxwell mode [104]l.

The Maxwell model is composed of a linear spring and a linear dashpot, connected in series (Figure 2.2a). Similarly, the Kelvin-Voigt model is composed of a linear spring and a linear dashpot, which are connected in parallel. More complex models such as the standard solid model (Figure 2.2b), which consist of combinations of springs and dashpots, tend to give a better representation of creep and relaxation phenomena compared with Maxwell or Kelvin-Voigt models [12, 70, 104].

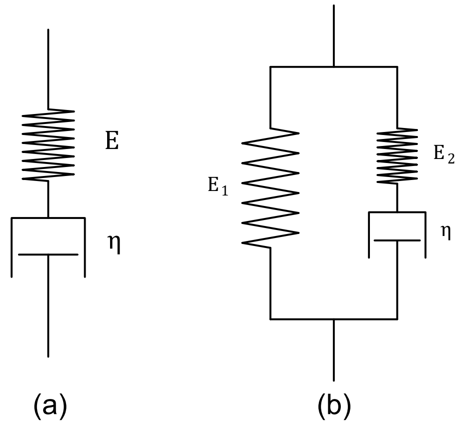

Figure 2.2: (a) Maxwell viscoelastic model (b) Maxwell form of the Standard Solid model

The constitutive equation for a Maxwell-type material is written as follows:

$$\sigma + \frac{\eta}{E}\dot{\sigma} = \eta\dot{\varepsilon} \tag{2.18}$$

where σ is the stress, η the dynamic viscosity of the viscous damper, E the elastic modulus of the spring, $\dot{\sigma}$ is the stress rate, and $\dot{\varepsilon}$ is the strain rate.

In stress relaxation, strain is constant over time, therefore $\dot{\varepsilon} = 0$, and $\varepsilon = \varepsilon_0$ is the imposed strain. Therefore, Equation (2.18) turns into a first order differential equation with initial condition $\sigma(\tau) = E \cdot \varepsilon_0$, where τ is the load duration [70]. For stress relaxation, the solution of Equation (2.18) can be expressed as follows

$$\sigma(t) = E \cdot \varepsilon_0 \cdot e^{\frac{-E}{\eta}(t-\tau)} \tag{2.19}$$

In creep, the stress is constant in time, therefore $\dot{\sigma} = 0$, and $\sigma = \sigma_0$ is the imposed stress. Equation (2.18) then turns into a first order differential equation with initial condition $\varepsilon(\tau) = \sigma_0/E$ where τ is the load duration [70].

Thus, for creep, the solution of Equation (2.18) can be expressed as follows

$$\varepsilon(t) = \frac{\sigma_0}{\eta}(t-\tau) + \frac{\sigma_0}{E} \tag{2.20}$$

The homogenised stress $\bar{\sigma}(t)$ and strain $\bar{\varepsilon}(t)$ can be constructed by evaluating Equations (2.3) and (2.8) at every time instant; while the macro material properties $\bar{E}$ and $\bar{\eta}$ can be evaluated by fitting the curves of $\bar{\sigma}(t)$ and $\bar{\varepsilon}(t)$ to Equations (2.19) and (2.20) depending on the loading condition. This homogenisation procedure is based on the assumption that the macro and micro constitutive models are expected to behave in a similar pattern, which motivated the use of the same constitutive law although with different values of the constitutive coefficients.

2.6.3 The Maxwell form of the Standard Solid Model for Viscoelastic Material

The Standard Solid model can give a better representation of both creep and stress relaxation phenomena. This is because the Standard Solid Model is enriched with a parallel spring that allows it to capture infinite elastic modulus and it allows for an exponential decay of both creep and stress relaxation. This model has two different forms, namely the Maxwell form and the Kelvin form. The Maxwell form of this model is constructed by connecting a linear spring element (elastic modulus E_1) in parallel with a Maxwell element (elastic modulus E_2 and dynamic viscosity η) as shown in Figure 2.2b, and this is the form that will be adopted in this study [12, 70, 104]. This form has been chosen because it is capable of representing the macro behaviour of composite unit cells such that the spring represent the elastic inclusion and the spring-dashpot represent the viscoelastic matrix.

The stress-strain relationship for the standard solid model is given as follows:

$$\sigma + \frac{\eta}{E_2}\dot{\sigma} = E_1\varepsilon + \left(1 + \frac{E_1}{E_2}\right)\eta\dot{\varepsilon} \tag{2.21}$$

When a viscoelastic material is subjected to a constant strain (i.e. a relaxation test), we can assume $\dot{\varepsilon} = 0$, and $\varepsilon = \varepsilon_0$ from time τ onwards. Therefore, Equation (2.21) is reduced to

$$\sigma + \frac{\eta}{E_2}\dot{\sigma} = E_1\varepsilon_0 \tag{2.22}$$

The first order ordinary differential equation (2.22) can be solved with initial condition $\sigma(\tau) = (E_1 + E_2) \cdot \varepsilon_0$, the solution of which can be written as

$$\sigma(t) = E_2\varepsilon_0 e^{\frac{-E_2}{\eta}(t-\tau)} + E_1\varepsilon_0 \tag{2.23}$$

E_1 is also equal to the long term (final) elastic modulus E_∞, after relaxation, while $E_1 + E_2$ can be defined as the initial elastic modulus E_0. This allows to reformulate the stress-strain relation in terms of micro-scale properties as a stress-strain relation in terms of macro-scale properties:

$$\sigma(t) = (E_0 - E_\infty)\varepsilon_0 e^{\frac{-(E_0-E_\infty)}{\eta}(t-\tau)} + E_\infty\varepsilon_0 \tag{2.24}$$

from which follows an expression for the time-dependent elastic modulus

$$E(t) = (E_0 - E_\infty) e^{\frac{-(E_0-E_\infty)}{\eta}(t-\tau)} + E_\infty \tag{2.25}$$

When a viscoelastic material is subjected to a constant stress (creep), we can assume $\dot{\sigma} = 0$, and $\sigma = \sigma_0$ from time τ. Therefore, Equation (2.21) is reduced to

$$\sigma_0 = E_1\varepsilon + \left(1 + \frac{E_1}{E_2}\right)\eta\dot{\varepsilon} \tag{2.26}$$

If the first order ordinary differential equation given in Equation (2.26) is completed with initial condition $\varepsilon(\tau) = \frac{\sigma_0}{E1+E2}$, the solution can be written as

$$\varepsilon(t) = \sigma_0\left(\frac{1}{E_1+E_2} - \frac{1}{E_1}\right) e^{\frac{-E_1E_2}{(E_1+E_2)\eta}(t-\tau)} + \frac{\sigma_0}{E_1} \tag{2.27}$$

Similar to relaxation, E_1 is equal to the long term (final) elastic modulus E_∞, while $E_1 + E_2$ can be defined as the initial Elastic modulus E_0. Thus,

$$\varepsilon(t) = \sigma_0 \left(\frac{1}{E_0} - \frac{1}{E_\infty} \right) e^{\frac{-E_\infty (E_0 - E_\infty)}{(E_0)\eta}(t-\tau)} + \frac{\sigma_0}{E_\infty} \tag{2.28}$$

Similar to section 2.6.2, Equations (2.3) and (2.8) from section 2.5 can be used to estimate the homogenised stress $\bar{\sigma}(t)$ and strain $\bar{\varepsilon}(t)$ at every time instant. Indeed, fitting the homogenised stresses $\bar{\sigma}$ and strains $\bar{\varepsilon}$ to Equations (2.24) and (2.28) can be used to obtain the macro material properties $\bar{E}_0$, $\bar{E}_\infty$ and $\bar{\eta}$. This homogenisation procedure is based on the assumption that the Maxwell form of the standard solid model represents the macro constitutive model, in the loading direction, of a unit cell made up with two materials (linear elastic matrix and Maxwell viscoelastic inclusion).

Chapter 3

Modelling methodology

3.1 Introduction

The aim of this research is to develop a programmed homogenisation tool to run parametric studies on periodic RVE. To achieve this aim, this chapter presents the methodology used to develop a numerical homogenisation tool for single inclusion RVEs. With reference to Section 2.4, a single inclusion unit cell of size (1 mm × 1 mm) was chosen as an RVE (Figure 3.1). By the end of this chapter, an automated code will be presented to run parametric studies on RVEs with different inclusion's aspect ratios, areas and inclination angle.

This chapter starts with RVE modeling where the Finite Element Method (FEM) was employed. Mesh criteria, time step convergence and element formulation are discussed in details in Section 3.2. The software package Abaqus was employed to produce the mesh for all RVEs, while the FE analysis was performed in LS-DYNA software package. Next, in Section 3.3, boundary conditions are discussed with emphasis on periodic boundary conditions. A criterion of implementing periodic boundary conditions in LS-DYNA is presented for RVEs modeled for creep and relaxation (Section 3.3.1), while a discussion for implementation of such bound-

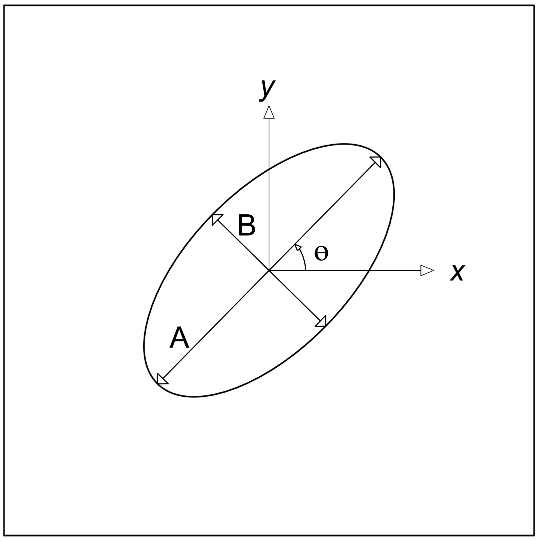

Figure 3.1: Representative volume element (1 mm × 1 mm)

ary conditions in dynamics is proposed in Section 3.3.2. An automated code is developed to run parametric studies on RVEs with different inclusion properties (Section 3.4). Finally, Section 3.5 presents the methodology at which the automated code works with, in this case, its shared memory parallel computing. This code will be used in the following chapters to study different RVEs.

3.2 Finite Element Modelling

As mentioned in Chapter 2, solving a microscale boundary value problem on an RVE is the first step in any numerical homogenisation scheme. In this thesis, the FEM is used to model RVEs. LS-DYNA FE software package was chosen, to model RVEs, for a number of reasons. First, a large number of material models are implemented in this software, which increase the freedom in choosing RVE materials. Thus, it makes the outcome of this research easier to be used in other studies or to be developed in the future. Furthermore, it is relatively easy to code a script that produces LS-DYNA input files in an automated manner, as well as interacting with high level programming languages makes it suitable to be used by someone with elementary knowledge of programming. LS-DYNA is capable of running multiple independent models simultaneously thus making it suitable for parallel computing. This feature has been employed in Section 3.5, resulting in a significant reduction of computational cost. Nevertheless, LS-DYNA, has a limitation of not having a meshing tool; this issue has been overcome by using a different software package, namely Abaqus, to perform meshing jobs.

LS-DYNA is a well established FE solver, which is commonly used in studies involving time integration. To name few: [19,67,69,86,91] have studied impact and stress waves, while [3, 88, 94, 108] have used LS-DYNA to model the viscoelastic response of different materials. To learn more about the development of LS-DYNA, element formulation, material models and theoretical background of this software, the reader is referred to [39].

The most commonly used algorithms to model a dynamic problem in FE are *implicit* or *explicit* time integration schemes. Implicit time integration use an implicit numerical integration method such as (Newmark, Newton Raphson, etc.); the quantities of displacement, velocity, and acceleration of the current time step (t_n) are computed from quantities of the previous time step (t_{n-1}). The equilibrum is achived at every time step, therefore it is considered to be unconditionally stable, however it is often computationally demanding, since it require matrix inversion at every time step [10]. On the other hand, explicit time integration commonly uses the central difference method, in which the nodal forces are used along with a inverted mass matrix to compute accelerations. This method is computationally less demanding due to the fact that mass matrix is diagonalised, thus it is easier to to be inverted [10]. In this thesis, both implicit and explicit solvers were employed in homogenising RVEs. The implicit solver was employed to simulate RVEs under quasi static loading condition (Chapter 3), while the explicit solver was utilised to model RVEs under dynamic loading (Chapter 4). The next Section (Section 3.2.1) presents the mesh criteria while a convergence study of time step is presented in Section 3.2.2; finally the choice of element formulation has been discussed and justified in Section 3.2.3.

3.2.1 Mesh criteria and convergence

A mapped mesh was considered, where possible, while refinement has been considered for the stress concentration areas, such as the tip of the inclusion. To obtain mapped meshes for RVEs with any inclusion, other than void, regardless of their inclusion's area, aspect ratio, or inclusion angle, partitions were created inside the inclusion. The partitions divide the inclusion into a square in the middle and linear partitions over the ellipse major and minor axis (as shown in Figure 3.2a). Meshing of all RVEs was obtained using Abaqus software package, while the automated script (Section 3.4) transfers the mesh file to LS-DYNA format.

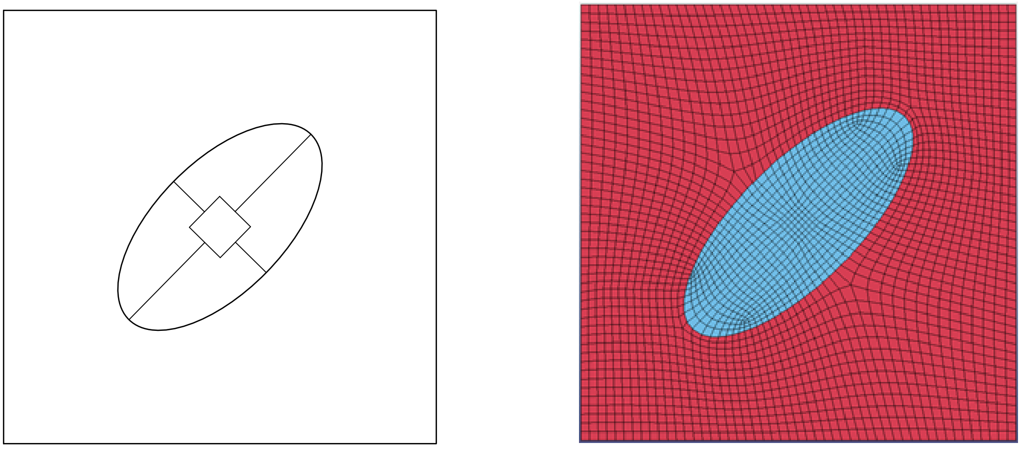

(a) Mesh partitions (b) Mesh

Figure 3.2: Mesh partitioning criteria

Throughout this study, the boundaries of any RVE, have been divided into equal sized mesh discretizations for each pair of parallel boundaries, e.g right and left boundaries. Hence, periodic boundary conditions can be implemented between boundaries as mentioned in Section 3.3. A mesh convergence study was conducted on several RVEs. Indeed, the homogenised results show negligible differences (around 1%) between element sizes of 0.1 mm and 0.001 mm for a 1 mm × 1 mm RVE. This is believed to happen due to the specific smooth geometry of the RVE inclusions, since there are no sharp edges and therefore, singularities were avoided. The conclusion has been drawn that this problem can be considered to be mesh independent.

3.2.2 Time step convergence

Under quasi-static loading conditions, the stability of the solution due to time step size is of no concern since the numerical method used to obtain the solution is unconditionally stable (implicit). However, in time dependent material models, the accuracy of the solution is influenced by the time step size. It is essential to use a time step that allows for sufficient solution points such that the numerical homogenisation scheme yields reasonable estimates for the time dependent parameters. A convergence study was carried out for all types of RVEs, at a converged mesh to obtain the optimum time step size to be used for the analysis. Figures 3.3 and 3.4 show a convergence study for an RVE with Maxwell viscoelastic material and a void inclusion; where Figure 3.3 shows the convergence of elastic modulus (E), and Figure 3.4 shows the convergence of dynamic viscosity (η). A maximum of 5 % difference, between the value of E or η and its successor, was used as a bench mark to conclude a converged value of E or η. Therefore, time step at that point is considered to be the converged value (in the case shown below a time step of 10^{-2}).

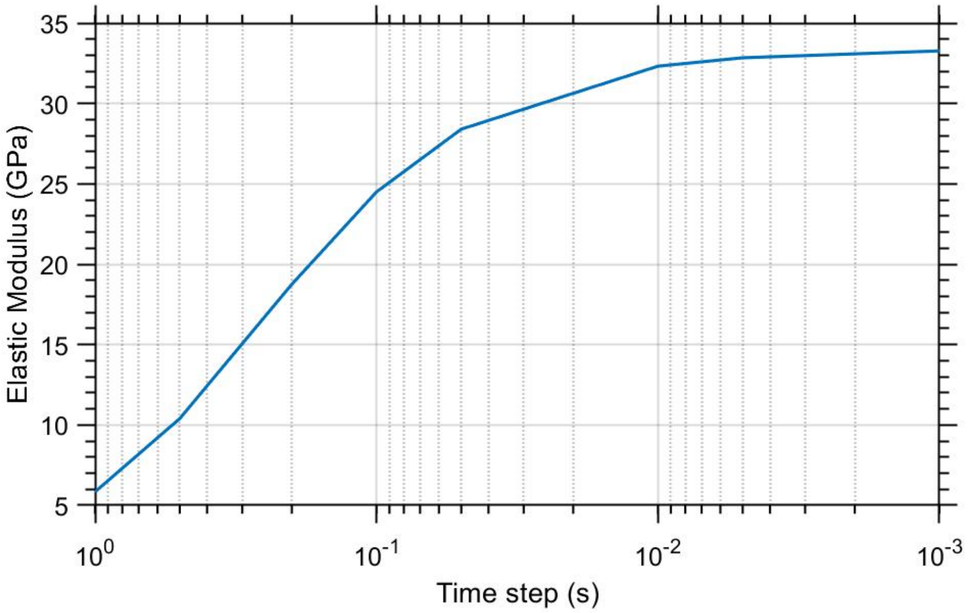

Figure 3.3: Convergence of elastic modulus

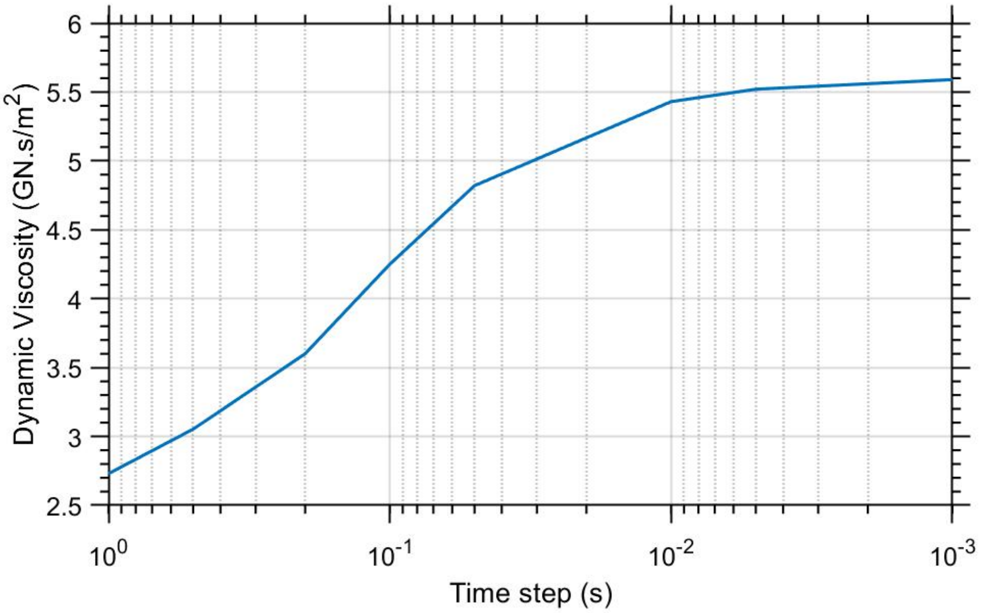

Figure 3.4: Convergence of dynamic viscosity

Under dynamic loading conditions, the stability of the solution is highly influenced by the time step size. In addition to the accuracy aspects discussed above, there are now also stability aspects to consider, since the Central Difference Method is conditionally stable [10]. To obtain meaningful results using explicit time integration, the time step should be smaller than the *critical time step* ($\Delta t < \Delta t_{crit}$); where the *critical time step* for linear elements is defined as the length of the smallest dimension of an element (l) divided by the speed of sound (c) in the media $\Delta t_{crit} = l/c$. The speed of sound in a 2 dimensional media is given by $c = \sqrt{\frac{E}{(1-\upsilon^2)\rho}}$, where E is the elastic modulus, ρ is the mass density and υ is the Poisson's ratio. The critical time step for higher order element formulations is usually lower than linear elements, for more details, the reader is referred to [6, 9, 51]. The mass density of RVE in static and quasi static loading condition was taken as $\rho = 7.8 \times 10^{-7}$ kN·s^2/m; however, the mass density has been taken as $\rho = 78$ kN·s^2/m in dynamic loading conditions to increase the time step required to obtain a stable solution. This increase in mass will change the natural frequencies of the system however the elastic modulus and dynamic viscosity (the properties of interest in this study) are not influenced by the change of mass density.

3.2.3 Element formulation

As the focus of this study is on 2D, plane stress[1] or plane strain [2] finite elements can be used. However the nature of our loading is uniaxial and an assumption of zero stresses in the third direction (thickness of RVE) is made; therefore, plane stress (referenced as EQ.12 in LS-DYNA) element formulation was employed to solve RVEs with elastic material properties. Using a reduced integration plane stress elements in viscoelastic RVEs resulted in an hourglass phenomena as shown in the following figure (Figure 3.5). This phenomena was reported to exist with reduced integration elements in strain rate dependent materials by several studies such as [14, 17, 20, 106]. Hourglass phenomena might cause meaningless results by allowing *zero energy* deformation modes. The artificial stiffness method, initially introduced by Flanagan and Belytschk [29], can be used to reduce the effect of hourglass. In this method, an extra stiffness is added to the elements to reduce the hourglass due to reduced integration [29]. This method can be implemented in LS-DYNA by the *CONTROL_HOURGLASS command. However, since the nature of this study address simple RVEs, using full integration element formulation will not have a restrictively adverse impact on the computational cost. Therefore, the full integration shell element formulation has been used (referenced as EQ.16 in LS-DYNA) for all viscoelastic RVEs to avoid the hourglass phenomena. The use of shell elements is because LS-DYNA does not support full integration plane stress elements. Since the loading is uniaxial, the rotational degrees of freedom where clamped, therefore it acted as a fully integrated plane stress.

---

[1] Plane stress: If the stress across one plane is very small or null, that plane can treated as a plane stress and the problem can be simplified to 2D.

[2] Plane strain: If the strain across one plane is very small or null, that plane can treated as a plane strain and the problem can be simplified to 2D.

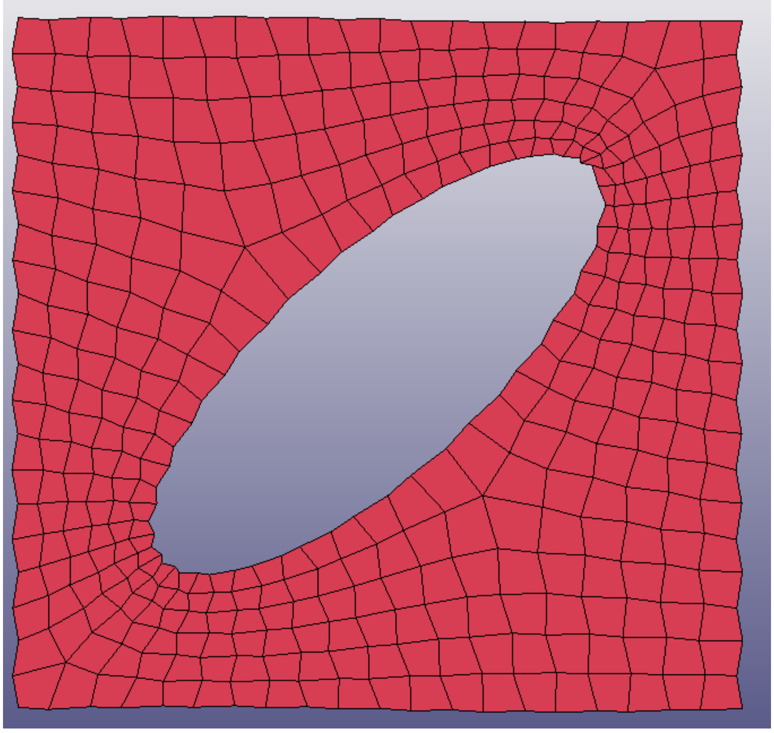

Figure 3.5: Hourglass in viscoelastic RVE (displacements are magnified 5 times)

3.3 Boundary conditions

To model the response of microscale unit cells, or RVEs, four different types of boundary conditions can be considered, namely uniform kinematic, uniform static, mixed and periodic boundary conditions [102, 103]. Uniform kinematic boundary conditions have an intuitive and direct link to the macroscopic strain tensor, but tend to overestimate the stiffness of the RVE. On the other hand, uniform static boundary conditions have a clear link to the macroscopic stress tensor but tend to underestimate the stiffness of the RVE. To balance the two effects of over and underestimating the RVE stiffness, mixed boundary conditions can be used in which some edges have prescribed displacements and the other edges have prescribed tractions.

Periodic boundary conditions avoid boundary effects and provide a better representation of an infinite model. Therefore, these type of boundary conditions are considered to be the best representative of a unit cell's physical properties. Periodic boundary conditions can be imposed to study the mechanical response of any heterogeneous material with relatively small unit cells [103]. In the literature, periodic boundary conditions have been widely used for the homogenisation of heterogeneous materials [31, 60, 103].

3.3.1 Boundary conditions under quasi-static loading

In a relaxation test, periodic boundary conditions (PBC) are established straight forwardly as follows. Firstly, the average horizontal normal strain is realised by imposing a displacement in the x-direction at two corner nodes of the unit cell (C2 and C3 in Figure 3.6 a), while the y translational degrees of freedom at these nodes are free. Also, the x and y translational degrees of freedom of the other two corner nodes (C1 and C4 in Figure 3.6 a) are fixed. Then, multi-point constraints are applied on the remaining edge nodes of the unit cell. In order to achieve this, the difference between x displacements of the right edge nodes (RN1, RN2, RN3, ...) and left edge nodes (LN1, LN2, LN3, ...) are coupled with the horizontal displacements of the corner node that is,

$$u_x^{RNi} - u_x^{LNi} = u_x^{C2} \tag{3.1}$$

In addition, the y displacements of the right edge nodes (RN1, RN2, RN3, ...) are coupled with the y displacements of the left edge nodes (LN1, LN2, LN3, ...),

$$u_y^{RNi} - u_y^{LNi} = u_y^{C2} \tag{3.2}$$

Similarly, x and y displacements of the top edge nodes (TN1, TN2, TN3, ...) are coupled with the x and y displacements of the bottom edge nodes (BN1, BN2, BN3, ...), respectively:

$$u_x^{TNi} - u_x^{BNi} = 0 \tag{3.3}$$

$$u_y^{TNi} - u_y^{BNi} = 0 \tag{3.4}$$

On the other hand, in a creep test, a constant force is imposed on an external node in the x direction, while the difference between x displacements of the right edge nodes (RN1, RN2, RN3, ...) and left edge nodes (LN1, LN2, LN3, ...) are coupled with this external node's displacement in the x direction (Figure 3.6 b),

$$u_x^{RNi} - u_x^{LNi} = u_x^{p} \tag{3.5}$$

The degrees of freedom at the remaining nodes are coupled following a similar

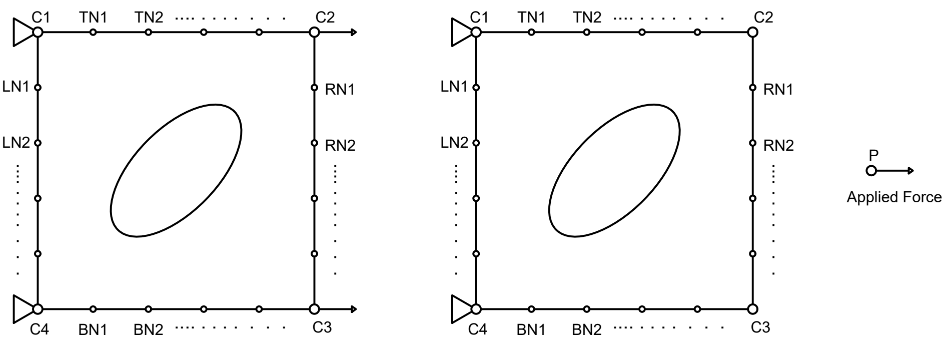

(a) (b)

Figure 3.6: Periodic boundary conditions: (a) Relaxation (b)Creep

approach that is used for the relaxation case (Equations (3.4) and (3.5)).

Periodic boundary conditions are applied in the LS-DYNA software package using the CONSTRAINED_MULTIPLE_GLOBAL command. Constraining of nodes, and preparation of the periodic boundary conditions file was achieved by the automated script as discussed in the following section. The script lines (of tying nodes and writing PBC file) are presented in Appendix A.1. This script allows modeling of RVEs with periodic boundary conditions in time domain and does not restrict material model to be linear elastic. There is an existing tool to obtain effective properties in the literature, this tool is called PBC Abaqus plugin tool [79]; this tool is well developed for elastic RVEs, however it doesn't model RVEs in time domain or with complex material models. The results of elastic RVEs modeled under PBC obtained using this script were verified and checked with the PBC Abaqus plugin tool [79]. For a given linear elastic RVE, the homogenised properties, obtained from this script and the Abaqus plugin tool [79], show a great match with each other.

3.3.2 Boundary conditions under dynamic loading

The periodic boundary conditions implementation methodology in Section 3.3.1 depend on constraining the displacement of two nodes with a prescribed displacement of the other node. This is known as the *stiffness penalty method*, where it can be visualised as a very stiff spring acting between the nodes of constraint [5,45]. Several studies reported that the *stiffness penalty method* reduces the critical time step enormously in conditionally stable time integration schemes [11,18]. Furthermore, it has been reported by [44,53] that the maximum eigenfrequency is significantly increased in solutions obtained while implementing this method.

Another approach of constraining nodes is the *inertia penalty method*, where an *artificial mass* or *moment inertia* can be used as a substitute to the degree of freedom constrains as presented in [43,54]. It can be visualized as a large mass acting on the boundary to nullify motion (such as the inerter in mechanical devices) [5,45]. Using such a method results in a lower critical time step for the analysis.

In addition to the mentioned limitations of both methods, they also tend to "limit the motion of the relevant degree of freedom" [5]. A promising solution, to overcome the limitations of the *stiffness* and *inertia* penalty methods, is the so-called *bipenalty method*, which was initially introduced by Askes *et al.* [5], and further developed by Hetherington *et al.* [44,45]. This method is a combination of both the stiffness and the inertia penalty approaches as illustrated with examples in the following studies [5,44,45]. To implement this approach in LS-DYNA, a user defined element formulation subroutine is required; due to the time and resources limitation this approach has been kept for future work.

To simulate the mechanical behaviour of RVEs in dynamics, the boundary conditions shown in Figure 3.7 were considered to get as close as possible to PBC. The top and bottom boundaries (A and B) were constrained for the vertical movement, and the left edge (C) was constrained for horizontal movement. The dynamic loading ($P(t)$) is considered to be applied horizontally on the free edge. This could be considered as the mixed-boundary conditions option, which was proven to be the second-best option in statics [102, 103].

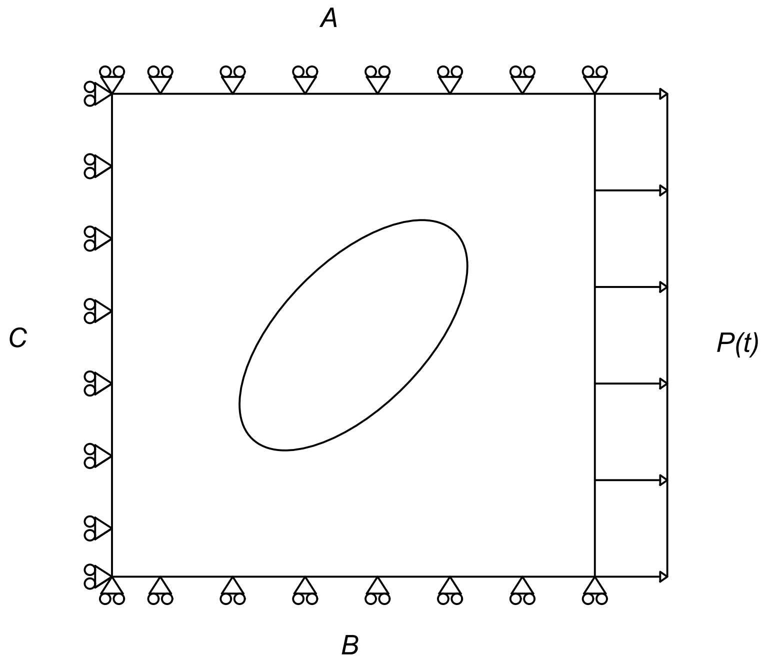

Figure 3.7: Proposed boundary conditions for dynamic excitation

3.4 Automated script

Once an RVE has been selected, the first step of any numerical homogenisation scheme is to simulate the mechanical behaviour of an RVE or unit cell numerically (using FEM in this research). Therefore, an automated script has been developed to perform unit cell analyses, since the nature of this research requires evaluating and optimizing different unit cells with different microstructural configurations, loading conditions and material models. As shown in Figure 3.8, three software packages, namely Abaqus, LS-DYNA and LS-prepost, have been employed to create the unit cell, perform the analysis and retrieve the results.

A Matlab code has been developed such that it organizes files and transfers them from one software package to another. The code starts with 3 for loops varying inclusion's aspect ratio, area and inclination angle respectively. In the first step, Matlab generates a python script as a first output file describing the geometry of the unit cell, and inclusion properties. The python script will run through Abaqus (step 2) to generate a mesh and elements description file (step 3). This file will be called by the Matlab code and transform the formatting into LS-DYNA format producing mesh.k and elements.k file (steps 4 and 5). The next step is generating an LS-DYNA input file by Matlab (step 6) and calling LS-DYNA to run the model and produce the results (steps 7 and 8). Retrieving the results is performed by LS-prespost, therefore the Matlab code produces a script that specifies the required results to be extracted from LS-prepost (step 9). LS-prepost will generate the specified results file from LS-DYNA output (steps 10 and 11). The final steps (12 and 13) are to record the results in a text file containing all iterations. The output file produced by Matlab is a text file that presents the configuration variables (aspect ratio, inclusion area and inclusion orientation) and the results (homogenised material properties) in one file to be further analysed. This code will be used to run series of different RVEs configurations and material properties. Examples of an Abaqus python script and LS-DYNA input file are given in Sections (A.2) and (A.3) of the Appendix respectively.

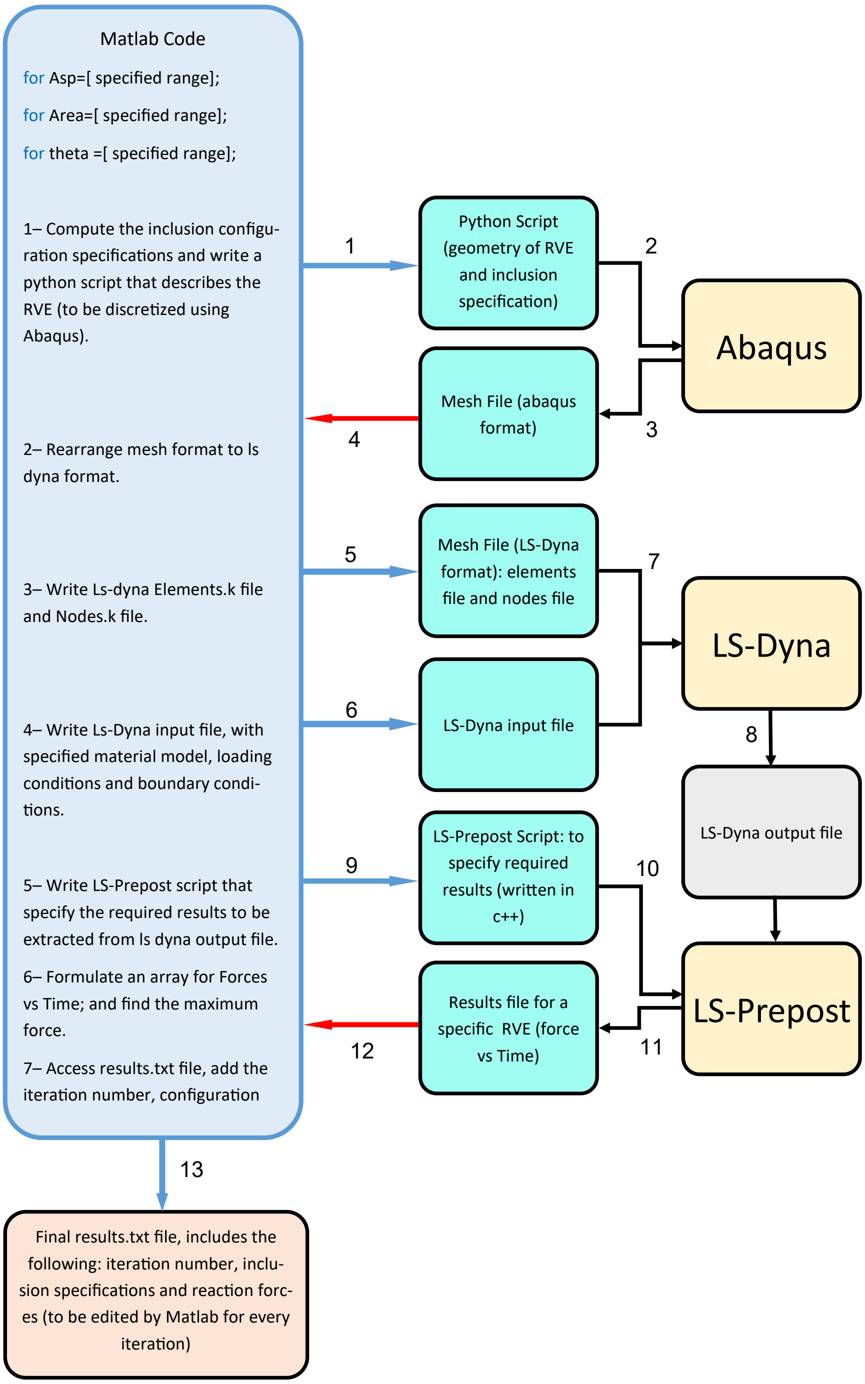
Matlab Code
for Asp=[specified range];
for Area=[specified range];
for theta =[specified range];
1– Compute the inclusion configuration specifications and write a python script that describes the RVE (to be discretized using Abaqus).
2– Rearrange mesh format to ls dyna format.
3– Write Ls-dyna Elements.k file and Nodes.k file.
4– Write Ls-Dyna input file, with specified material model, loading conditions and boundary conditions.
5– Write LS-Prepost script that specify the required results to be extracted from ls dyna output file.
6– Formulate an array for Forces vs Time; and find the maximum force.
7– Access results.txt file, add the iteration number, configuration
1
Python Script (geometry of RVE and inclusion specification)
2
Abaqus
3
Mesh File (abaqus format)
4
5
Mesh File (LS-Dyna format): elements file and nodes file
7
LS-Dyna
6
LS-Dyna input file
8
LS-Dyna output file
9
LS-Prepost Script: to specify required results (written in c++)
10
LS-Prepost
Results file for a specific RVE (force vs Time)
11
12
13
Final results.txt file, includes the following: iteration number, inclusion specifications and reaction forces (to be edited by Matlab for every iteration)

Figure 3.8: Flowchart for the analysis code

3.5 Parallel computing

The nature of this research requires analysing a very large amount of RVEs to obtain sufficient knowledge about macro structural behaviour. Therefore, implementation of the concept of parallel computing would be beneficial to lower the analysis time and to increase the efficiency of the code by allowing many RVEs to be analysed simultaneously (given in Figure 3.8). Parallel computing can be implemented with different logic methodologies, such as shared and distributed memory algorithms. For further details about parallel computing methodologies, implementations and examples, the reader is referred to [35, 82]. In this work, the concept of shared memory was employed such that each iteration, for a given inclusion's geometry properties, is performed on a different core while using a shared memory of the system (Figure 3.9). Such approach can be applied in MATLAB using the batch function, while specifying a command file for each specific RVE, as shown in Appendix A.4.

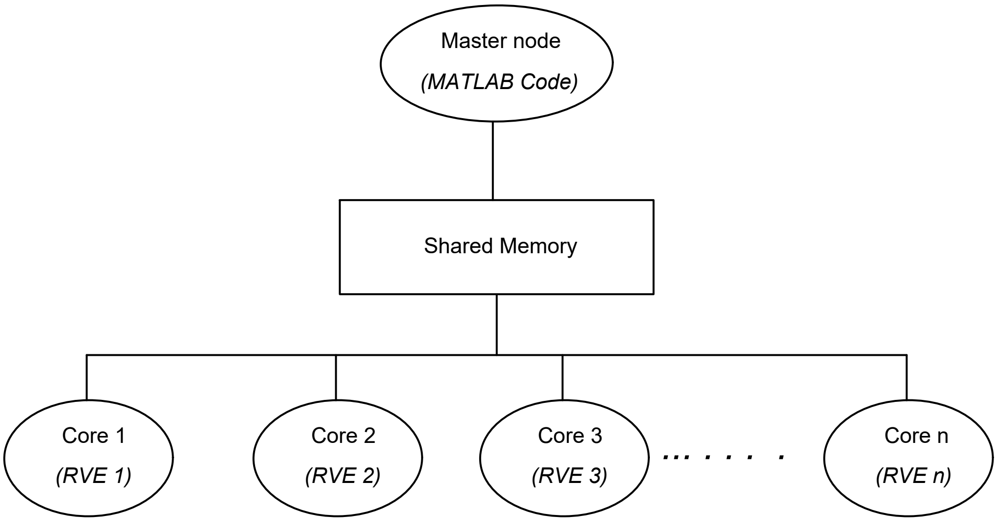

Figure 3.9: Parallel computing architecture

Chapter 4

Quasi-static loading conditions

4.1 Introduction

Under quasi-static loading conditions, two main aspects influence the homogenised properties of an RVE. These aspects are the micro structural configuration and the constitutive material models at micro level. In a simple RVE, such as the one mentioned in Chapter 3 (Figure 3.1), the micro structural configuration can be assessed by the inclusion geometrical properties such as the elliptical inclusion's aspect ratio, area and inclination angle. Meanwhile, the constitutive material models at micro level can be assessed by matrix and inclusion material properties. To investigate the inclusion's geometrical effect on the response of RVE, the codes developed in Chapter 3 were employed to run series of parametric studies. In these simulations, the RVE dimensions are 1 mm × 1 mm, the inclusion's aspect ratio AsR varies between 1 and 3 with 0.5 increments, the area A_r ranges from 0.1 mm^2 to 0.175 mm^2 with 0.025 mm^2 increments, and the inclination angle θ varies between 0° to 180° with 10° increments. As the area of the RVE is 1 mm^2, the value of the volume fraction of an RVE is always equal to the numeric value of the inclusion's area. The loading conditions in this chapter are quasi-static, all homogenised results in this chapter were obtained while implementing periodic boundary conditions along the RVE edges. Elastic unit cells are studied under constant prescribed displacement loading conditions. On the other hand, unit cells that exhibit viscoelastic response are tested under creep and relaxation conditions; macro material properties extracted from creep tests coincide with the ones extracted from relaxation tests as shown in sections 4.3 and 4.4.

The studied properties are the homogenised elastic modulus for a linear elastic RVE (section 4.2); while the homogenised initial elastic modulus and homogenised dynamic viscosity were studied for viscoelastic RVEs (section 4.3). In the case of a composite unit cell, of elastic matrix and viscoelastic inclusion, the homogenised initial and final elastic moduli and the homogenised dynamic viscosity were investigated (section 4.4). This chapter has been summarised and published in an open source journal paper [1].

4.2 Linear elastic RVE with void inclusion

First we consider a linear elastic unit cell with a single elliptical void (Figure 3.1) to determine the homogenised elastic modulus $\bar{E}$. Three different elastic moduli are assumed for the linear elastic matrix: $E = 105$ GPa, 210 GPa and 420 GPa. Poisson's ratio v of the matrix material is set to null to avoid boundary effects; furthermore, setting the Poisson's ratio to null allow us to study the emergent Poisson's effect due to the inclusion. All the numerical simulations, including mesh convergence and boundary conditions, were complemented with correspondence to the methodology mentioned in Chapter 3.

The variation of the homogenised elastic modulus $\bar{E}$ vs inclination angle θ with respect to different aspect ratios is shown in Figure 4.1. This figure shows the results of RVEs with A_r=0.175 mm^2 and $E = 210$ GPa . Indeed, all simulations with different inclusion areas and elastic moduli followed the same pattern. A simple method to verify the results is the so called rule of mixtures [16], where the homogenised elastic modulus has to be between two bonds, upper bond[1] and lower bond[2] as described in the footnote. In this case the upper bound is 173 GPa and the lower bound is 0 GPa; All results in Figure 4.1 fall between these two bonds.

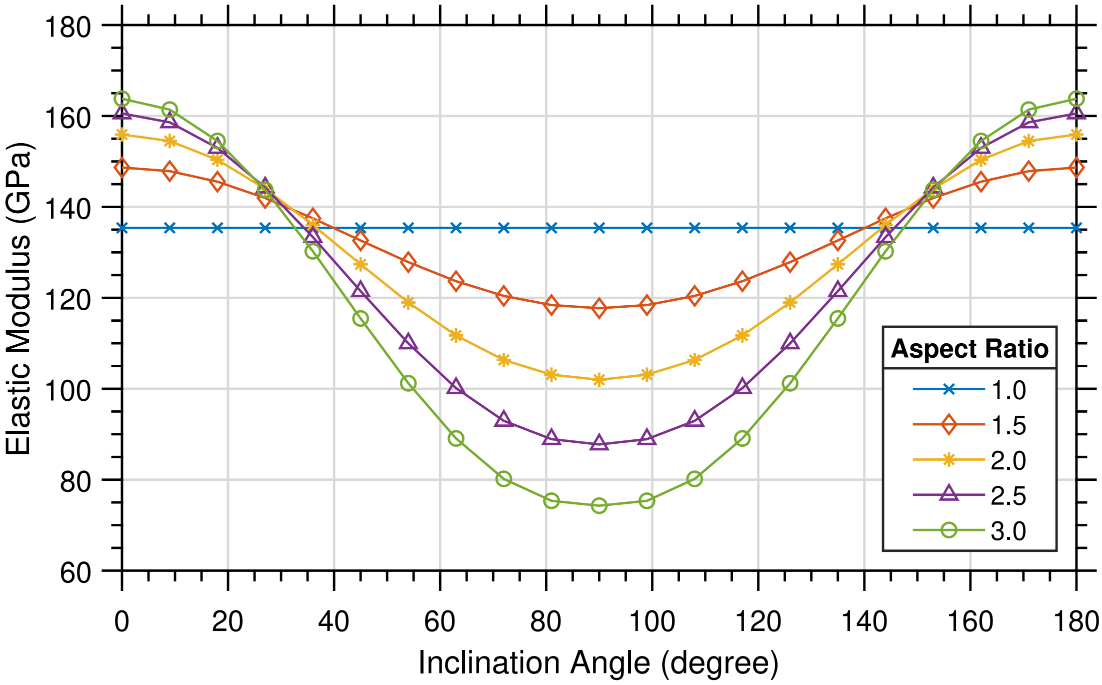

Figure 4.1: Variation of homogenised elastic modulus $\bar{E}$ with inclusion's inclination angle θ for different aspect ratios and constant inclusion's area A_r=0.175 mm^2

Although the material model of the matrix, at micro level, was an isotropic linear elastic, it is noted that the macroscopic constitutive model, homogenised material properties, exhibits an anisotropic linear elastic behaviour [1]. Furthermore Figure 4.2 shows the variation of homogenised Poisson's ratio $\bar{\upsilon}$ with inclination angel. The homogenised Poisson's ratio has been computed as described in section 2.6.1 (Equation 2.17). It is noted that inclusions induce some Poisson's effect although the material model has null Poisson's ratio.

---

[1] Rule of mixtures upper bound: $\bar{E} = V_f E_{inc} + (1 - V_f) E_M$ where $\bar{E}$ is the homogenised elastic modulus, V_f is the volume fraction of the inclusion and (E_{inc}, E_M) are the inclusion and matrix moduli.

[2] Rule of mixtures lower bound: $\bar{E} = \frac{E_{inc} E_M}{V_f E_M + (1-V_f) E_{inc}}$

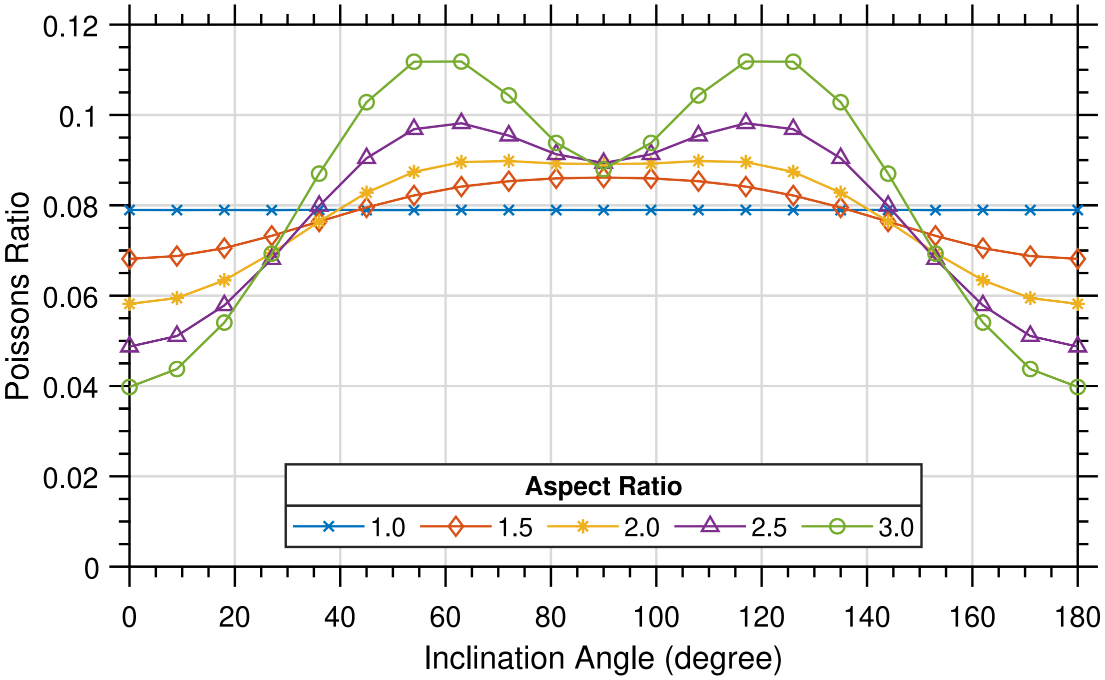

Figure 4.2: Variation of homogenised Poisson's ratio $\bar{v}$ with inclusion's inclination angle θ for different aspect ratios and constant inclusion's area A_r=0.175 mm^2

A closed-form expression (Equation (4.1)) can be obtained through fitting a trigonometric curve to represent the variation of homogenised elastic modulus $\bar{E}$ with inclination angle θ for the RVE. That is,

$$\bar{E}(\theta) = E\left(x_0\cos(2\theta) + \sum_{i=1}^{n} x_i \cos\left(\frac{\pi - 2\theta}{2^i}\right) + C\right) \tag{4.1}$$

where x_0, x_i, and C are constants representing configurational parameters, which depend on the microstructure of the unit cell. In this equation, a summation of higher-order trigonometric functions can be used to increase the degree of accuracy of the results. In the fundamental curve fit (i.e. neglecting the summation)

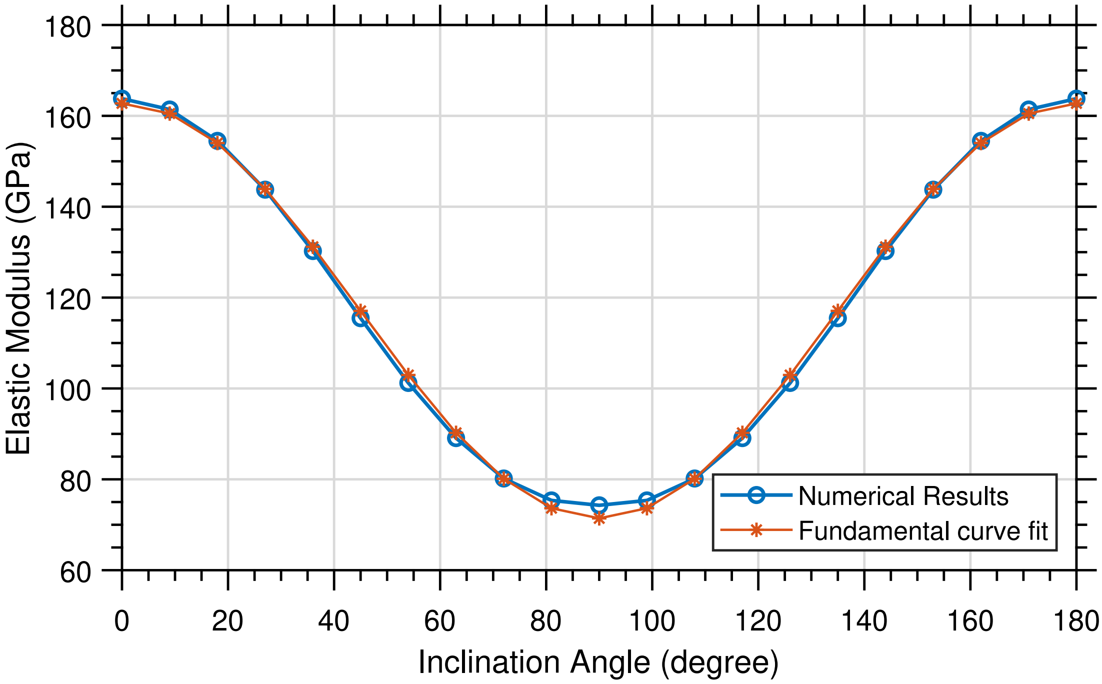

Figure 4.3: Comparison between the FE homogenised elastic modulus $\bar{E}$ and its prediction along different inclination angles θ (A_r=0.175 mm^2 and AsR=3)

approximation of Equation (4.1), C is inversely proportional with both the inclusion area A_r and aspect ratio AsR, however x_0 is directly proportional with the inclusion area A_r and aspect ratio AsR. The values of x_0 and C for different combinations of aspect ratios and inclusion area can be found in Appendix B (Tables B.1 and B.2).

The fundamental curve fit prediction for the variation of homogenised elastic modulus $\bar{E}$ with inclination angle θ for the unit cell made of linear elastic material with single elliptical void is presented in Figure 4.3 together with the FE results. As one can observe from this figure, the fundamental curve fit prediction yields accurate results. The higher order terms in Equation (4.1) very marginally improve the prediction [1].

4.3 Viscoelastic RVE with void inclusion

Secondly, a series of FE analyses is conducted on a linear viscoelastic 2D unit cell with a single elliptical void. MAT_VISCOELASTIC material model of LS-DYNA, which is based on Maxwell's standard solid model of viscoelasticity, has been utilized to model a linear isotropic viscoelastic medium in LS-DYNA. The input parameters for this material model are: initial shear modulus G_0, final shear modulus G_∞, decay constant β and bulk modulus k. In this section, an RVE with elastic modulus of E=210 GPa, dynamic viscosity of $\eta = 190$ GN·s/m^2 and Poisson's ratio of $\upsilon = 0$ has been used to conduct this study. To input these material parameters in LS-DYNA the initial shear modulus can be written as $G_0 = \frac{E}{2(1+\upsilon)}$. Meanwhile, the final shear modulus G_∞=0 since Maxwell viscoelastic material doesn't accommodate a finite long term stiffness, decay constant $\beta = \frac{E}{\eta}$ and bulk modulus $k = \frac{E}{3(1-2\upsilon)}$ by definition. The material parameters used in the FE analysis are shown in Table 4.1.

Table 4.1: Linear viscoelastic material model parameters

Behaviour	LS-DYNA Model	G_0 (GPa)	G_∞ (GPa)	k (GPa)	β(1/s)
Viscoelastic	MAT_VISCOELASTIC	105.00	0.00	70.00	1.10

In the numerical simulations, two different loading conditions, namely creep and stress relaxation (both represented with the Maxwell model), are considered for the 2D unit cell with a single elliptical void (Figure 3.1). In these simulations, the variations of the homogenised elastic modulus $\bar{E}$ and homogenised dynamic viscosity $\bar{\eta}$ with inclination angle θ are evaluated. Evaluation of homogenised elastic modulus and dynamic viscosity has been carried out as per the criteria mentioned in chapter 2. The details of the numerical models such as mesh convergence, time steps and element formulation were conducted with correspondence to the methodology mentioned in Chapter 3. The time of the analysis has been

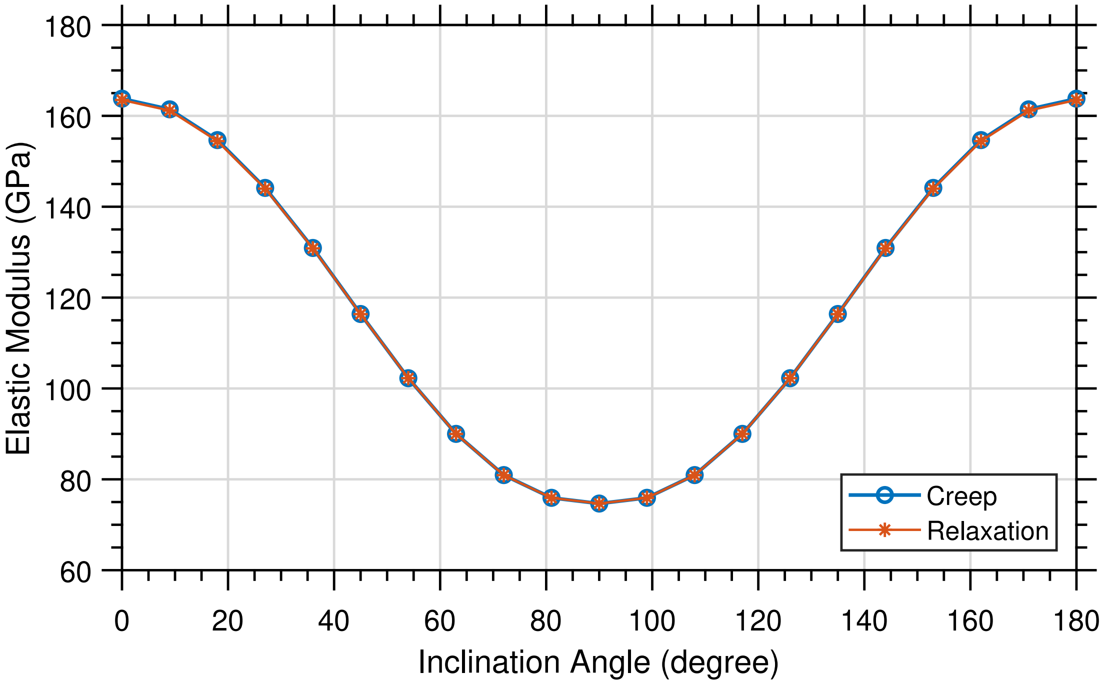

Figure 4.4: Variation of homogenised elastic modulus $\bar{E}$ with inclination angle θ using creep and relaxation tests (A_r=0.175 mm^2 and AsR=3)

chosen to be sufficient to visualise the full stress relaxation behaviour.

As one can observe from Figures 4.4 and 4.5, the FE models for viscoelastic unit cells with creep and stress relaxation (using inclusion area A_r=0.175 mm^2 and aspect ratio AsR=3) show good correlation for the variation of homogenised elastic modulus $\bar{E}$ and dynamic viscosity $\bar{\eta}$ with inclination angle θ; the same variation pattern is observed for all other inclusion area and aspect ratios. As expected the macro material model was Maxwell linear viscoelastic; however it exhibit an anisotropic behaviour [1].

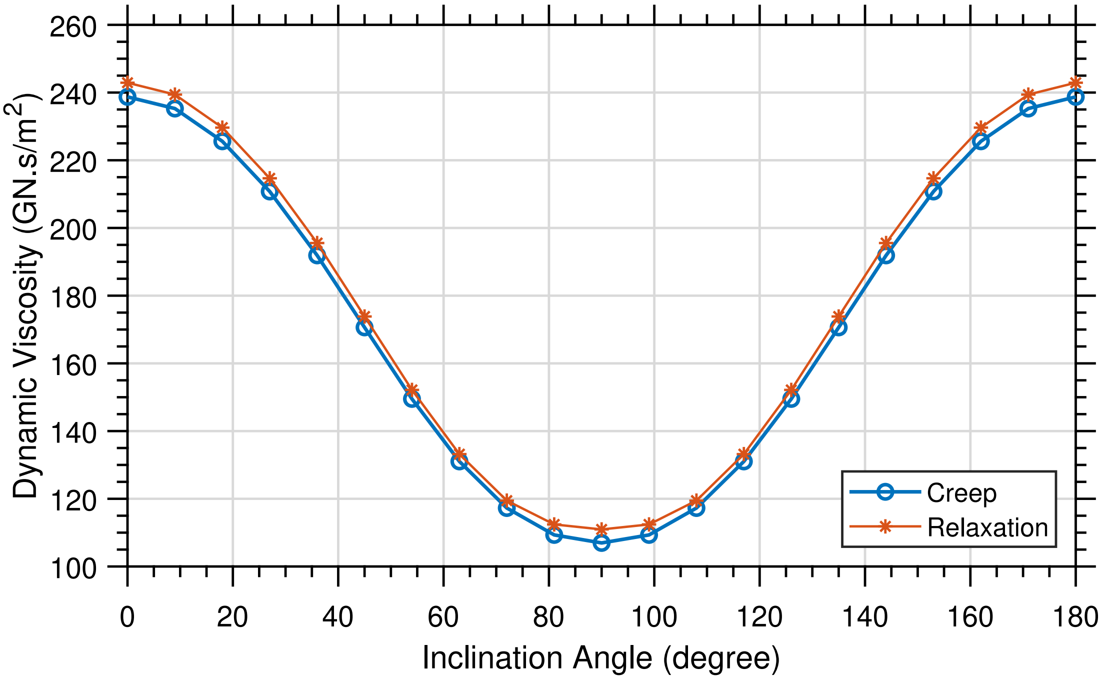

Figure 4.5: Variation of homogenised dynamic viscosity $\bar{\eta}$ with inclination angle θ using creep and relaxation tests (A_r=0.175 mm^2 and AsR=3)

Similar to the linear elastic case, simple formulas are derived through curve fitting to represent the variation of homogenised elastic modulus $\bar{E}$ and homogenised dynamic viscosity $\bar{\eta}$ with inclination angle θ for the viscoelastic 2D unit cell with a single elliptical void:

$$\bar{E}(\theta) = E\left(x_0\cos(2\theta) + \sum_{i=1}^{n} x_i \cos\left(\frac{\pi - 2\theta}{2^i}\right) + C\right) \tag{4.2}$$

$$\bar{\eta}(\theta) = \eta\left(x_0\cos(2\theta) + \sum_{i=1}^{n} x_i \cos\left(\frac{\pi - 2\theta}{2^i}\right) + C\right) \tag{4.3}$$

The homogenised elastic modulus $\bar{E}$ is related to the micro elastic modulus E (Equation (4.2)). It is noted that the constants C, x_0 and x_i in this equation are the same for a linear elastic RVE, discussed in section 4.2. However, Equation (4.3) relates the homogenised dynamic viscosity $\bar{\eta}$ with the microscale dynamic viscosity η, whereby C, x_0 and x_i in this equation are quite different from the elastic modulus equation and the fundamental fit constants (C and x_0) are presented in Appendix B (Tables B.3 and B.4).

4.4 Composite RVE (linear elastic matrix with viscoelastic inclusion)

Next, a composite unit cell consisting of a linear elastic matrix (Material 1) with a Maxwell viscoelastic inclusion (Material 2) is created as shown in Figure 4.6.

A parametric study is performed by varying the material properties of the inclusion, while the material properties of the matrix ($E = 210$ GPa and $\upsilon = 0$) are kept constant as shown in Table 4.2. Six different composite unit cells are considered. In composite unit cells 1 to 3, the elastic modulus of the viscoelastic inclusion (E_{inc}) is varied, while keeping the dynamic viscosity η constant. On the other hand, the composite unit cells 4 to 6 the elastic modulus E_{inc} and the dynamic viscosity η of the viscoelastic inclusion are varied but keeping their ratio β constant. The details of the numerical models such as mesh convergence, time steps and element formulation were conducted with correspondence to the methodology mentioned in Chapter 3. The time of the analysis has been chosen to be sufficient to visualise the full stress relaxation behaviour. Similar to the parametric studies presented in the previous sections, in these simulations, the aspect ratio AsR varies between 1 and 3 with 0.5 increments, the area A_r ranges from 0.1 mm^2 to 0.175 mm^2 with 0.025 mm^2 increments, and inclination angle θ varies between 0° to 180° with 10° increments.

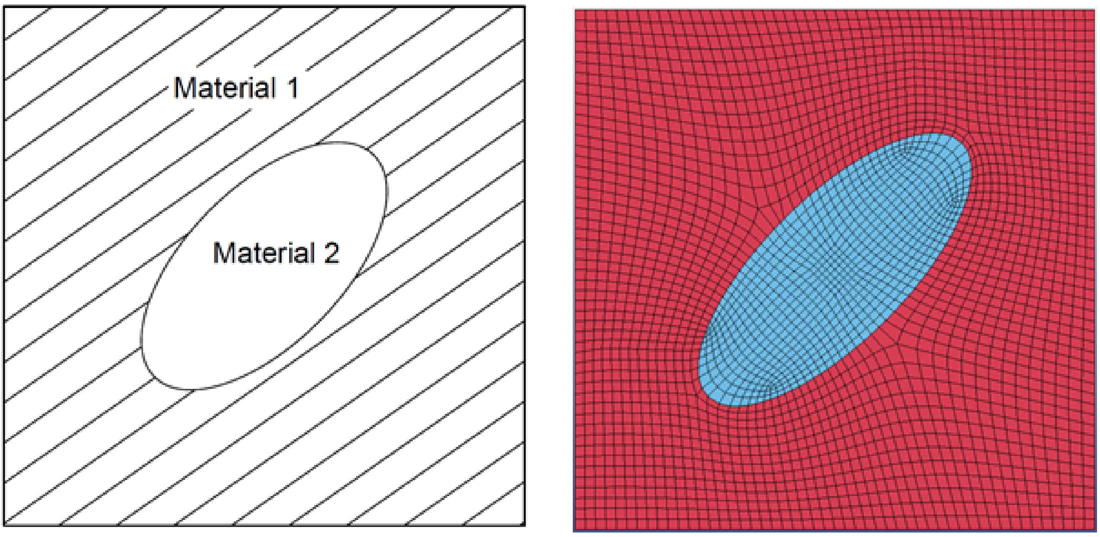

Figure 4.6: Composite unit cell with viscoelastic inclusion

Table 4.2: Material Properties of the composite unit cells

Composite No.	Material	E (GPa)	E_∞ (GPa)	η (GN·s/m^2)	β (1/s)
Composite unit cell 1	Elastic	E=210.00	-	-	-
	Maxwell Viscoelastic	E_{inc}=105.00	0.00	300.00	0.35
Composite unit cell 2	Elastic	E=210.00	-	-	-
	Maxwell Viscoelastic	E_{inc}=210.00	0.00	300.00	0.70
Composite unit cell 3	Elastic	E=210.00	-	-	-
	Maxwell Viscoelastic	E_{inc}=420.00	0.00	300.00	1.40
Composite unit cell 4	Elastic	E=210.00	-	-	-
	Maxwell Viscoelastic	E_{inc}=105.00	0.00	95.46	1.10
Composite unit cell 5	Elastic	E=210.00	-	-	-
	Maxwell Viscoelastic	E_{inc}=210.00	0.00	190.91	1.10
Composite unit cell 6	Elastic	E=210.00	-	-	-
	Maxwell Viscoelastic	E_{inc}=420.00	0.00	381.81	1.10

For the composite unit cells given in Table 4.2, the homogenised properties consist of elastic and viscoelastic parts. Therefore, new parameters appear in the homogenised response, Macro level, that do not exist in the linear elastic nor viscoelastic unit cells with a single elliptical void. For instance, in a stress relaxation test (Figure 4.7), the infinite elastic modulus $\bar{E}_\infty$ is not null for the homogenised solution (Figure 4.7-c) compared with null $\bar{E}_\infty$ in the inclusion (Figure 4.7-b). Furthermore, the decay constant β has a different definition on the macro level in comparison to its micro level properties. Indeed, the homogenised dynamic viscosity, at macro level, change with the inclination angle of the inclusion while the dynamic viscosity of the inclusion is constant at any given area and aspect ratio. Similarly, in a creep test (Figure 4.8), an exponential growth of the strain in time is observed, compared to a linear growth in the Maxwell viscoelastic inclusion and constant strain in the linear elastic matrix at the micro level. Indeed, the macro constitutive model exhibits anisotropic behaviour due to the configuration of the inclusion [1].

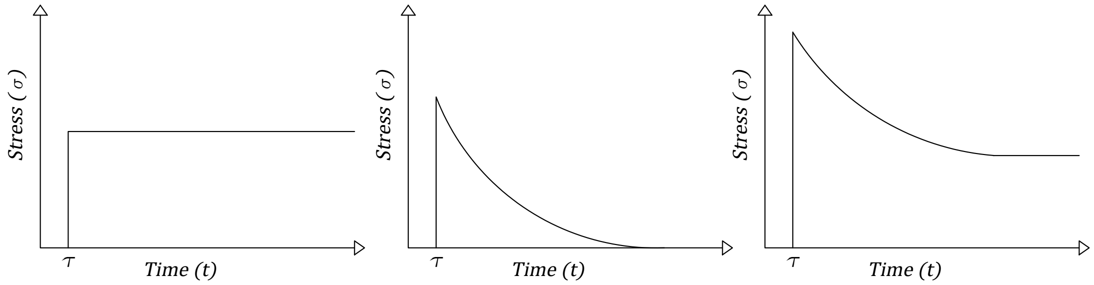

(a) Matrix (linear elastic) (b) Inclusion (Maxwell viscoelastic) (c) Homogenised Macro behaviour

Figure 4.7: Relaxation: Micro behaviours of matrix (a) and inclusion (b), Macro behaviour of a composite unit cell (c)

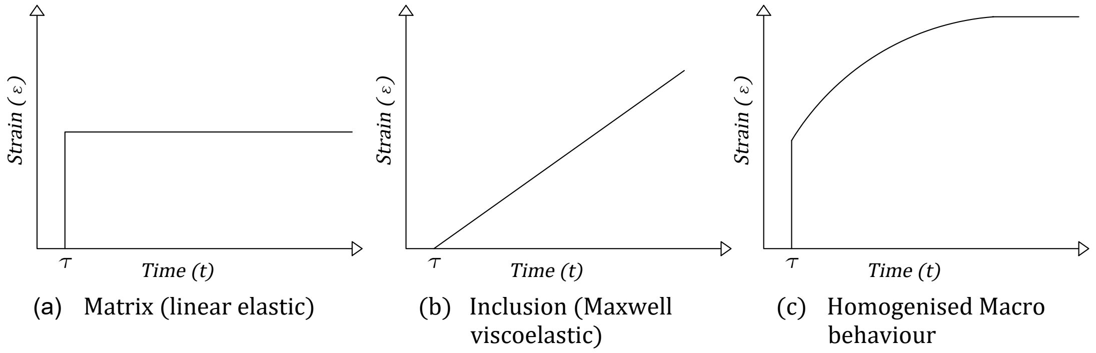

(a) Matrix (linear elastic) (b) Inclusion (Maxwell viscoelastic) (c) Homogenised Macro behaviour

Figure 4.8: Creep: Micro behaviours of matrix (a) and inclusion (b), Macro behaviour of a composite unit cell (c)

Figures 4.9 to 4.12 show the variation of the homogenised initial elastic modulus $\bar{E}_0$, the homogenised infinite elastic modulus $\bar{E}_\infty$, and the homogenised dynamic viscosity $\bar{\eta}$ with the inclination angle θ for the composite unit cells given in Table 2. FE analysis results show that the variation of the initial elastic modulus $\bar{E}_0$ with the inclination angle θ for composite unit cells 1 and 4, composite unit cells 2 and 5, and composite unit cells 3 and 6 are identical. On the other hand, the variation of the infinite elastic modulus $\bar{E}_\infty$ with the inclination angle θ is identical for the all composite unit cells, since $\bar{E}_\infty$ depends only on the elastic matrix properties. The variation of the homogenised dynamic viscosity $\bar{\eta}$ with the inclination angle θ show differences for composite unit cells 4 to 6. The dynamic viscosity is largest for a 90° inclination angle, in which case the composite behaviour resembles most closely that of a series connection between elastic matrix and viscoelastic inclusion [1].

To verify the suitability of this test to simulate both creep and stress relaxation, independent studies have been conducted. The figures below show the homogenised material model parameters ($\bar{E}_0$, $\bar{E}_\infty$ and $\bar{\eta}$) from the two tests. These figures are extracted from combination 5 (Table 4.2) using an aspect ratio of 3 and an inclusion area of 0.175 mm^2 – but note that the same pattern was observed in all other combinations of material and geometrical properties.

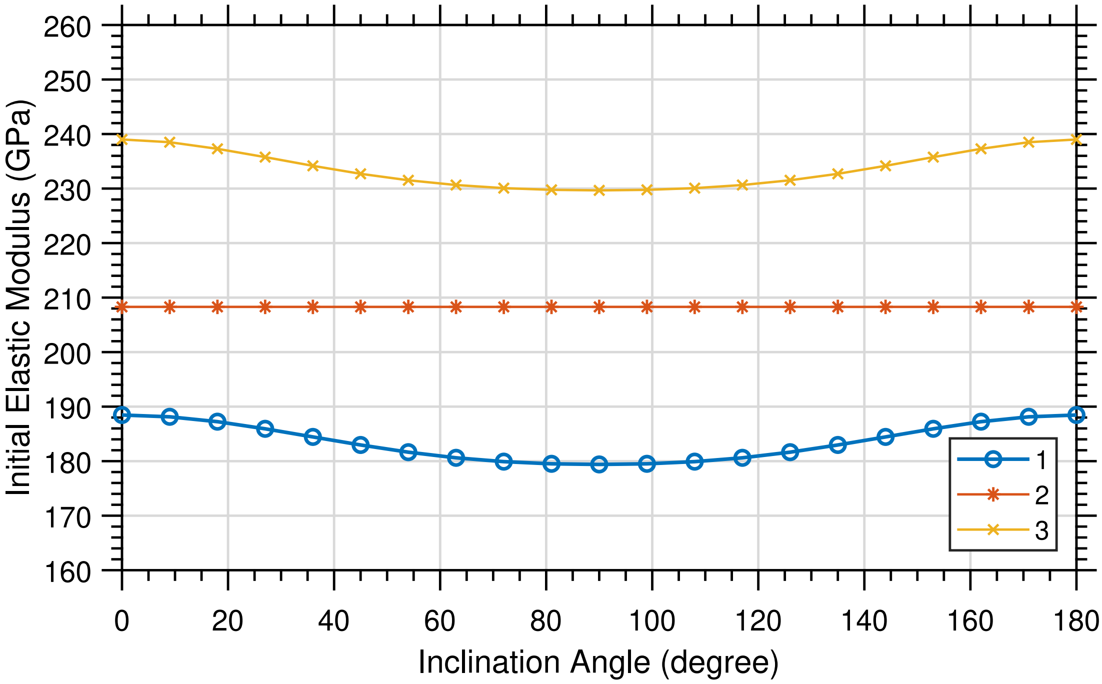

Figure 4.9: Variation of homogenised initial elastic modulus $\bar{E}_0$ with the inclination angle θ for the composite unit cells 1 to 3 given in Table 4.2 (A_r=0.175 mm^2)

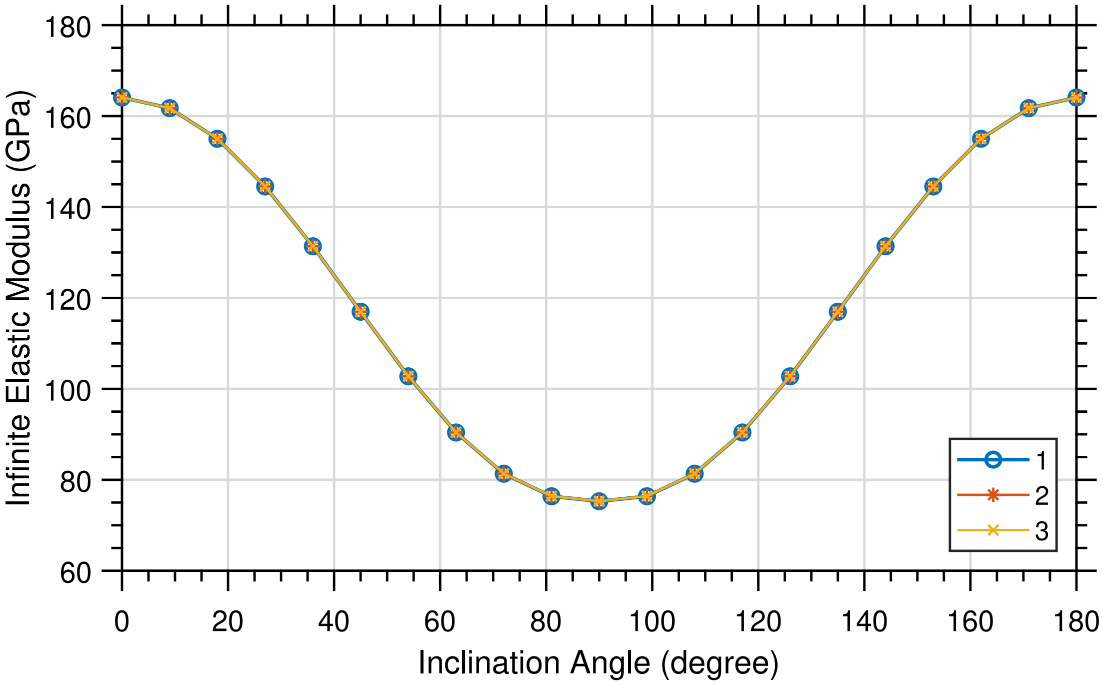

Figure 4.10: Variation of homogenised infinite elastic modulus $\bar{E}_\infty$ with the inclination angle θ for composite unit cells 1 to 3 given in Table 4.2 (A_r=0.175 mm^2)

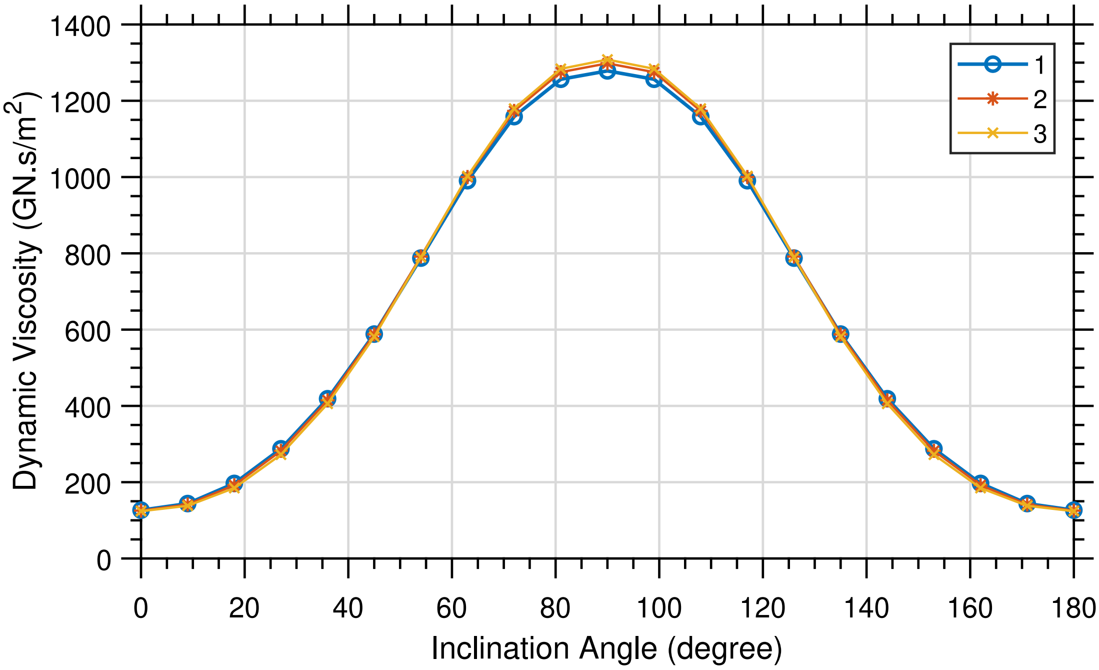

Figure 4.11: Variation of homogenised dynamic viscosity $\bar{\eta}$ with the inclination angle θ for composite unit cells 1 to 3 given in Table 4.2 (A_r=0.175 mm^2)

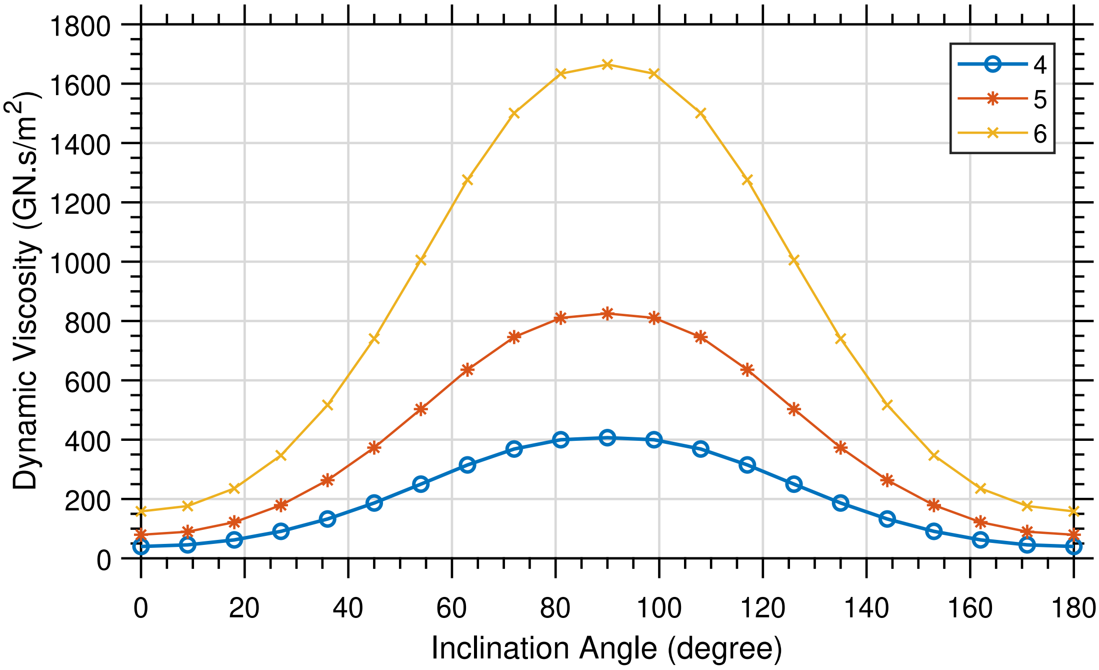

Figure 4.12: Variation of homogenised dynamic viscosity $\bar{\eta}$ with the inclination angle θ for composite unit cells 4 to 6 given in Table 4.2 (A_r=0.175 mm^2)

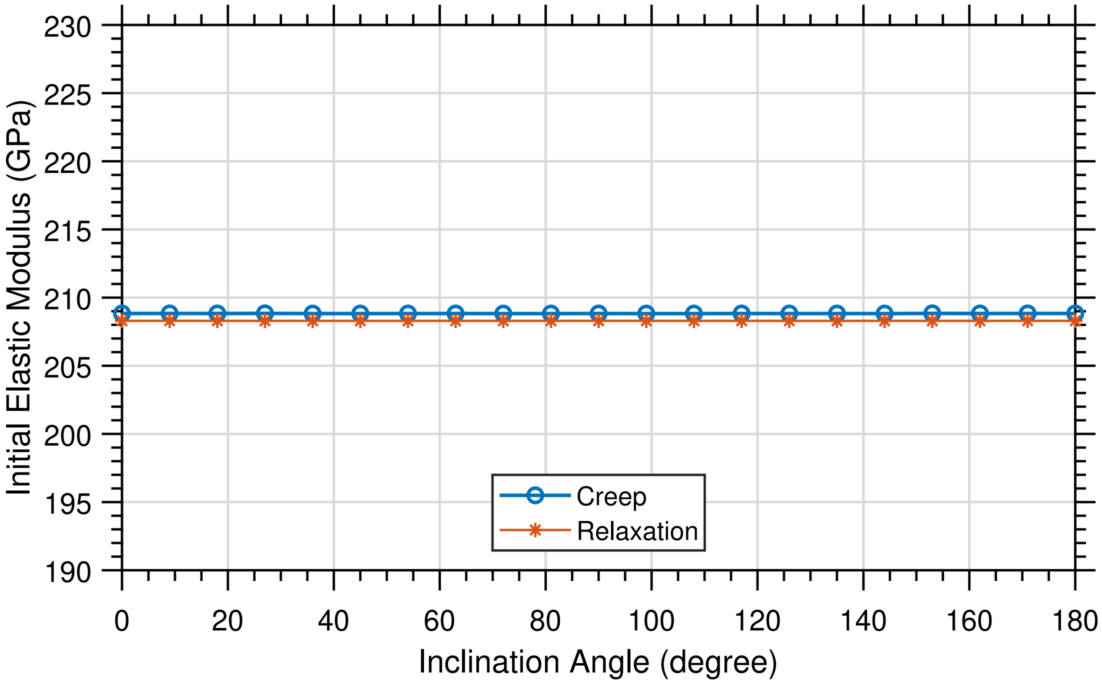

Figure 4.13: Variation of homogenised initial elastic modulus $\bar{E}_0$ with the inclination angle θ for composite unit cell 5 given in Table 4.2 (A_r=0.175 mm^2 and AsR=3)

Simple formulas are derived through curve fitting to represent the variation of homogenised infinite elastic modulus $\bar{E}_\infty$ and homogenised dynamic viscosity $\bar{\eta}$ with inclination angle θ for the elastic 2D unit cell with a single viscoelastic inclusion (Figure 4.6):

$$\bar{E}_\infty(\theta) = E\left(x_0\cos(2\theta) + \sum_{i=1}^{n} x_i \cos\left(\frac{\pi - 2\theta}{2^i}\right) + C\right) \tag{4.4}$$

$$\bar{\eta}(\theta) = \eta\left(x_0\cos(2\theta) + \sum_{i=1}^{n} x_i \cos\left(\frac{\pi - 2\theta}{2^i}\right) + C\right) \tag{4.5}$$

The homogenised infinite elastic modulus $\bar{E}_\infty$ depends on the elastic modulus of the matrix E. Again, the constants C, x_0 and x_i in this equation are same for a linear elastic (Section 4.2) and Maxwell viscoelastic (Section 4.3) RVEs (Tables B.1 and B.2). However, Equation (4.5) relates the macro dynamic viscosity $\bar{\eta}$ with

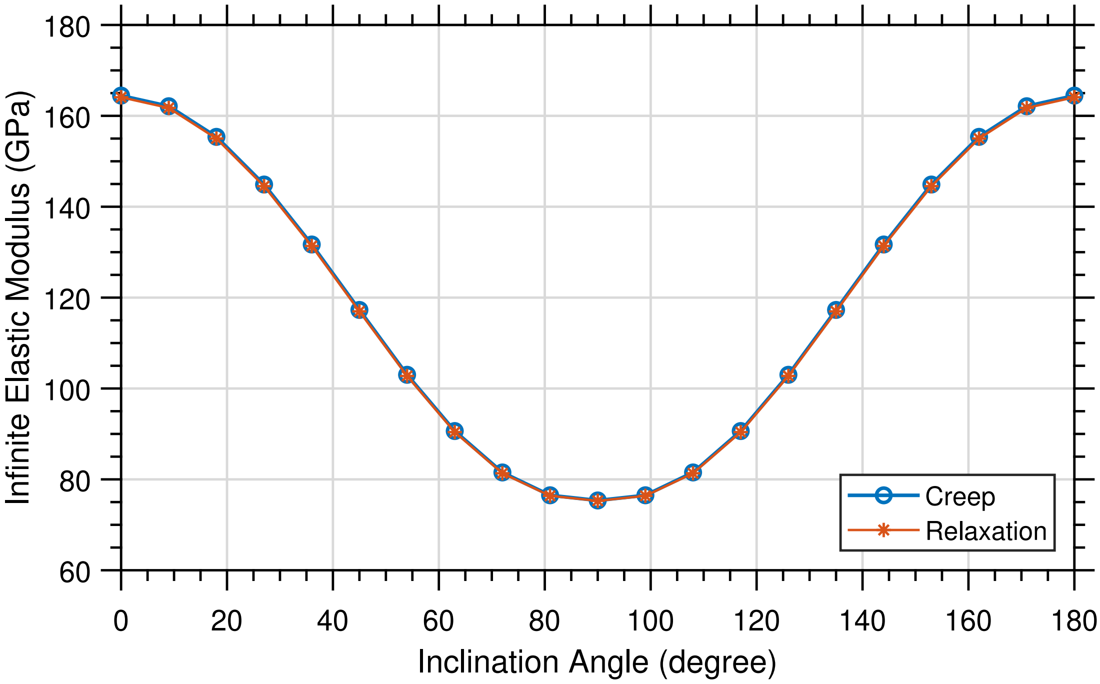

Figure 4.14: Variation of homogenised infinite elastic modulus $\bar{E}_\infty$ with the inclination angle θ for composite unit cell 5 given in Table 4.2 (A_r=0.175 mm^2 and AsR=3)

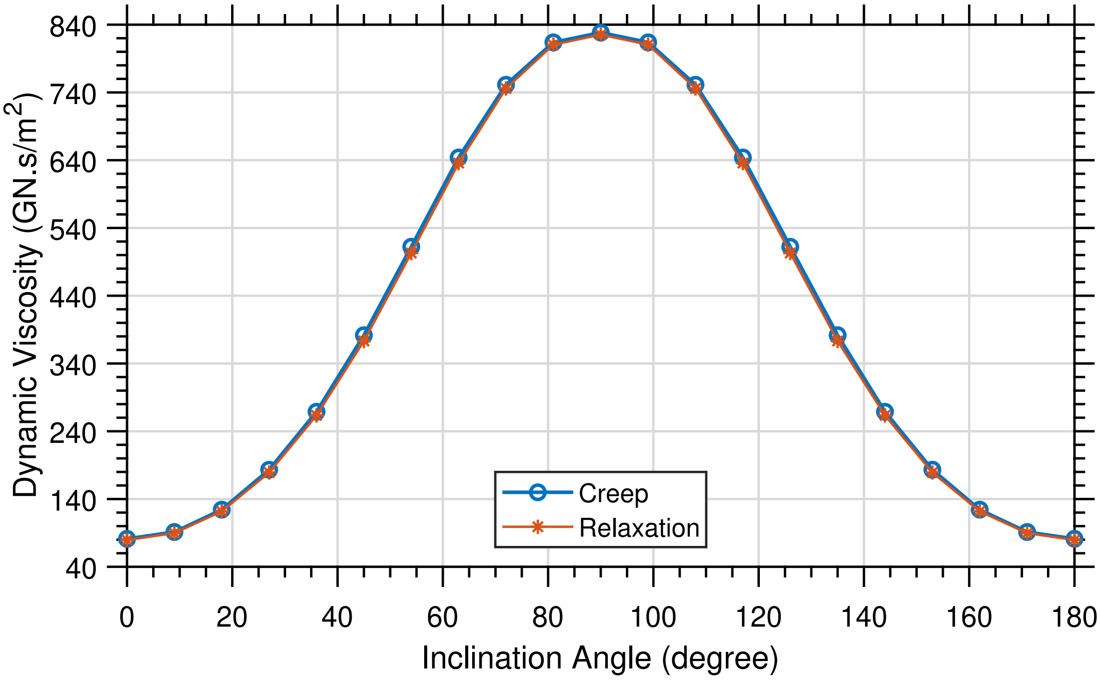

Figure 4.15: Variation of homogenised dynamic viscosity $\bar{\eta}$ with the inclination angle θ for composite unit cell 5 given in Table 4.2 (A_r=0.175 mm^2 and AsR=3)

the micro dynamic viscosity η; C, x_0 and x_i in this equation are quite different from of the dynamic viscosity fit parameters , Section 4.3, and presented in tables B.5 and B.6 of Appendix B.

4.5 Summary, evaluation and applicability

This chapter study the homogenised material properties of simple elastic and viscoelastic unit cells. The aim of this chapter to test the developed methodology in quasi static loading conditions and understand the effect of micro structure on macro mechanical properties. Thus, a priority was given to test more micro structures, inclusion's properties, while fixing material parameters. However, the same concept apply to other materials with the same constitutive models. More results for generalised materials are available in Appendix C. Where section C.1 shows normalised results of elastic RVEs, where the elastic modulus was 1 GPa for aspect ratio 1. Figure C.1 shows the results of all other aspect ratios; furthermore, Figure C.2 shows the prediction of elastic modulus using Equation (4.1) where it shows very similar accuracy to the analysis shown in this chapter. Similarly, section C.2 shows normalised results for viscoelastic RVEs where elastic modulus of the matrix was taken as 1 GPa and dynamic viscosity of 1 GN·s/m^2. Coincidence of results between creep and relaxation was observed for homogenised elastic modulus (Figure C.3) and homogenised dynamic viscosity (Figure C.4). Finally section C.3 shows results for composite RVEs, where Figures C.5 and C.6 show the coincidence of homogenised properties between creep and relaxation tests. The same pattern was observed comparing to the analysis presented in this chapter. A conclusion can be drawn that this approach is applicable for any linear elastic or Maxwell linear viscoelastic unit cell with single inclusion.

Chapter 5

Dynamic Loading conditions

5.1 Introduction

In this chapter, the homogenised behaviour of unit cells under dynamic loading conditions is studied. First, the principles of dynamics for the three studied unit cell cases are reviewed and analytical solutions for the dynamic equations of motions are formulated (Section 5.2). Second, the loading conditions are discussed and a link between analytical solution and loading cases have been developed (Section 5.3). The numerical homogenisation scheme mentioned earlier in Section 2.5 has been employed to obtain the homogenised response of displacement with respect to time. Boundary conditions of the studied unit cells were implemented with accordance to methodology presented in Section 3.3.2. The results of unit cells with linear elastic with void, viscoelastic with void, and linear elastic with viscoelastic inclusion are presented in Sections 5.4, 5.5 and 5.6 respectively. The accuracy of the analytical solution prediction compared with the homogenised time domain response of displacement and velocity is discussed in detail with possible improvement tips for future work.

5.2 Principles of dynamics

To understand the homogenised behaviour of unit cells in dynamics, a derivation of the dynamic equation of motion is necessary. In this section a brief summary will be given of the dynamic response of single degree of freedom (SDoF) systems for the three considered types of unit cells (elastic with void inclusion, viscoelastic with void inclusion and elastic with viscoelastic inclusion). In a single degree of freedom system, the response of the elastic unit cell with void inclusion has been assumed to act as a spring connected to a lumped mass; while the viscoelastic unit cell, with void inclusion, has been assumed to act as a spring connected with a lumped mass and dashpot in series, similar to the Maxwell viscoelastic constitutive model in quasi static loading mentioned in Section 2.6.2. On the other hand, the elastic unit cell with Maxwell viscoelastic inclusion has been assumed as a lumped mass connected with a spring that is connected, in parallel, with a spring and a dashpot; similar to the standard solid constitutive model in quasi static loading mentioned in Section 2.6.3.

Unlike quasi static constitutive models (Section 2.6), in this section, all derivations will be performed with respect to stiffnesses (k, k_1 and k_2) and damping constant (c), to obtain an expression for the equation of motion with respect to time. The formulation of the dynamic equation of motion solution for the elastic case (Section 5.2.1) follows the methodology and derivation presented by Chopra [23]. However, in cases of viscoelastic unit cell and elastic unit cell with viscoelastic inclusion (Sections 5.2.2 and 5.2.3), the obtained solutions of dynamic equation of motion were derived and formulated based on basics of Newtons second law and following the same criteria of Chopra for spring mass system. The solutions for three material behaviours were obtained for the cases of free vibration and constant loading. Meanwhile these solutions can be extended to simulate the response due to a pulse loading by specifying an appropriate initial conditions, as shown in Section 5.3.

5.2.1 SDoF: Linear spring

In the absence of damping, the single degree of freedom of a linear elastic unit cell can be simplified to a mass spring system as follows (Figure 5.1); where M is the mass of the system, $P(t)$ is the dynamic force function with time, and k is the stiffness of a linear spring which can be determined from the elastic modulus of an unit cell. The derivation in this section was carried out in accordance with the methodology and formulation described by Chopra [23].

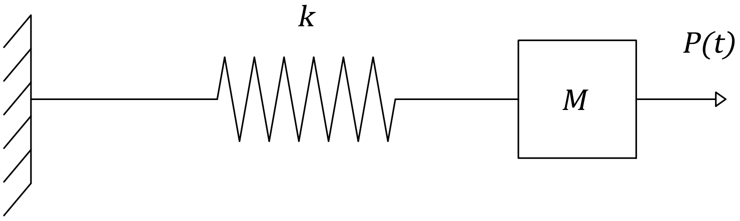

Figure 5.1: Linear spring-mass model

The equation of motion can be written as:

$$f_k(t) + f_I(t) = P(t) \tag{5.1}$$

where $f_k(t) = ku(t)$ is the force in the spring and $f_I(t) = M\ddot{u}(t)$ is the inertial force.

$$ku(t) + M\ddot{u}(t) = P(t) \tag{5.2}$$

Equation (5.2) is a second order ordinary differential equation. A homogeneous solution (for a free vibration case) can be written, in the form of trigonometric function, as follows:

$$u(t) = Acos(\omega t) + Bsin(\omega t) \tag{5.3}$$

In case the loading is a constant force ($P(t) = P_0$) the solution is a combination of the homogeneous solution (Equation (5.3)) and a particular solution (P_0/k) as follows:

$$u(t) = Acos(\omega t) + Bsin(\omega t) + P_0/k \tag{5.4}$$

The constant ω is a property of the dynamic system, therefore it depends solely on the system properties (stiffness k and mass M).

$$\omega = \sqrt{\frac{k}{M}} \tag{5.5}$$

On the other hand, the constants A and B depend on the initial conditions of the system (of displacement $u(0)$ and velocity $\dot{u}(0)$) and the applied force $P(t)$. Indeed constants A and B, in the case of free vibration, can be determined by solving Equation (5.3) with its time derivative (simultaneously) while equating them to the initial conditions respectively. In case of free vibration, constants A and B read as follows:

$$A = u(0) \tag{5.6}$$

$$B = \frac{\dot{u}(0)}{\omega} \tag{5.7}$$

In case of applied constant forces $P(t) = P_0$, constants A and B can be obtained by solving Equation (5.4) and its time derivative simultaneously while equating them to the initial conditions ($u(0)$ and $\dot{u}(0)$) as follows:

$$A = u(0) - \frac{P_0}{k} \tag{5.8}$$

$$B = \frac{\dot{u}(0)}{\omega} \tag{5.9}$$

A MATLAB function was coded to obtain ODE symbolic solution, and used to verify the solution of this ODE (Equation (5.2)), the function can be also used to model spring mass dynamic problem (Appendix A.5). The MATLAB solution was found to be perfectly matching the analytical solution presented in this section.

5.2.2 SDoF: Linear spring and a dashpot in series

The Maxwell viscoelastic model can be simplified as linear spring and a dashpot connected in series with a mass as follows (Figure 5.2); where M is the lumped mass of the system or unit cell and $P(t)$ is the dynamic force function. The stiffness of the spring k can be evaluated from the elastic modulus of a Maxwell viscoelastic unit cell E, while c is the damping coefficient of the dashpot, which can be obtained from the dynamic viscosity of Maxwell viscoelastic unit cell η.

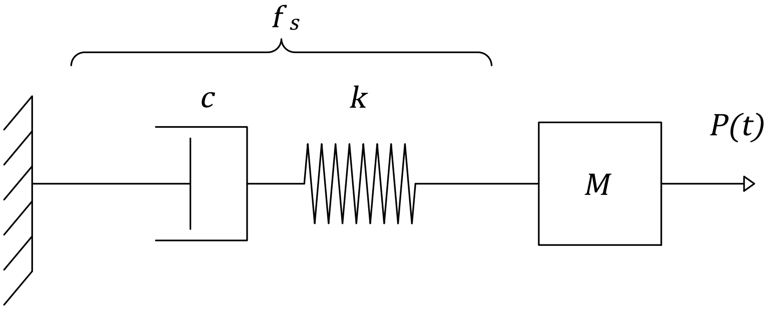

Figure 5.2: Linear spring-dashpot in series model

Using Newton's second law, the equation of motion can be written as follows:

$$f_s(t) + f_I(t) = P(t) \tag{5.10}$$

where $f_I(t) = M\ddot{u}(t)$ is the inertial force and $f_s(t)$ is the force in the spring dashpot system.

$$f_s(t) + M\ddot{u}(t) = P(t) \tag{5.11}$$

Since the spring and dashpot are connected in series, at any time t, the forces in the spring $f_k(t) = ku_k(t)$ and damper $f_c(t) = c\dot{u}_c(t)$ are equal to each other (Equation (5.12)). Furthermore, the displacement of the system $u(t)$ is equivalent to sum of the displacements of the spring $u_k(t)$ and the dashpot $u_c(t)$ as shown in Equation (5.13).

$$f_s(t) = f_c(t) = f_k(t) \tag{5.12}$$

$$u(t) = u_c(t) + u_k(t) \tag{5.13}$$

$f_s(t)$ can be written only in terms of $u_c(t)$ or $u_k(t)$; therefore, its essential to write $u(t)$ in terms of either $u_c(t)$ or $u_k(t)$ to have a consistent ODE with one differential variable.

From Equation (5.12) we can obtain the following:

$$c\dot{u}_c(t) = ku_k(t) \tag{5.14}$$

Substituting u_k from Equation (5.14) into Equation (5.13), we can obtain an expression of u in terms of u_c as follows:

$$u(t) = u_c(t) + \frac{c}{k}\dot{u}_c(t) \tag{5.15}$$

The equation of motion (Equation (5.11)) can be written, as follows, in terms of $u_c(t)$ by substituting $f_s(t) = f_c(t) = c\dot{u}_c(t)$ and $u(t)$ from Equation (5.15).

$$c\dot{u}_c + M(\ddot{u}_c + \frac{c}{k}\dddot{u}_c) = P(t) \tag{5.16}$$

Rearranging the variables, the equation of motion reads as follows:

$$\frac{Mc}{k}\dddot{u}_c + M\ddot{u}_c + c\dot{u}_c = P(t) \tag{5.17}$$

The equation of motion for this system is a third order ordinary differential equation. In case of free vibration ($P(t) = 0$), the following can be written as a solution (homogeneous solution).

$$u_c(t) = e^{\alpha t}(Acos(\omega t) + Bsin(\omega t)) + C \tag{5.18}$$

The solution can be written as follows in case the force has a constant value ($P(t) = P_0$).

$$u_c(t) = e^{\alpha t}(Acos(\omega t) + Bsin(\omega t)) + C + \frac{P_0}{c}t \tag{5.19}$$

Both solutions depend on the properties of the system and initial conditions. Solving the characteristic equation of the ODE yield the values of α and ω as follows:

$$\alpha = \frac{-k}{2c} \tag{5.20}$$

$$\omega = \frac{\sqrt{4M\,c^2k - M^2k^2}}{2Mc} \tag{5.21}$$

To evaluate constants A, B and C, three initial conditions are required, namely Equations (5.22), (5.23), and (5.24) which have been written in with respect to the initial conditions of the full system ($u(0)$ and $\dot{u}(0)$).

First, at $t = 0$, all the displacement is carried by the spring; therefore the the initial displacement of the dashpot is null:

$$u_c(0) = 0 \tag{5.22}$$

Second, initial velocity of the dashpot can be obtained from Equation (5.14) as follows, where $u_k(0) = u(0)$:

$$\dot{u}_c(0) = \frac{k}{c}u_k(0) \tag{5.23}$$

Third, initial acceleration of the dashpot can be obtained by differentiating Equation (5.14) with respect to time as follows, while $\dot{u}_k(0) = \dot{u}(0) - \dot{u}_c(0)$.

$$\ddot{u}_c(0) = \frac{k}{c}\dot{u}_k(0) \tag{5.24}$$

Applying the initial conditions mentioned above (Equations (5.22), (5.23), and (5.24)) to the equation of motion (Equation (5.18)), and its first and second time derivatives, we may write the following expressions for A, B and C (for free vibration case).

$$A = \frac{2\alpha\omega\dot{u}_c(0) - \omega\ddot{u}_c(0)}{\omega(\alpha^2 + \omega^2)} \tag{5.25}$$

$$B = \frac{(\omega^2 - \alpha^2)\dot{u}_c(0) + \alpha\ddot{u}_c(0)}{\omega(\alpha^2 + \omega^2)} \tag{5.26}$$

$$C = \frac{(\alpha^2 + \omega^2)u_c(0) - 2\alpha\dot{u}_c(0) + \ddot{u}_c(0)}{\alpha^2 + \omega^2} \tag{5.27}$$

To obtain expressions of A, B and C in the case of constant applied force ($P(t) = P_0$), Equation (5.19) and its first and second time derivatives can be solved simultaneously while equating them to the initial conditions (Equations (5.22), (5.23), and (5.24)). The expressions read as follows:

$$A = \frac{2\alpha\omega c\dot{u}_c(0) - \omega c\ddot{u}_c(0) - 2\alpha\omega P_0}{\omega c(\alpha^2 + \omega^2)} \tag{5.28}$$

$$B = \frac{(\omega^2 - \alpha^2)c\dot{u}_c(0) + \alpha c\ddot{u}_c(0) + (\alpha^2 - \omega^2)P_0}{\omega c(\alpha^2 + \omega^2)} \tag{5.29}$$

$$C = \frac{(\alpha^2 + \omega^2)cu_c(0) - 2\alpha c\dot{u}_c(0) + c\ddot{u}_c(0) + 2\alpha P_0}{c(\alpha^2 + \omega^2)} \tag{5.30}$$

Once $u_c(t)$ is formulated, the equation of motion of the whole system $u(t)$ can be obtained from Equation (5.15). To verify our solution, a MATLAB function was coded, based on ODE symbolic solution, and used to check the solution of this ODE (Equation (5.17)). The function can be also used to model Maxwell viscoelastic dynamic problem (Appendix A.6). Comparing the analytical solution, presented in this section, with the MATLAB function solution, they show a perfect match.

5.2.3 SDoF: Linear spring and a dashpot in series connected in parallel with another Linear spring

The Maxwell form of standard solid model (SSM) has been modeled as a mass connected to a spring in parallel with a spring-dashpot system (connected in series) as shown in Figure 5.3. M present the lumped mass of the system, while $P(t)$ is the dynamic load function with time. k_1 and k_2 are the stiffnesses of the two springs; they can be quantified from E_0 and E_∞ of an SSM, while c is the dashpot damping constant, which can be evaluated from the dynamic viscosity η of SSM. In this section, an analytical solution to solve this model under dynamic loading is presented.

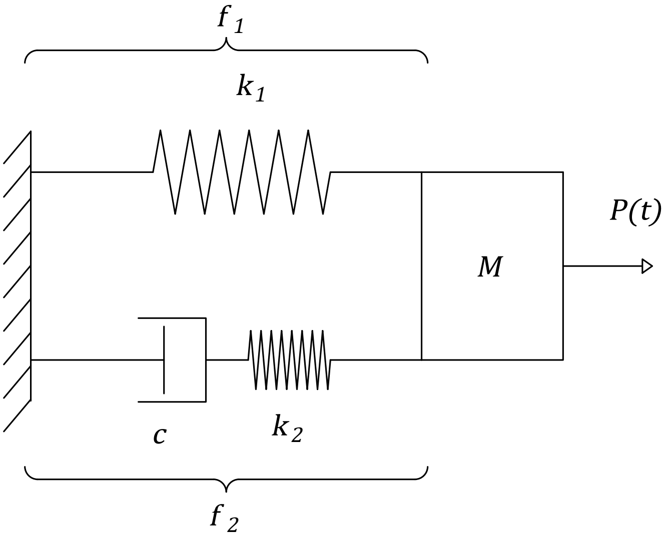

Figure 5.3: Linear spring-dashpot (in series) connected in parallel with a linear spring

The equation of motion for this system can be written as follows:

$$f_1(t) + f_2(t) + f_I(t) = P(t) \tag{5.31}$$

where $f_I(t) = M\ddot{u}$ is the inertial force, $f_1(t) = k_1 u_{k1}(t)$ is the force in the upper spring and and $f_2(t)$ is the force in the spring dashpot system. Therefore, we have:

$$f_1(t) + f_2(t) + M\ddot{u}(t) = P(t) \tag{5.32}$$

Similar to the concept of Maxwell model, $f_2(t)$ can be written as follows, since the spring k_2 and the dashpot c are connected in series:

$$f_2(t) = f_c(t) = f_{k2}(t) \tag{5.33}$$

On the other hand, the overall displacement of the second system $u_2(t)$ can be written as a summation of the displacements of the spring $u_{k2}(t)$ and dashpot $u_c(t)$.

$$u_2(t) = u_c(t) + u_{k2}(t) \tag{5.34}$$

Using the identity $f_c(t) = f_{k2}(t)$ from Equation (5.33), where $f_c(t) = c\dot{u}_c(t)$ and $f_{k2}(t) = k_2 u_{k2}(t)$, we can obtain the following:

$$c\dot{u}_c(t) = k_2 u_{k2}(t) \tag{5.35}$$

Since the upper spring k_1 is connected in parallel, to one bulk mass, with the spring dashpot system, the overall displacement of the system $u(t)$ is equal to the displacement of the upper spring $u_1(t)$ and the displacement of the spring dashpot system $u_2(t)$. Employing this identity with Equation (5.34) and substituting for $u_{k2}(t)$ from Equation (5.35), we can obtain an expression of $u(t)$ in terms of $u_c(t)$

and $\dot{u}_c(t)$ as follows:

$$u(t) = u_2(t) = u_c(t) + \frac{c}{k_2}\dot{u}_c(t) \tag{5.36}$$

Substituting $f_1(t) = k_1 u_1(t) = k_1 u(t)$ and $f_2 = c\dot{u}_c$ in Equation (5.32) to formulate the equation of motion:

$$k_1 u(t) + c\dot{u}_c + M\ddot{u}(t) = P(t) \tag{5.37}$$

The equation of motion of the full system can be written with respect of one function $u_c(t)$, and its time derivatives, by substituting $u(t)$ from Equation (5.36) as follows:

$$k_1\left(u_c + \frac{c}{k_2}\dot{u}_c\right) + c\dot{u}_c + M(\ddot{u}_c + \frac{c}{k_2}\dddot{u}_c) = P(t) \tag{5.38}$$

Rearranging Equation (5.38) leads to the following expression:

$$\frac{Mc}{k_2}\dddot{u}_c + M\ddot{u}_c + \left(c + \frac{k_1 c}{k_2}\right)\dot{u}_c + k_1 u_c = P(t) \tag{5.39}$$

The equation of motion for this system is a third order ordinary differential equation. In case of free vibration ($P(t) = 0$), the following can be written as a solution (homogeneous solution).

$$u_c = e^{\alpha t}(Acos(\omega t) + Bsin(\omega t)) + Ce^{\gamma t} \tag{5.40}$$

On the other hand, in case of a constant force $P(t) = P_0$ the solution can be written as a summation of the homogeneous solution (Equation (5.40)) and a particular solution of (P_0/k_1) as follows:

$$u_c(t) = e^{\alpha t}(Acos(\omega t) + Bsin(\omega t)) + Ce^{\gamma t} + \frac{P_0}{k_1} \tag{5.41}$$

The homogeneous solution dependence on properties of the dynamic system is presented in constants α, ω and γ. Furthermore, the initial conditions, namely initial displacement $u(0)$ and initial velocity $\dot{u}(0)$ of the system, play a role in the homogeneous solution and they are presented in the constants A, B and C. However the particular solution depends on the applied force P_0 and the stiffness of spring 1 (k_1).

Writing mathematical expressions for the parameters α, ω and γ leads to lengthy expressions that lack insight. Therefore, the constants R and D were defined to write a more compact expression for α, ω and γ.

$$\begin{aligned} R = {} & \frac{1}{\sqrt{M}}\left(4M^2 k_1\, k_2{}^4 + 8M\, c^2 k_1{}^2 k_2{}^2 - 20M\, c^2 k_1\, k_2{}^3 - M\, c^2 k_2{}^4\right)^{\frac{1}{2}} \\ & + \frac{1}{\sqrt{M}}\left(4c^4 k_1{}^3 + 12c^4 k_1{}^2 k_2 + 12c^4 k_1\, k_2{}^2 + 4c^4 k_2{}^3\right)^{\frac{1}{2}} \end{aligned} \tag{5.42}$$

$$D = \left(\left(-8k_2{}^3 M - 72k_1 k_2\, c^2 + 36c^2 k_2{}^2 + 12\sqrt{3}Rc\right) M^2\right)^{\frac{1}{3}} \tag{5.43}$$

The solution parameters α, ω and γ expressions can be written as follows with respect to the system parameters (M, $k1$, $k2$ and c) and the constant D.

$$\alpha = -\frac{D}{12Mc} - \frac{k_2{}^2 M - 3c^2 k_1 - 3c^2 k_2}{3cD} - \frac{k_2}{3c} \tag{5.44}$$

$$\omega = \frac{\sqrt{3}}{2}\left(\frac{D}{6Mc} - \frac{2\left(k_2{}^2 M - 3c^2 k_1 - 3c^2 k_2\right)}{3cD}\right) \tag{5.45}$$

$$\gamma = \frac{D}{6Mc} + \frac{2\left(k_2{}^2 M - 3c^2 k_1 - 3c^2 k_2\right)}{3cD} - \frac{k_2}{3c} \tag{5.46}$$

To evaluate constants A, B and C of the equation of motion solutions (Equations (5.40) and (5.41)), three initial conditions are required, namely Equations (5.47), (5.48), and (5.50):

First, at $t = 0$, all the displacement is carried by the springs $k1$ and $k2$; therefore the the initial displacement of the dashpot is null:

$$u_c(0) = 0 \tag{5.47}$$

Second, initial velocity of the dashpot can be obtained from Equation (5.36) as follows, where $u_{k2}(0) = u(0)$:

$$\dot{u}_c(0) = \frac{k_2}{c} u_{k2}(0) = \frac{k_2}{c} u(0) \tag{5.48}$$

Third, initial acceleration of the dashpot can be obtained by differentiating Equation (5.36) with respect to time as follows:

$$\ddot{u}_c(t) = \frac{k_2}{c} \dot{u}_{k2}(t) \tag{5.49}$$

By differentiating Equation (5.34), $\dot{u}_{k2}(t)$ can be written as $\dot{u}_{k2}(t) = \dot{u}(t) - \dot{u}_c(t)$, so that we can write the following as a third initial condition:

$$\ddot{u}_c(0) = \frac{k_2}{c} \dot{u}_{k2}(0) = \frac{k_2}{c} (\dot{u}(0) - \dot{u}_c(0)) \tag{5.50}$$

Theses initial conditions (Equations (5.48), (5.49), and (5.50)) can be equated (while substituting $t = 0$) to the equation of motion (Equations (5.40)), and its first and second time derivatives respectively. Solving the three equations simultaneously yields the following expressions for A, B and C (for the free vibration case):

$$A = \frac{(\gamma^2 - 2\alpha\gamma)\omega u_c(0) + 2\alpha\omega\dot{u}_c(0) - \omega\ddot{u}_c(0)}{\omega(\gamma^2 - 2\gamma\alpha + \alpha^2 + \omega^2)} \tag{5.51}$$

$$B = -\frac{(\alpha\gamma^2 - \alpha^2\gamma + \omega^2\gamma)u_c(0) + (\alpha^2 - \omega^2 - \gamma^2)\dot{u}_c(0) + (\gamma - \alpha)\ddot{u}_c(0)}{\omega(\gamma^2 - 2\gamma\alpha + \alpha^2 + \omega^2)} \tag{5.52}$$

$$C = \frac{(\alpha^2 + \omega^2)u_c(0) - 2\alpha\dot{u}_c(0) + \ddot{u}_c(0)}{\gamma^2 - 2\gamma\alpha + \alpha^2 + \omega^2} \tag{5.53}$$

In the case of constant applied force $P(t) = P_0$, equation of motion (Equation (5.41)) can be solved along with its first and second time derivatives while equating them to the initial conditions (Equations (5.48), (5.49), and (5.50)) respectively. This gives:

$$A = \frac{(\gamma^2 - 2\alpha\gamma)\omega k_1 u_c(0) + 2\alpha\omega k_1\dot{u}_c(0) - \omega k_1\ddot{u}_c(0) + (2\gamma\alpha - \gamma^2)\omega P_0}{\omega k_1(\gamma^2 - 2\gamma\alpha + \alpha^2 + \omega^2)} \tag{5.54}$$

$$\begin{aligned} B = -&\frac{(\alpha\gamma^2 - \alpha^2\gamma + \omega^2\gamma)k_1 u_c(0) + (\alpha^2 - \omega^2 - \gamma^2)k_1\dot{u}_c(0)}{\omega k_1(\gamma^2 - 2\gamma\alpha + \alpha^2 + \omega^2)} \\ &- \frac{(\gamma - \alpha)k_1\ddot{u}_c(0) + (\gamma\alpha^2 - \alpha\gamma^2 - \gamma\omega^2)P_0}{\omega k_1(\gamma^2 - 2\gamma\alpha + \alpha^2 + \omega^2)} \end{aligned} \tag{5.55}$$

$$C = \frac{(\alpha^2 + \omega^2)k_1 u_c(0) - 2\alpha k_1\dot{u}_c(0) + k_1\ddot{u}_c(0) - (\alpha^2 + \omega^2)P_0}{k_1(\gamma^2 - 2\gamma\alpha + \alpha^2 + \omega^2)} \tag{5.56}$$

Similar to Section 5.2.2, the equation of motion of the whole system $u(t)$ can be obtained from Equation (5.36), once $u_c(t)$ is formulated. To check the analytical solution, developed in this section, a MATLAB function was coded based on ODE symbolic solver to obtain a solution of Equation (5.39). The solution obtained from the MATLAB functions perfectly match the analytical solution. The MATLAB script is referenced in Appendix A.7, and it can be used model the sdof dynamic behaviour of a standard solid model.

5.3 Loading conditions

To examine the dynamic behaviour of linear elastic unit cell with void inclusion; a number of unit cells have been modeled under a sudden constant loading and a pulse force. Numerical homogenisation criteria were applied for the displacement and velocity in time domain. To verify the suitability of numerical homogenisation in dynamics, homogenised material properties, obtained from quasi-static loading case were used to obtain analytical solutions and compare them with the dynamic numerical homogenised time domain response. In this chapter two dynamic loading scenarios will be considered, a sudden constant loading and a pulse loading. In which the analytical solution of the sudden constant loading can be obtained straight forwardly from Section 5.2.

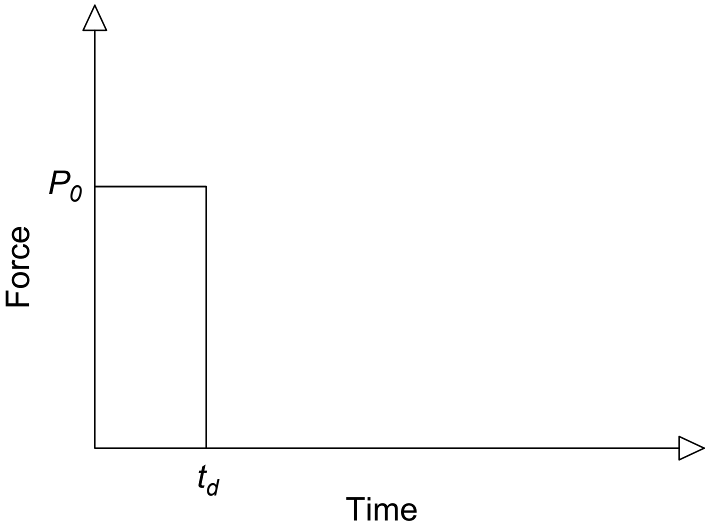

Figure 5.4: Impulse loading

The impulsive loading conditions can be obtained by applying a large force for a short duration of time (Figure 5.4). Depending on the unit cell type, Equations (5.3), (5.19) and (5.41) can be solved in the time domain (0 to t_d) to obtain the analytical solution during loading time period. This is followed by solving

Equations (5.2), (5.18) and (5.40) for post loading time ($t > t_d$), where the unit cell vibration is considered to be free vibration beyond t_d. These equations are summarised below in Equation (5.57) for elastic unit cells, Equation (5.58) for viscoelastic unit cells and Equation (5.59) for composite unit cells. To evaluate A, B and C, initial conditions of $u(0) = 0$ and $\dot{u}(0) = 0$ for Equation (5.57), while $u_c(0) = 0$, $\dot{u}_c(0) = 0$ and $\ddot{u}_c(0) = 0$ for Equations (5.58) and (5.59). Finally, A_p, B_p and C_p can be evaluated using the values of displacement, velocity and acceleration by the end of the loading period (t_d). These values would be $u(t_d)$ and $\dot{u}(t_d)$ for Equation (5.57), while $u_c(t_d)$, $\dot{u}_c(t_d)$ and $\ddot{u}_c(t_d)$ for Equations (5.58) and (5.59).

$$u(t) = \begin{cases} Acos(\omega t) + Bsin(\omega t) + P_0/k, & \text{if } t \leq t_d \\ A_p cos(\omega(t - td)) + B_p sin(\omega(t - td)), & \text{if } t > t_d \end{cases} \tag{5.57}$$

$$u_c(t) = \begin{cases} e^{\alpha t}(Acos(\omega t) + Bsin(\omega t)) + C + \frac{P_0}{c}t, & \text{if } t \leq t_d \\ e^{\alpha(t-td)}(A_p cos(\omega(t - td)) + B_p sin(\omega(t - td))) + C_p, & \text{if } t > t_d \end{cases} \tag{5.58}$$

$$u_c(t) = \begin{cases} e^{\alpha\tau}(Acos(\omega t) + Bsin(\omega t)) + Ce^{\gamma t} + \frac{P_0}{k_1}, & \text{if } t \leq t_d \\ e^{\alpha(t-td)}(A_p cos(\omega(t - td)) + B_p sin(\omega(t - td))) + C_p e^{\gamma(t-td)}, & \text{if } t > t_d \end{cases} \tag{5.59}$$

5.4 Linear elastic unit cell

with void inclusion Similar to Section 4.2 in chapter 4, this section present a study of elastic unit cells with single void inclusion. However, in this section, dynamic loading conditions will be applied to assess the homogenised dynamic response of unit cells, and test the suitability of quasi-static homogenised properties to represent dynamic behaviour. The dynamic loading conditions were applied as mentioned in Section 5.3. unit cells of elastic modulus $E = 3300$ MPa, and the Poisson's ratio has been set to null, since the focus of this study is on uni-axial loading. Boundary conditions were used with accordance to the methodology mentioned earlier in Section 3.3.2.

A constant loading of 20 N has been used to examine the response of the unit cell subjected to a sudden permanent loading. Meanwhile the homogenised material properties of the unit cell under creep, quasi static conditions, has been used to evaluate the analytical solution of the dynamic problem. The main property required, in this case, is the homogenised elastic modulus of $\bar{E} = 1844.4$ MPa which contributes to a stiffness of $k = 1844.4$ N/mm. The mass in the analytical solution has been taken as $M = \frac{\rho V_R}{2}$, where ρ is the mass density, V_R is the volume of the unit cell. In this section, the mass density is taken as $\rho = 78$ kN·s^2/m to increase the time step required to obtain a stable solution. This increase in mass will change the natural frequencies of the system however the elastic modulus and dynamic viscosity (the properties of interest in this study) are not influenced by the change of mass density. The mass is divided by 2 since while are obtaining a homogenised solution based on a single degree of freedom model, where one half of the total mass is assumed to be free to move while the other is assumed to be lumped to the support.

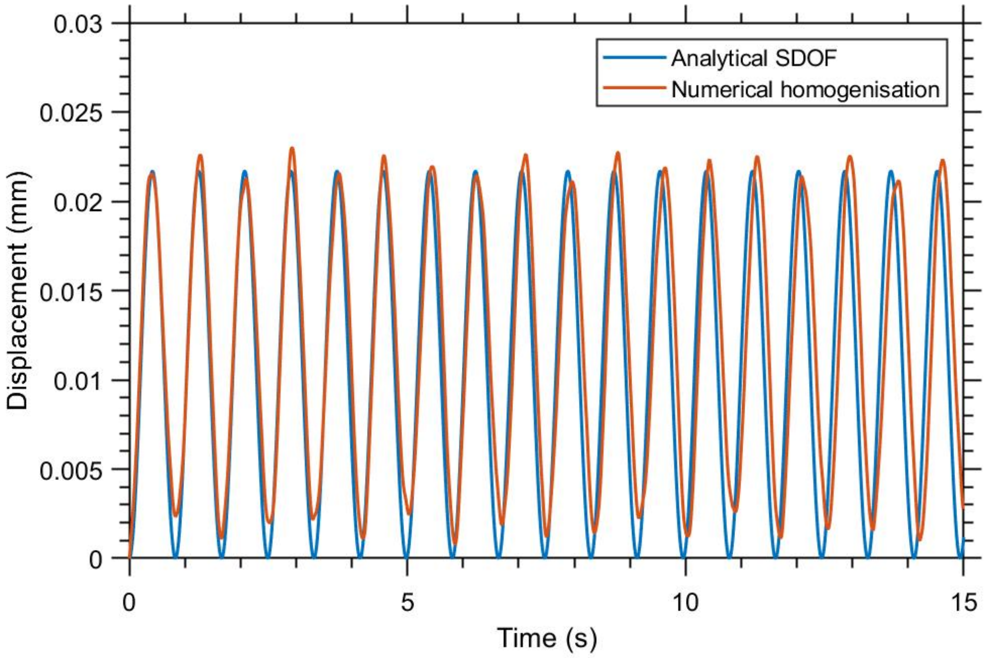

Figure 5.5: Displacement vs time due to a sudden constant load applied on a linear elastic unit cell

with void inclusion (A_r=0.175 mm^2, ASP=3 and $\theta = 45°$)

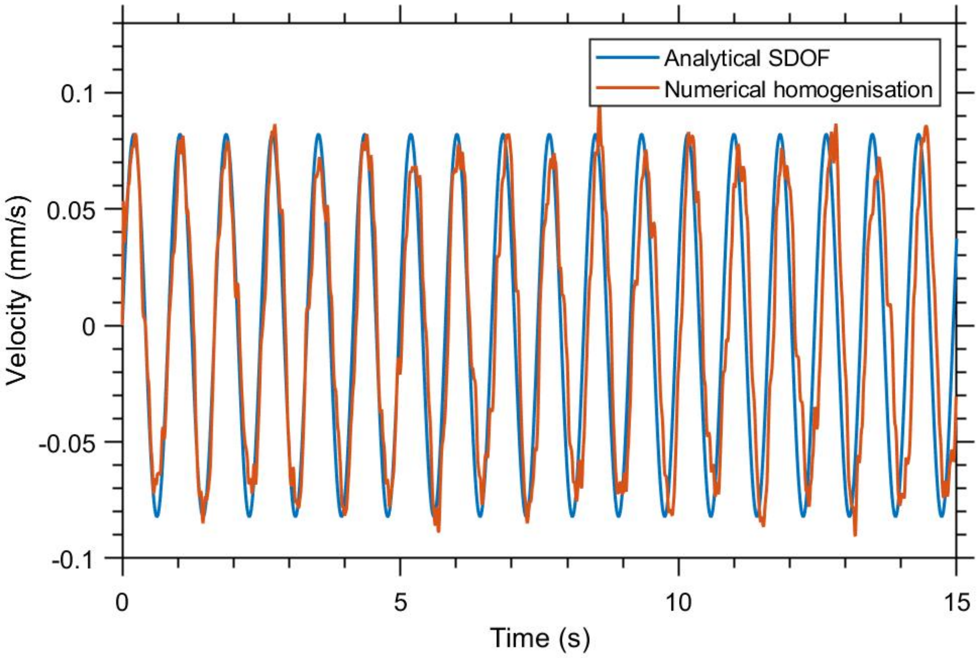

Figure 5.6: Velocity vs time due to a sudden constant load applied on a linear elastic unit cell

with void inclusion (A_r=0.175 mm^2, ASP=3 and $\theta = 45°$)

Figures 5.5 and 5.6 show the time response of displacement and velocity respectively. The numerical homogenised solution of an unit cell can be predicted with good accuracy by the analytical model of single degree of freedom while using properties obtained from quasi static tests.

To test this homogenisation approach under impulsive loading (Figure 5.4), a unit cell was modeled while applying a pulse force (P_0) of 20N, and a loading duration (t_d) of 1 second. Similar to the case of sudden constant loading the analytical solutions of displacement and velocity yield good approximation of the responses vs time as shown in Figures 5.7 and 5.8. The figures presented in this section were obtained from unit cells with inclusion's area of 0.175, inclination angle of 45° and aspect ratio of 3. All other combinations of inclusions parameters (areas, aspect ratios, and inclination angles) tend to yield similar accuracy.

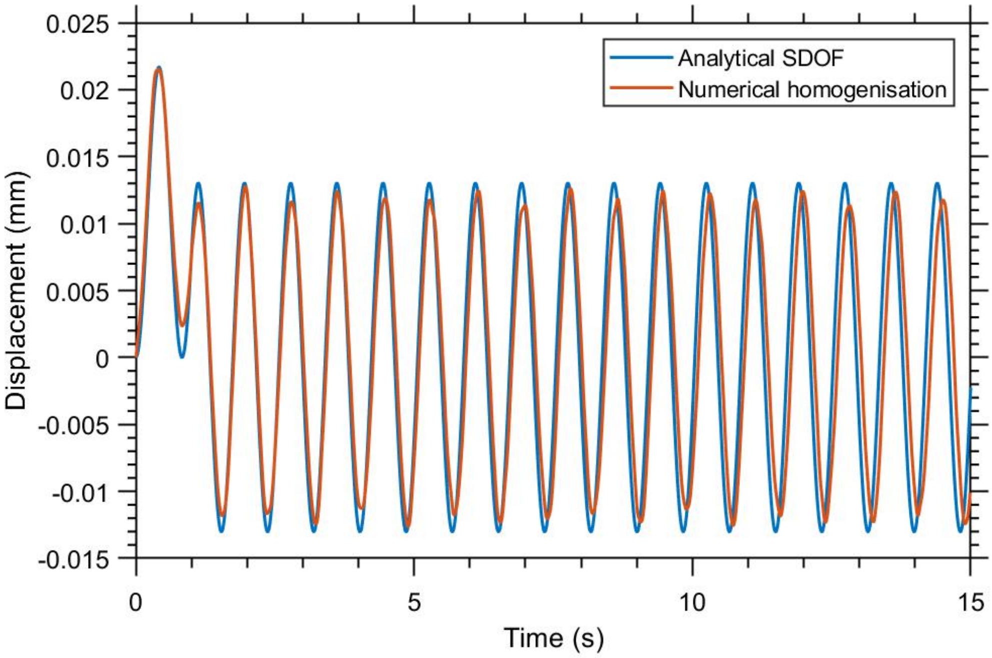

Figure 5.7: Displacement vs time due to an impulsive load applied on a linear elastic unit cell

with void inclusion (A_r=0.175 mm^2, ASP=3 and $\theta = 45°$)

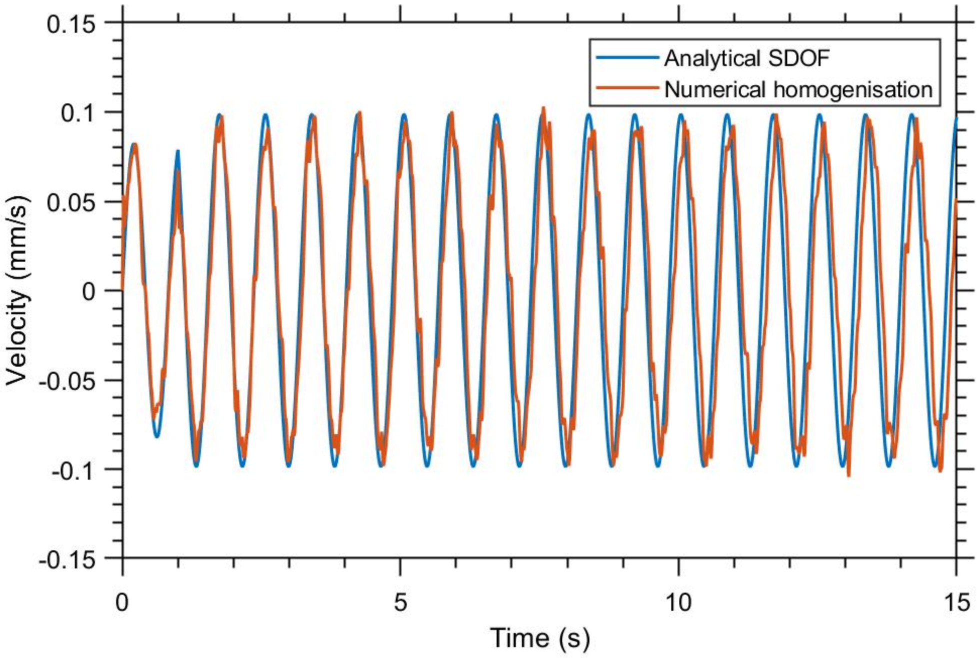

Figure 5.8: Velocity vs time due to an impulsive load applied on a linear elastic unit cell

with void inclusion (A_r=0.175 mm^2, ASP=3 and $\theta = 45°$)

5.5 Viscoelastic unit cell

with void inclusion In this section, Maxwell viscoelastic unit cells with void inclusion have been studied under dynamic loading conditions. Similar to the previous section, the numerical homogenised time response will be compared to the analytical solution. The unit cell materials properties at micro level are elastic modulus (E) of 3300 MPa and dynamic viscosity (η) of 1650 N·s/mm^2. Similar to the quasi static case (Section 4.3), Maxwell has been modeled using the MAT_VISCOELASTIC material model in LS-DYNA. Homogenised macro level properties under creep loading conditions while implementing boundary conditions from Section 3.3.2 are $\bar{E}$ of 1853 MPa and $\bar{\eta}$ of 1319 N·s/mm^2. Since the unit cells used in this study have a 1 mm boundaries, the stiffness and damping coefficient are equal to the numeric values of $\bar{E}$ and $\bar{\eta}$ (k=1853 N/mm, c=1319 N·s/mm). Since this approach is based on a single degree of freedom, the mass in the analytical model has been assumed to be equal to one half of the unit cell mass.

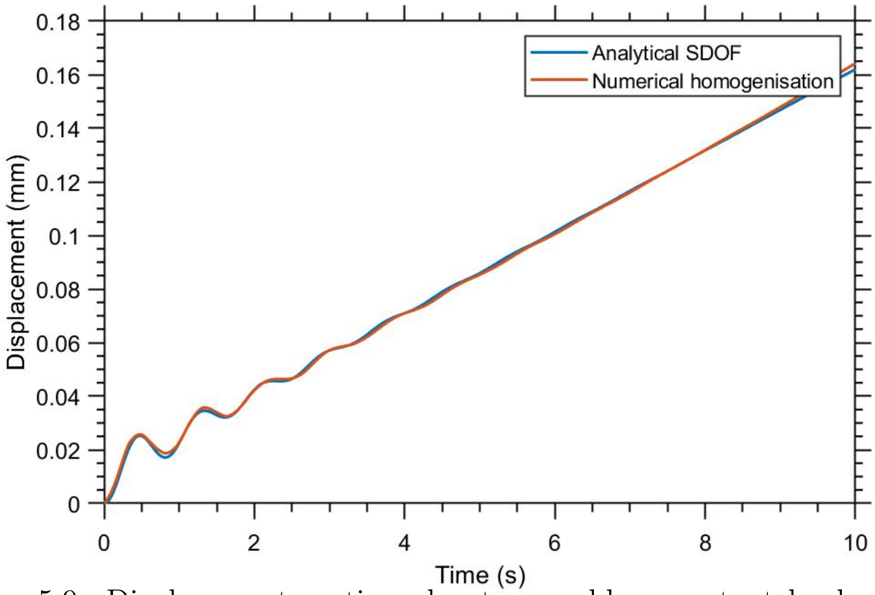

Figure 5.9: Displacement vs time due to a sudden constant load applied on a viscoelastic unit cell

with void inclusion (A_r=0.175 mm^2, ASP=3 and $\theta = 45°$).

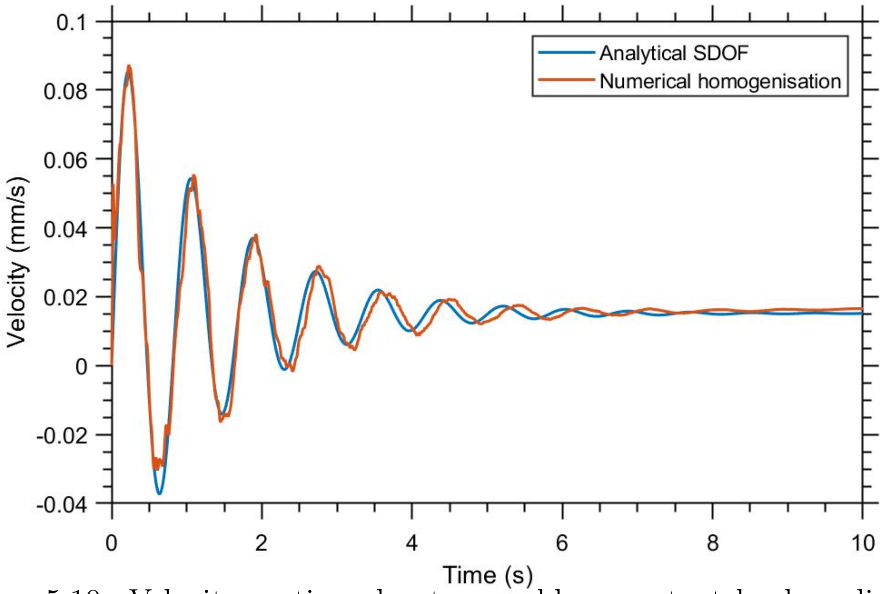

Figure 5.10: Velocity vs time due to a sudden constant load applied on a viscoelastic unit cell

with void inclusion (A_r=0.175 mm^2, ASP=3 and $\theta = 45°$)

Similar to the previous section, the unit cells were modeled under a sudden constant loading and an impulsive loading as with accordance to Section 5.3. The applied constant load has a magnitude of 20 N, while the pulse force magnitude (P_0) is 20N, and a loading duration (t_d) of 1 second. The time domain response has been compared with the analytical solution obtained from quasi static homogenised properties. Figures 5.9 and 5.10 show the displacement and velocity due to a sudden constant loading; the analytical solution is clearly capturing the time response with good accuracy. Furthermore, Figures 5.11 and 5.12 show the displacement and velocity response due to a pulse force. It is noted that the analytical solution and the numerical homogenised solution tend to yield very similar values for the vibration period and peak displacement. A slight shift between the analytical solution and the numerical homogenisation is believed to be due to the absence of periodic boundary conditions in dynamics as discussed in Section 3.3.2. The figures presented in this section show results obtained from a unit cell with inclusion's area of 0.175, inclination angle of 45° and aspect ratio of 3, while All other combinations of inclusions parameters yield similar accuracy.

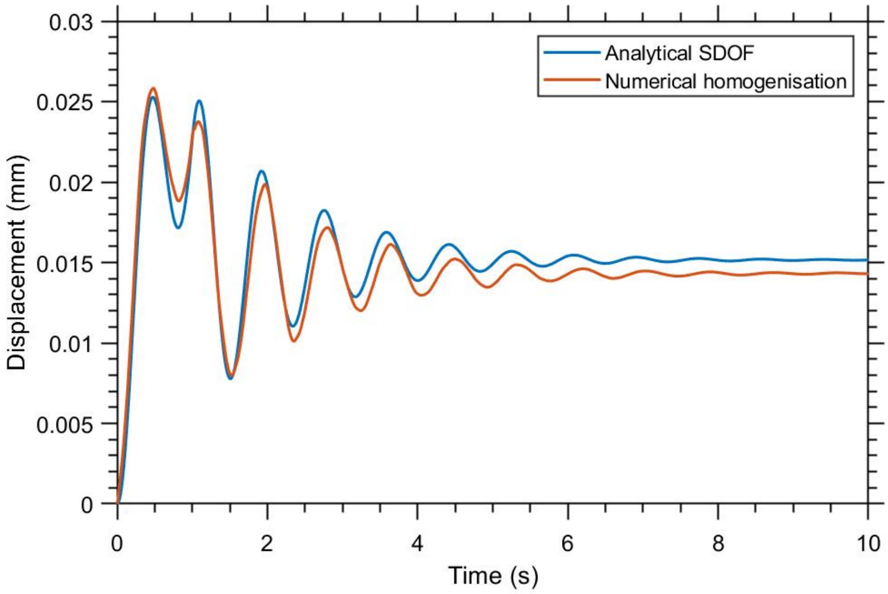

Figure 5.11: Displacement vs time due to an impulsive load applied on a viscoelastic unit cell

with void inclusion (A_r=0.175 mm^2, ASP=3 and $\theta = 45°$)

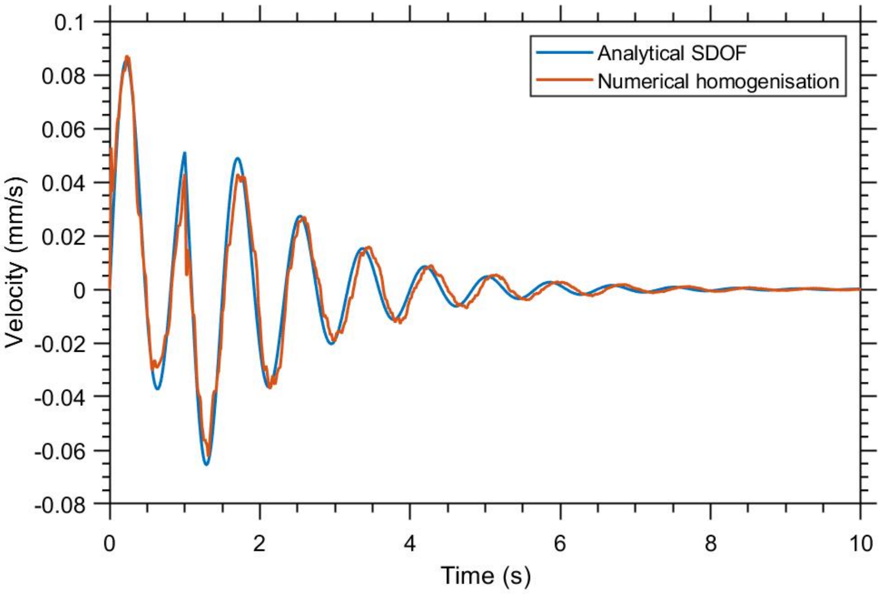

Figure 5.12: Velocity vs time due to an impulsive load applied on a viscoelastic unit cell

with void inclusion (A_r=0.175 mm^2, ASP=3 and $\theta = 45°$)

5.6 Composite unit cell

(linear elastic matrix with viscoelastic inclusion) In this section, a composite unit cell that consists of a linear elastic matrix and a viscoelastic inclusion has been studied under dynamic loading conditions. The unit cell elastic matrix micro properties are elastic modulus (E) of 9000 MPa, with the inclusion micro properties elastic modulus (E) of 9000 MPa and a dynamic viscosity (η) of 1800 N·s/mm^2. The homogenised macro model for this type of unit cells follows the Maxwell form of the standard solid model, which yields, in this case, the following homogenised properties: initial elastic modulus ($\bar{E}_0$) of 9000 MPa, final elastic modulus ($\bar{E}_\infty$) of 4610 MPa and dynamic viscosity ($\bar{\eta}$) of 4929 N·s/mm^2. These properties have been employed in the analytical solution (mentioned in Sections 5.2.3 and 5.3), where $k_1 = \bar{E}_f \cdot l$, $k_2 = (\bar{E}_i - \bar{E}_f) \cdot l$ and $c = \bar{\eta} \cdot l$, where l is the length of the unit cell in the direction of loading. The lumped mass in the analytical solution has been assumed to be equal to one half of the unit cell mass, due to the single degree of freedom assumption.

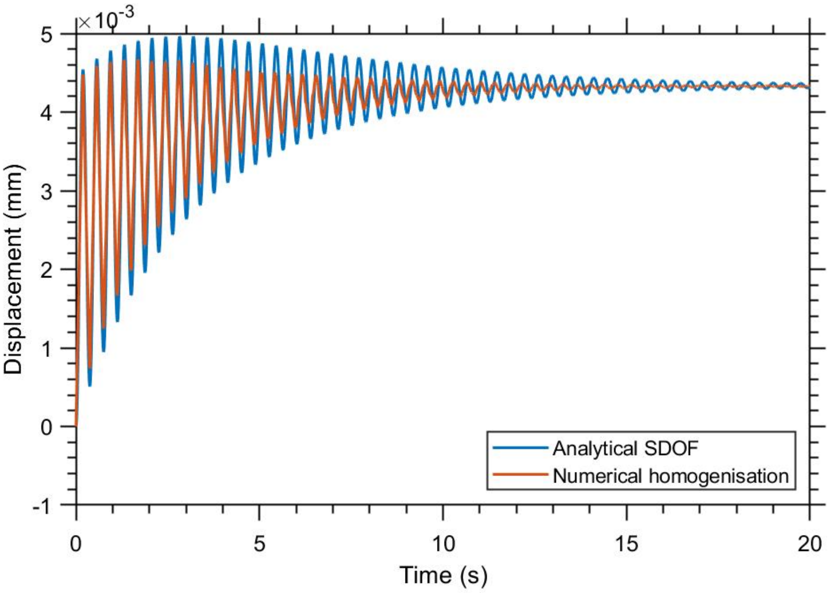

Figure 5.13: Displacement vs time due to a sudden constant load applied on an elastic unit cell

with viscoelastic inclusion (A_r=0.175 mm^2, ASP=3 and $\theta = 45°$).

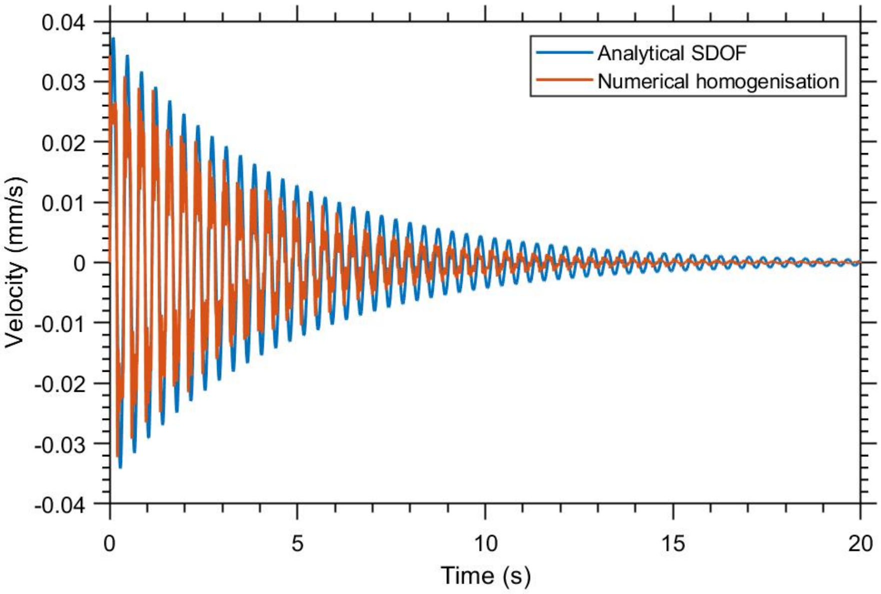

Figure 5.14: Velocity vs time due to a sudden constant load applied on an elastic unit cell

with viscoelastic inclusion (A_r=0.175 mm^2, ASP=3 and $\theta = 45°$)

Similar to previous sections, the unit cell has been studied under a sudden constant loading of 20 N. Figures 5.13 and 5.14 show the time domain response of displacement and velocity. Furthermore, the response due to an impulsive loading has been examined by modelling the unit cell subjected to a force pulse of a magnitude (P_0) is 20N, and a loading duration (t_d) of 1 second. Figures 5.15 and 5.16 show the time domain response of displacement and velocity due to an impulsive loading. In both loading cases, it is noted that the period of oscillations were captured with great accuracy by both numerical homogenisation and the analytical solution. However, the accuracy of, displacement or velocity, magnitudes at each oscillation tend to be over estimated by the analytical solution. This is believed to occur due to two main reasons; first, the boundary conditions in these sections were imposed with the methodology specified in Section 3.3.2, while the use of periodic boundary conditions would improve the accuracy of prediction. Second, the unit cells used in this section consist of 2 material models at micro level, in which the elastic material Poisson's ratio can be ensured to be null; while, the viscoelastic part is specified with accordance to the material model (MAT_VISCOELASTIC), in which its required to input the material parameters of bulk modulus, initial shear modulus, final shear modulus and a decay constant. Applying the material parameters as bulk and shear moduli, allow us to define a null Poisson's ratio initially by specifying a bulk and initial shear moduli initially. However, as time progress and the shear modulus changes while bulk modulus is constant, therefore, the homogenised Poisson's ratio change with time. Thus, the homogenised response is not solely uniaxial. To test this hypothesis, the lowest effect of Poisson's ratio occurs when the inclusion's inclination angle is null while the maximum effect occurs with inclination angle of 90°. The analytical solution tends to yield better prediction of the numerical homogenised time response for cases with inclination angles of null, as shown in Appendix D.1, compared with a lower accuracy prediction for the 90° in as shown in Appendix D.2. To account for the change in Poisson's ratio, it is essential to study the anisotropic nature of unit cell; due to the limitations of time and resources, the development of an automated script to study the anisotropy behaviour have been kept for the future work.

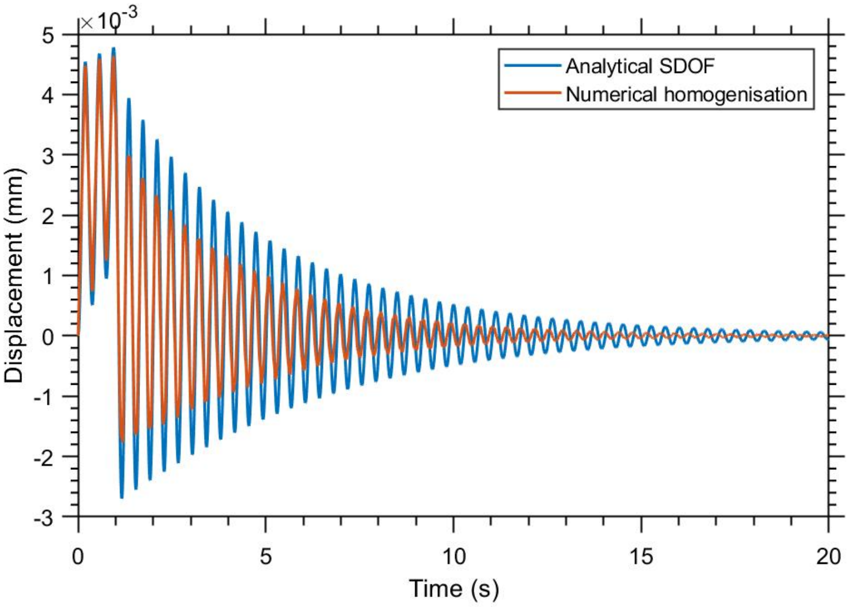

Figure 5.15: Displacement vs time due to an impulsive load applied on an elastic unit cell

with viscoelastic inclusion (A_r=0.175 mm^2, ASP=3 and $\theta = 45°$)

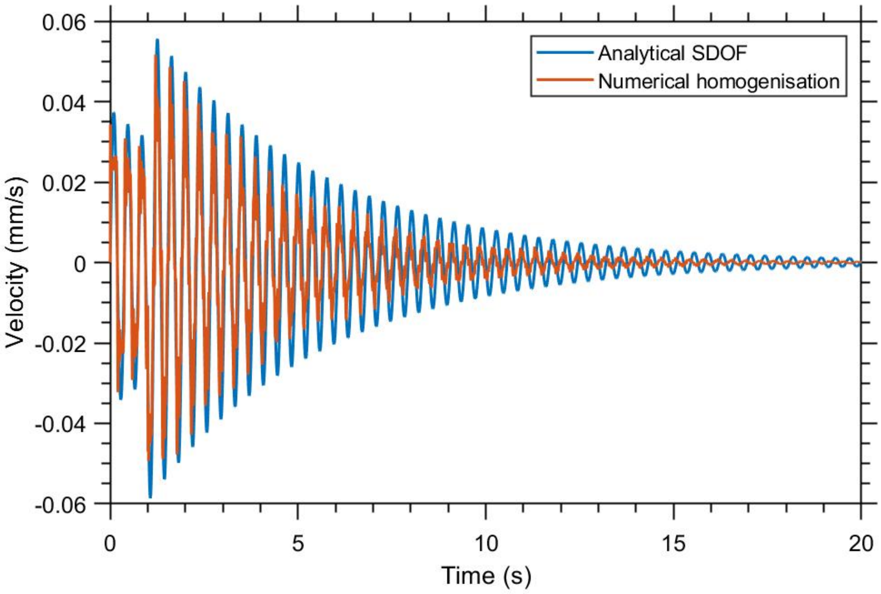

Figure 5.16: Velocity vs time due to an impulsive load applied on an elastic unit cell

with viscoelastic inclusion (A_r=0.175 mm^2, ASP=3 and $\theta = 45°$)

5.7 Unit cell response in dynamics and effective mechanical properties

In this section the suitability of considering a unit cell as an RVE for obtaining mechanical properties from dynamic response will be studied. To do so, first we will consider a single unit cell with single inclusion, inclined at 45° as shown in Figure 5.17. The material of this unit cell are considered to be steel with an elastic modulus of 210 GPa and a mass density of 7800 kg/m^3.

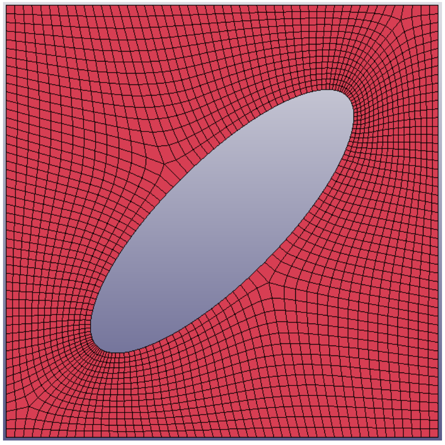

Figure 5.17: Single unit cell with void inclusion (A_r=0.175 mm^2, ASP=3 and $\theta = 45°$) (dimensions 1 mm × 1 mm)

Modeling this unit cell yield a homogenised elastic modulus of $\bar{E}$ is 117.6 GPa. To verify if this elastic modulus is representative of macro level in dynamics, I consider modeling of 2 × 2, Figure 5.18a, (dimensions of 2 mm × 2 mm) and 4 × 4, Figure 5.18b, (dimensions of 4 mm × 4 mm) with a sudden constant dynamic load. Then elastic modulus obtained from single unit cell ($\bar{E}$=117.6 GPa) will be used along with analytical solutions from section 5.2.1 to predict the response of the 2 × 2 and 4 × 4 models. While the mass in the analytical solution is 4 times the mass of a single unit cell for the 2 × 2 model and 16 times for the 4 × 4 model.

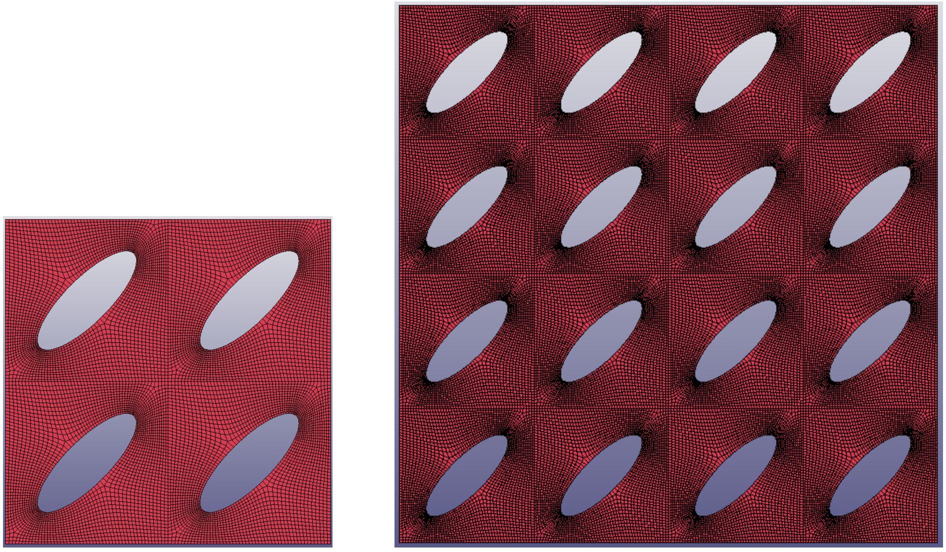

(a) 2×2 (b) 4×4

Figure 5.18: Macro models of 2×2 unit cells (a) and 4×4 unit cells

Figures 5.19 and 5.21 show the displacement vs time plots of the 2 × 2 and 4 × 4 macro levels respectively. It is noted that the prediction of the analytical solution (using single unit cell mechanical properties) matches very well with macro response for both models. On the other hand, Figures 5.20 and 5.22 show the velocity vs time plots of the 2 × 2 and 4 × 4 macro levels respectively. Similar to the displacements; velocity response of both cases can be captured with good accuracy using the homogenised elastic modulus of single unit cell and single degree of freedom solution.

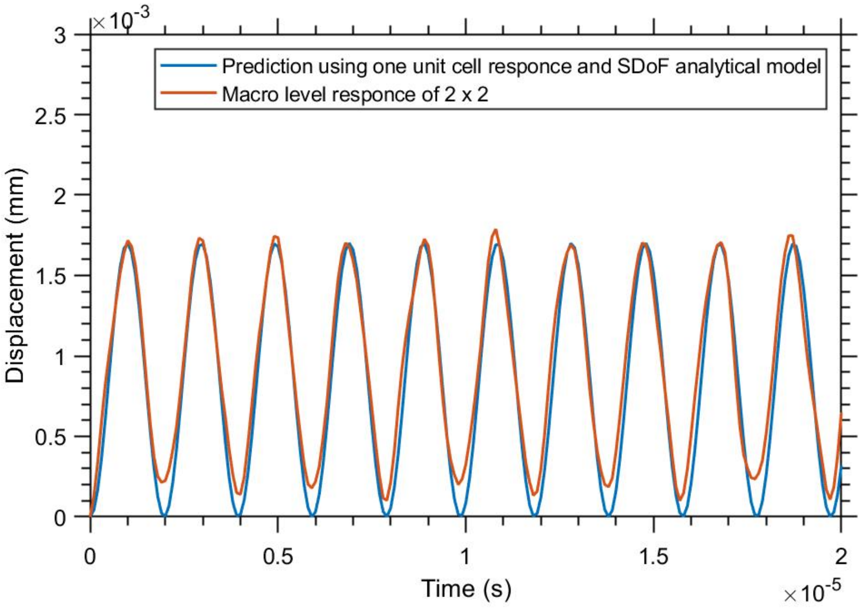

Figure 5.19: Displacement vs time due to a sudden load applied on an elastic 2 × 2 unit cell macro model with void inclusion (A_r=0.175 mm^2, ASP=3 and $\theta = 45°$)

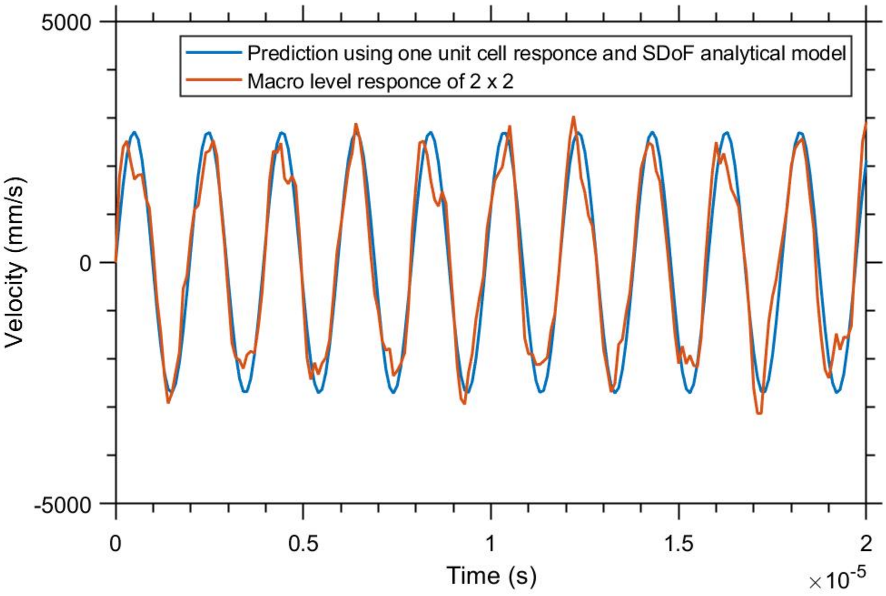

Figure 5.20: Velocity vs time due to a sudden load applied on an elastic 2 × 2 unit cell macro model with void inclusion (A_r=0.175 mm^2, ASP=3 and $\theta = 45°$)

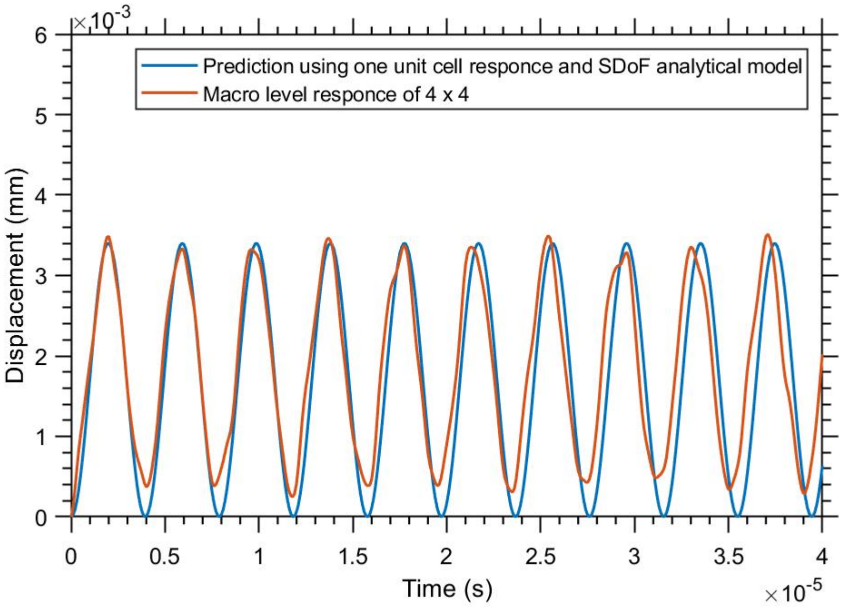

Figure 5.21: Displacement vs time due to a sudden load applied on an elastic 4 × 4 unit cell macro model with void inclusion (A_r=0.175 mm^2, ASP=3 and $\theta = 45°$)

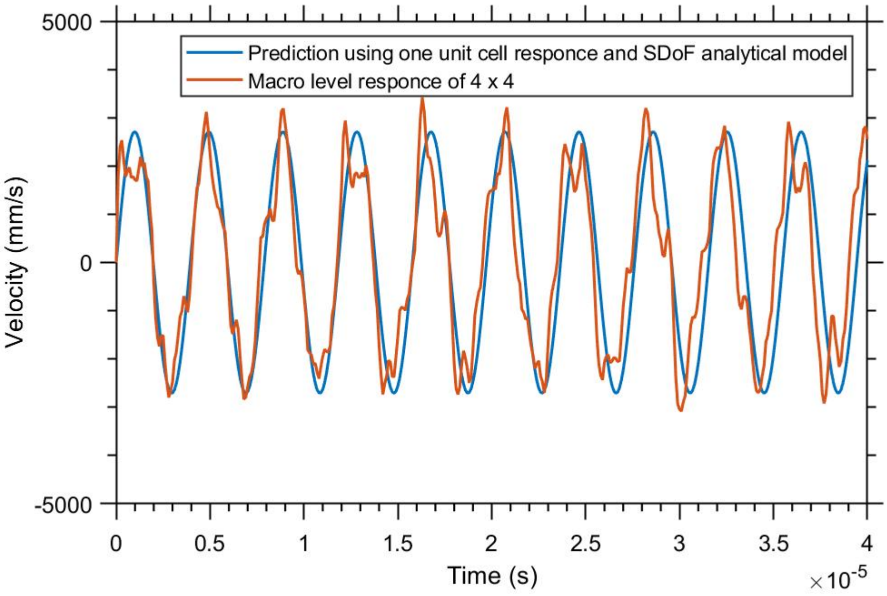

Figure 5.22: Velocity vs time due to a sudden load applied on an elastic 4 × 4 unit cell macro model with void inclusion (A_r=0.175 mm^2, ASP=3 and $\theta = 45°$)

Given the results obtained above, the homogenised elastic modulus of a single unit cell ($\bar{E}$=117.6 GPa) worked well in predicting the dynamic behaviour of 2 × 2 and 4 × 4 macro levels. Thus, a single unit cell can be considered as an RVE, in statics and dynamics, to obtain mechanical properties such as elastic modulus and dynamic viscosity. It is noted from the analysis in this section that this approach works very well with real engineering materials as the modeled material represent steel properties. High computational cost in both models was observed, namely 23 minutes for the 2 × 2 model and 108 minutes for the 4 × 4 model. This is due to two reasons, the large number of elements, and the relatively low density which resulted in smaller time step for the explicit analysis.

Chapter 6

Time Homogenisation

6.1 Introduction

To obtain the macro scale, homogenised, material properties from the solution of an RVE under dynamic loading might be challenging, due to the highly oscillatory response of homogenised stresses and strains. A *time averaging* approach is introduced in this chapter to smoothen the stress and strain curves and thus obtain the macro material properties (elastic modulus and dynamic viscosity) with less scope for ambiguity. The so-called *time homogenisation* or *time averaging* approach consists of averaging the space homogenised stress and strain in time and obtaining their physical meaning from relevant constitutive models. Similar to space averaging, the time averaging of a quantity ψ can be obtained by the following integral (Equation (6.1)); In which $\bar{\bar{\psi}}$ is the averaged quantity in time and space, and $\bar{\psi}$ is the space averaged quantity as defined by Equation (6.2).

$$\bar{\bar{\psi}} = \frac{1}{t} \int_{t_0}^{t} \bar{\psi}(t)\, dt \tag{6.1}$$

$$\bar{\psi} = \frac{1}{\Omega} \int\limits_{\Omega} \psi(x, y)\, d\Omega \tag{6.2}$$

In this chapter, the concept of time homogenisation is applied to elastic and viscoelastic unit cells with void inclusions, in addition to an elastic unit cell with a viscoelastic inclusion. It should be noted that the use of word ”homogenised” in this chapter is refereed to averaged quantities, not effective or representative quantities. A discussion of the physical meaning of time homogenised stress to strain ratio is presented for the three material models. Unit cells were tested with different loading conditions and the obtained time homogenised solution was compared to the corresponding behaviour under quasi static loading conditions. This approach can be employed to obtain material properties for desired dynamic behaviour with increased confidence compared to non-time homogenised results.

6.2 Time homogenisation of linear elastic unit cells

In a linear elastic unit cell, the homogenised elastic modulus in static loading conditions can be obtained via $\bar{E} = \frac{\bar{\sigma}}{\bar{\varepsilon}}$. Conversely, obtaining the homogenised elastic modulus from the space homogenised stresses and strain curves under dynamic loading is much more challenging due to the vibrations in strain and fluctuations of stress as shown in Figure 6.1. In particular, it is conceivable that singular results for the homogenised elastic modulus are obtained in case the homogenised strain happens to be near-zero for a particular time instant. Time homogenisation of stress and strain curves can be used to smoothen the fluctuations and yet obtain a reliable estimate of the homogenised elastic modulus.

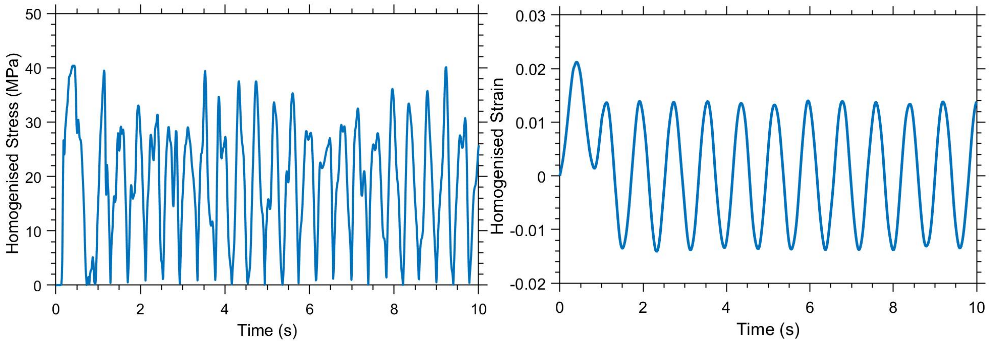

(a) (b)

Figure 6.1: Space homogenised stress (a) and strain (b)

To examine the concept of time homogenisation on elastic unit cells, a unit cell of elastic modulus 3300 MPa has been modeled under dynamic loading of pulse and a sudden constant loading. The time homogenised elastic modulus was estimated as follows:

$$\bar{\bar{E}} = \frac{\bar{\bar{\sigma}}}{\bar{\bar{\varepsilon}}} \tag{6.3}$$

where $\bar{\bar{\sigma}}$ is the time homogenised stress and $\bar{\bar{\varepsilon}}$ is the time homogenised strain, in which both values of $\bar{\bar{\sigma}}$ and $\bar{\bar{\varepsilon}}$ are obtained using Equation (6.1) taking $t_0 = 0$ s.

As shown below in Figure 6.2, the time homogenised elastic modulus from different loading conditions gives a reasonable estimate of the effective elastic modulus obtained from quasi-static loading. It can be seen, in particular for the case of a pulse load, that a certain time is required for the results to attain values within the vicinity of the benchmark results. This is due to the fact that the suggested time homogenisation is carried out up to the particular time instant of the analysis and a certain lead-in time is required before results start to stabilise.

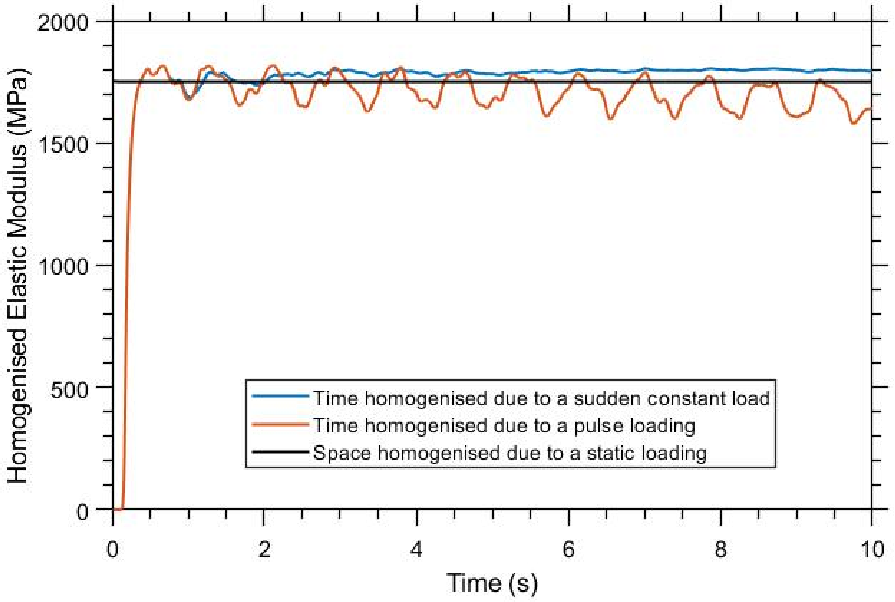

Figure 6.2: Homogenised elastic modulus vs time due to different loading conditions.

6.3 Time homogenisation of viscoelastic unit cells

The advantage of using time averaging is even more recognisable in viscoelastic unit cells since space homogenised stresses and strains are more fluctuating with time. In Maxwell viscoelastic unit cells, the relation between stresses and strains is governed by a differential equation as discussed in chapter 2 (section 2.6.2); therefore, it is not possible to write an independent mathematical expression for each of the material parameters. However, time homogenisation can be used to obtain expressions that are valid for specific loading conditions. To recall, the Maxwell viscoelastic equation reads as follows:

$$\sigma + \frac{\eta}{E}\dot{\sigma} = \eta\dot{\varepsilon} \tag{6.4}$$

so that the ratio between time homogenised stress $\bar{\bar{\sigma}}$ and $\bar{\bar{\varepsilon}}$ strain yields the following

$$\frac{\bar{\bar{\sigma}}}{\bar{\bar{\varepsilon}}} = \frac{\int_{t_0}^{t} \bar{\eta}\dot{\bar{\varepsilon}} - \frac{\bar{\eta}}{\bar{E}}\dot{\bar{\sigma}}\,dt}{\int_{t_0}^{t} \bar{\varepsilon}\,dt} \tag{6.5}$$

The right hand side of Equation (6.5) is dependent on the loading conditions, therefore the physical meaning of the ratio between time homogenised stress and strain is not a material property. In this section, the solution is presented for 2 loading cases, namely a constant sudden dynamic load (equivalent to creep test in quasi statics), and a sudden constant displacement (equivalent to relaxation test in quasi statics). Since the time homogenised results should eliminate the effect of inertia, an assumption has been made that the time homogenised stress rate is null in the case of constant force. Similarly, the time homogenised strain rate is assumed to be null in case of sudden constant displacement. In the case of a constant force Equation (6.5) reads as follows:

$$\frac{\bar{\bar{\sigma}}}{\bar{\bar{\varepsilon}}} = \frac{\int_{t_0}^{t} \bar{\eta}\dot{\bar{\varepsilon}}\,dt}{\int_{t_0}^{t} \bar{\varepsilon}\,dt} \tag{6.6}$$

Substituting $\bar{\varepsilon} = \frac{\sigma_0}{\bar{\eta}}t + \frac{\sigma_0}{\bar{E}}$ and its time derivative for $\dot{\bar{\varepsilon}}$ in Equation (6.6) that yields the following:

$$\frac{\bar{\bar{\sigma}}}{\bar{\bar{\varepsilon}}} = \frac{\int_{t_0}^{t} \sigma_0\,dt}{\int_{t_0}^{t} \frac{\sigma_0}{\bar{\eta}}t + \frac{\sigma_0}{\bar{E}}\,dt} = \frac{\bar{\eta}\bar{E}t}{\bar{E}t^2/2 + \bar{\eta}t} \tag{6.7}$$

In a constant displacement test, the stress rate $\dot{\bar{\sigma}}$ in Equation (6.5) can be written as the time derivative of the relaxation stress i.e. $\dot{\bar{\sigma}}(t) = -\frac{\bar{E}^2}{\bar{\eta}}\cdot\varepsilon_0\cdot e^{\frac{-\bar{E}}{\bar{\eta}}t}$. Therefore, the resulting Equation (6.8) is the basis for a physical interpretation of the ratio between time homogenised stress and strain for Maxwell viscoelastic unit cells under constant displacement.

$$\frac{\bar{\bar{\sigma}}}{\bar{\bar{\varepsilon}}} = \frac{\int_{t_0}^{t} -\frac{\bar{\eta}}{\bar{E}}\dot{\bar{\sigma}}\,dt}{\int_{t_0}^{t} \bar{\varepsilon}\,dt} = \frac{\int_{t_0}^{t} \bar{E}\varepsilon_0 e^{\frac{-\bar{E}}{\bar{\eta}}t}\,dt}{\int_{t_0}^{t} \varepsilon_0\,dt} = \frac{\bar{\eta}(1 - e^{\frac{-\bar{E}}{\bar{\eta}}t})}{t} \tag{6.8}$$

Taking the limit of t approaching zero of the right hand sides of Equations (6.7) and (6.8) gives

$$\lim_{t\to 0}\frac{\bar{\eta}\bar{E}t}{\bar{E}t^2/2+\bar{\eta}t}=\lim_{t\to 0}\frac{\bar{\eta}(1-e^{\frac{-\bar{E}}{\bar{\eta}}t})}{t}=\bar{E} \tag{6.9}$$

This can be viewed in Figures 6.3 and 6.4, where the ratio of time homogenised stress to strain due to a sudden constant load is compared with a creep test, and the time homogenised stress to strain ratio of a sudden displacement is compared to a relaxation test. Indeed, $\bar{\eta}$ can be estimated by fitting each figure to their mathematical formulation i.e. Equations 6.8 and 6.7, respectively. It is noted that there is a delay in the time homogenised response of both dynamic cases. This delay is believed to be the result of the time that stress waves require to propagate to the opposite support boundary. It is also noticeable that Figure 6.3 yield smother representation compared with Figure 6.4. This is believed to be due to nature of this material model, as the space homogenised stress which is used to generate Figure 6.4 is very noisy compared with the space homogenised strain as shown in Section D.3 of Appendix D (Figures D.9 and D.10).

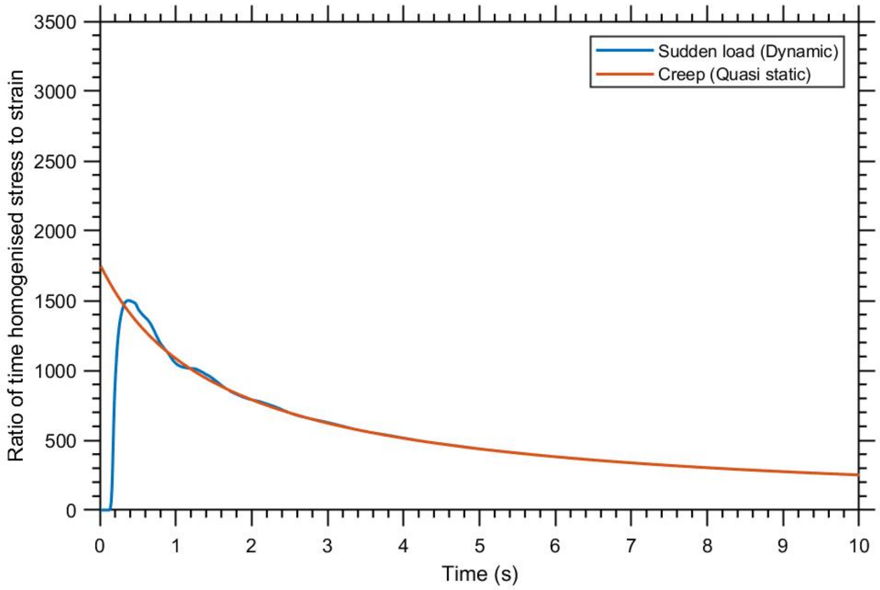

Figure 6.3: Ratio of time homogenised stress and strain vs time due to quasi static and dynamic loading.

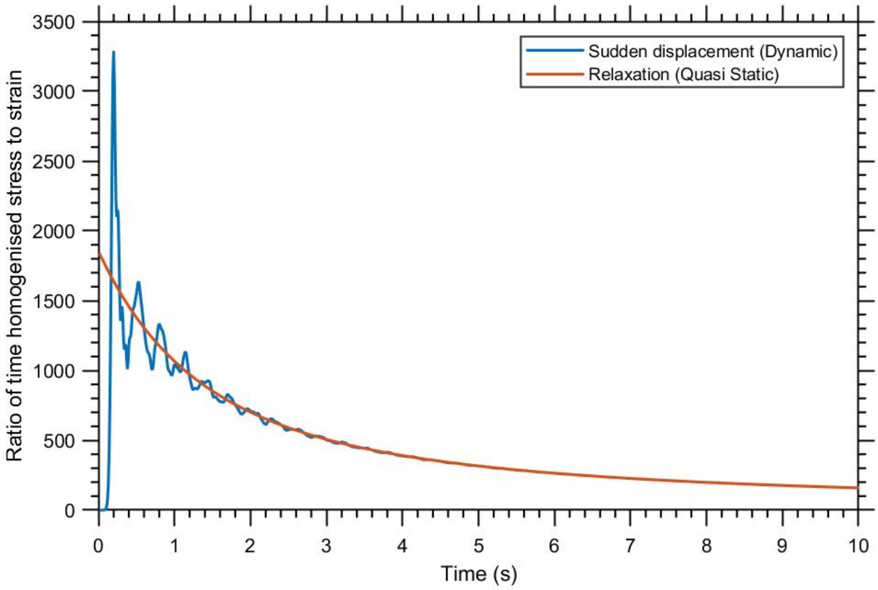

Figure 6.4: Ratio of time homogenised stress and strain vs time due to quasi static and dynamic constant displacements.

In loading conditions where neither stress rate nor strain rate can be assumed to be null, the time homogenisation approach can be applied to the constitutive model as follows:

$$\int_{t_0}^{t} \bar{\sigma}\, dt + \frac{\bar{\eta}}{\bar{E}} \int_{t_0}^{t} \bar{\dot{\sigma}}\, dt = \bar{\eta} \int_{t_0}^{t} \bar{\dot{\varepsilon}}\, dt \tag{6.10}$$

To obtain the homogenised material properties using Equation (6.10) numerically, an advanced curve fitting tool, such as neural network algorithms, should be used to fit the right and left hand sides of the equation and equate them to each other, thus an estimate of the homogenised material properties can be obtained.

6.4 Time homogenisation of composite unit cells

Similar to previous sections, the concept of time homogenisation is applied to the solutions of composite unit cells, which consist of an elastic matrix and a viscoelastic inclusion. The macro level constitutive model of such unit cells follows the standard solid model as follows:

$$\sigma + \frac{\bar{\eta}}{\bar{E}_0 - \bar{E}_\infty}\dot{\sigma} = \bar{E}_\infty \varepsilon + \left(1 + \frac{\bar{E}_\infty}{\bar{E}_0 - \bar{E}_\infty}\right)\bar{\eta}\dot{\varepsilon} \tag{6.11}$$

Since it is challenging to obtain a mathematical expression of the ratio between stress and strain from Equation (6.11), the focus of this section will be on special cases of constant sudden loading and constant sudden displacement. The ratio of time homogenised stress and strain due to a sudden constant load will be compared to a creep test. On the other hand, the ratio of time homogenised stress and strain due to a sudden constant displacement will be compared to a relaxation test. In a creep case the stress can be assumed to be σ_0 and strain is a function of time; therefore, $\bar{\bar{\sigma}}/\bar{\bar{\varepsilon}}$ can be written as follows:

$$\frac{\bar{\bar{\sigma}}}{\bar{\bar{\varepsilon}}} = \frac{\int_{t_0}^{t} \sigma_0 \, dt}{\int_{t_0}^{t} \bar{\varepsilon}(t) \, dt} \tag{6.12}$$

where $\bar{\varepsilon}(t) = \sigma_0 \left(\frac{1}{\bar{E}_0} - \frac{1}{\bar{E}_\infty}\right) e^{\frac{-\bar{E}_\infty(\bar{E}_0 - \bar{E}_\infty)}{(\bar{E}_0)\bar{\eta}}t} + \frac{\sigma_0}{\bar{E}_\infty}$; therefore, the denominator in Equation (6.12) reads as follows:

$$\int_{t_0}^{t} \bar{\varepsilon}(t) \, dt = \frac{\bar{E}_0 \bar{\eta} \sigma_0}{\bar{E}_\infty(\bar{E}_0 - \bar{E}_\infty)} \left(\frac{1}{\bar{E}_0} - \frac{1}{\bar{E}_\infty}\right) \left(1 - e^{\frac{-\bar{E}_\infty(\bar{E}_0 - \bar{E}_\infty)}{(\bar{E}_0)\bar{\eta}}t}\right) + \frac{\sigma_0}{\bar{E}_\infty} t \tag{6.13}$$

Substituting Equation (6.13) back in Equation (6.12) yields the following

$$\frac{\bar{\bar{\sigma}}}{\bar{\bar{\varepsilon}}} = \frac{t}{\frac{\bar{E}_0 \bar{\eta}}{\bar{E}_\infty(\bar{E}_0 - \bar{E}_\infty)} \left(\frac{1}{\bar{E}_0} - \frac{1}{\bar{E}_\infty}\right) \left(1 - e^{\frac{-\bar{E}_\infty(\bar{E}_0 - \bar{E}_\infty)}{(\bar{E}_0)\bar{\eta}}t}\right) + \frac{t}{\bar{E}_\infty}} \tag{6.14}$$

Similarly, the sudden constant displacement is compared with the relaxation test. In the quasi static relaxation loading conditions, the stress is given by $\bar{\sigma}(t) = (\bar{E}_0 - \bar{E}_\infty)\varepsilon_0 e^{\frac{-(\bar{E}_0 - \bar{E}_\infty)}{\bar{\eta}}t} + \bar{E}_\infty \varepsilon_0$. The ratio of time homogenised stress to strain can be written as:

$$\frac{\bar{\bar{\sigma}}}{\bar{\bar{\varepsilon}}} = \frac{\int_{t_0}^{t} (\bar{E}_0 - \bar{E}_\infty)\varepsilon_0 e^{\frac{-(\bar{E}_0 - \bar{E}_\infty)}{\bar{\eta}} t} + \bar{E}_\infty \varepsilon_0 \, dt}{\int_{t_0}^{t} \varepsilon_0 \, dt} = \frac{\bar{\eta}(1 - e^{\frac{-(\bar{E}_0 - \bar{E}_\infty)}{\bar{\eta}} t}) + \bar{E}_\infty t}{t} \tag{6.15}$$

The initial homogenised elastic modulus $\bar{E}_0$ can be obtained by taking the limit as t approaches zero of Equation (6.14) or (6.15).

$$\lim_{t \to 0} \frac{t}{\frac{\bar{E}_0 \bar{\eta}}{\bar{E}_\infty(\bar{E}_0 - \bar{E}_\infty)} \left(\frac{1}{\bar{E}_0} - \frac{1}{\bar{E}_\infty} \right) \left(1 - e^{\frac{-\bar{E}_\infty(\bar{E}_0 - \bar{E}_\infty)}{(\bar{E}_0)\bar{\eta}} t} \right) + \frac{t}{\bar{E}_\infty}} = \bar{E}_0 \tag{6.16}$$

$$\lim_{t \to 0} \frac{\bar{\eta}(1 - e^{\frac{-(\bar{E}_0 - \bar{E}_\infty)}{\bar{\eta}} t}) + \bar{E}_\infty t}{t} = \bar{E}_0 \tag{6.17}$$

Figure 6.5 shows the ratio of time homogenised stress to strain due to a sudden constant load and compares it with the quasi-static creep case. On the other hand, Figure 6.6 presents the time homogenised stress to strain due to a sudden constant displacement and compares it with the quasi-static relaxation case. In both loading conditions the time homogenised solution seems to work very well in approximating the quasi static response from the dynamic response.

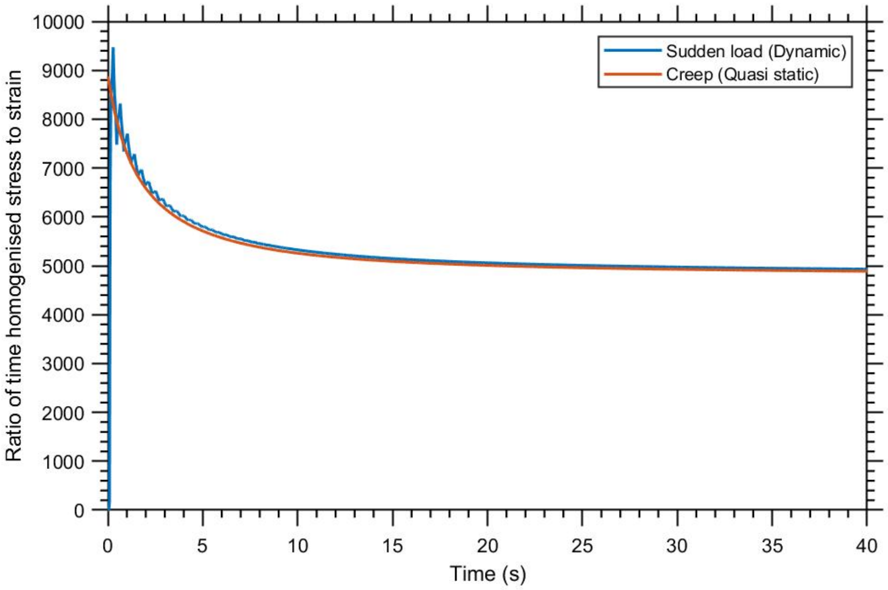

Figure 6.5: Ratio of time homogenised stress and strain vs time due to quasi static and dynamic loading.

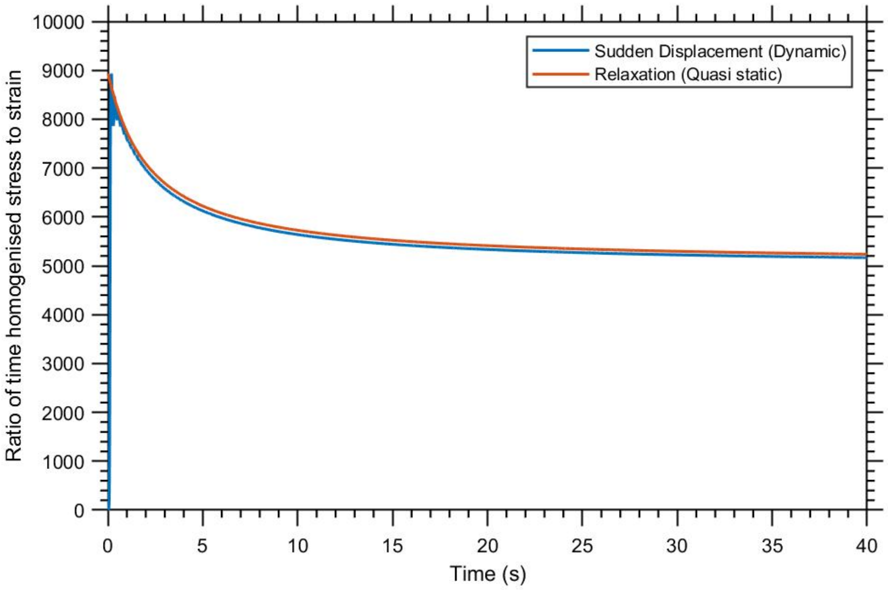

Figure 6.6: Ratio of time homogenised stress and strain vs time due to quasi static and dynamic constant displacements.

Similar to the previous section, the other homogenised material properties $\bar{\eta}$ and $\bar{E}_\infty$ can be extracted by curve fitting the time homogenised ratio curves to Equation (6.14) or Equation (6.15) respectively. In loading conditions where the stress and strain rates are not both null, Equation (6.18) can be used to apply time homogenisation:

$$\int_{t_0}^{t} \bar{\sigma}\, dt + \frac{\bar{\eta}}{\bar{E}_0 - \bar{E}_\infty} \int_{t_0}^{t} \dot{\bar{\sigma}}\, dt = \bar{E}_\infty \int_{t_0}^{t} \bar{\varepsilon}\, dt + \left(1 + \frac{\bar{E}_\infty}{\bar{E}_0 - \bar{E}_\infty}\right) \bar{\eta} \int_{t_0}^{t} \dot{\bar{\varepsilon}}\, dt \tag{6.18}$$

Similar to Equation (6.10), homogenised material properties can then be obtained via advance curve fitting tools.

Chapter 7

Conclusion and Future Research

7.1 Summary and evaluation

Numerical homogenisation can be used to understand the macro material properties of metamaterials with relatively low cost. Unit cells with a single void or with a viscous inclusion were modelled under periodic boundary conditions for quasi static loading conditions. Systematic parametric studies were conducted to investigate the effect of inclusion area, aspect ratio and inclination angle on the macroscopic material properties. In this thesis, the extension towards dynamic behaviour was also made; where linear elastic RVEs can be captured, with great accuracy, using numerical homogenisation. On the other hand, viscoelastic and composite RVEs dynamic behaviour can be captured with good accuracy. Finally, the concept of time homogenisation was introduced as novel concept to obtain effective material properties from the dynamic behaviour of the RVE.

The macroscopic material properties of elastic unit cells studied in this thesis can be captured with good accuracy using trigonometric functions, whereas the viscous unit cells show a multiplicative decomposition that consists of a linear elastic trigonometric function and a viscous exponential decay. Unit cells with voids show a macroscale constitutive model similar to the microscale one. On the other hand, the macroscale mechanical properties of the elastic unit cell with viscous inclusion show an enriched constitutive model at the macro level while using two simple models, linear elastic and Maxwell viscoelastic, for the micro level. This enriched macroscale behaviour can be captured accurately with the Standard Solid Model of viscoelasticity. Consistent results were obtained for creep and relaxation tests using a nonlinear regression curve fitting tool to fit stresses and strains with time and obtain the macroscale properties.

The analytical solution of the dynamic equation of motion can be used to simulate the dynamic behaviour of RVEs; where the spring and dashpot constants can be obtained from quasi static homogenised material properties. The homogenised material properties of elastic RVEs can be captured from dynamic loading response using the time homogenisation approach as shown in Chapter 6. Similarly, viscoelastic and composite RVEs effective properties can be obtained through time homogenisation; however, the ratio of time homogenised stress to strain, tends to depend somewhat on the strain and stress rates. Therefore, a distinctive expression was derived for 2 loading scenarios, which are a sudden constant displacement, and a sudden constant force. For the general case in which strain and stress rates are taken into account the time homogenised macro material model can be used to obtain the effective properties from any dynamic loading.

7.2 Potential Future Work

In this section, a discussion is presented on the potential future work along with some thoughts on their implementation. Potential development of this research can be made by considering 3D RVEs, where no conceptual difficulties are expected to do so. Therefore, exploring the anisotropic behaviour of RVEs and constructing a full constitutive matrix can be feasible. Furthermore, exploring the suitability of numerical homogenisation with alternative micro material models, such as nonlinear viscoelasticity, and unit cell microstructure would allow us to use this approach to study further metamaterials. In addition, consideration of further loading conditions, such as dynamic periodic loading, would help in understanding the behaviour of metamaterials in the frequency domain.

An improvement can be made to the homogenised solution of RVEs under dynamic loading, by implementing periodic boundary conditions. This can be made by defining an LS-DYNA user-defined element formulation of the *bipenalty method* as discussed in Section 3.3. A development to the time homogenisation approach can be made by implementing the concept to the full macro constitutive models, therefore, the concept can be used to study RVE under any dynamic loading where stress and strain rates are not null. This is possible by programming an advanced curve fitting tool or a neural network algorithm that is capable of fitting multiple independent variables.

Bibliography

[1] I. H. A. Abuzayed, Z. Ozdemir, and H. Askes. Time domain homogenisation of elastic and viscoelastic metamaterials. *Mechanics of time-dependent materials*, 2022.

[2] M. Al Nashar and A. Sutradhar. Design of hierarchical architected lattices for enhanced energy absorption. *Materials*, 14(18):5384, 2021.

[3] A. Almagableh and P. Raju M. Experimental and finite element modeling of vinyl ester nanocomposites under blast and quasi-static flexural loading. *J. Appl. Polym. Sci*, 126(6):1895–1905, 2012.

[4] M. Askari, D. A. Hutchins, P. J. Thomas, L. Astolfi, R. L. Watson, M. Abdi, M. Ricci, S. Laureti, L. Nie, S. Freear, R. Wildman, C. Tuck, M. Clarke, E. Woods, and A. T. Clare. Additive manufacturing of metamaterials: A review. *Additive manufacturing*, 36:101562, 2020.

[5] H. Askes, M. Caramés-Saddler, and A. Rodríguez-Ferran. Bipenalty method for time domain computational dynamics. *Proceedings of The Royal Society A*, 466(2117):1389–1408, 2010.

[6] H. Askes, A. Rodríguez-Ferran, and J. Hetherington. The effects of element shape on the critical time step in explicit time integrators for elastodynamics. *International journal for numerical methods in engineering*,

101(11):809–824, 2015.

[7] B. Audoly and Y. Pomeau. *Elasticity and geometry : from hair curls to the non-linear response of shells.* Oxford University Press, Oxford ; New York, 2010.

[8] E. Barchiesi, M. Spagnuolo, and L. Placidi. Mechanical metamaterials: a state of the art. *Mathematics and Mechanics of Solids*, 24(1):212–234, 2019.

[9] T. Belytschko and J. I. Lin. Eigenvalues and stable time steps for the bilinear mindlin plate element. *International journal for numerical methods in engineering*, 21(9):1729–1745, 1985.

[10] T. Belytschko, W. Liu, B. Moran, and K. Elkhodary. *Nonlinear Finite Elements for Continua and Structures.* Chichester, England : Wiley, 2014, Chichester, England, second edition. edition, 2014.

[11] T. Belytschko and M. O. Neal. Contact-impact by the pinball algorithm with penalty and lagrangian methods. *International journal for numerical methods in engineering*, 31(3):547–572, 1991.

[12] G. Bernhard. *Mathematical structure of the theories of viscoelasticity.* Hermann, Paris, 1953.

[13] K. Bertoldi, P. M. Reis, S. Willshaw, and T. Mullin. Negative poisson's ratio behavior induced by an elastic instability. *Advanced materials (Weinheim)*, 22(3):361–366, 2009.

[14] P. Broumand and A. R. Khoei. X-fem modeling of dynamic ductile fracture problems with a nonlocal damage-viscoplasticity model. *Finite elements in analysis and design*, 99:49–67, 2015.

[15] G. Bruno, A. M. Efremov, A. N. Levandovskyi, and B. Clausen. Con-

necting the macro- and microstrain responses in technical porous ceramics: modeling and experimental validations. *Journal of materials science*, 46(1):161–173, 2011.

[16] W. D. Callister and D. G. Rethwisch. *Materials science and engineering.* Wiley, Hoboken, New Jersey, ninth edition, si version. edition, 2015.

[17] A. Cangiani, G. Manzini, A. Russo, and N. Sukumar. Hourglass stabilization and the virtual element method. *Int. J. Numer. Meth. Engng*, 102(3-4):404–436, 2015.

[18] N. J. Carpenter, R. L. Taylor, and M. G. Katona. Lagrange constraints for transient finite element surface contact. *International journal for numerical methods in engineering*, 32(1):103–128, 1991.

[19] R. Castedo, C. Reifarth, A. P. Santos, J. Losada, L. M. López, M. Chiquito, and J. M. Mancilla. Application of grid convergence index to shock wave validated with ls-dyna and prosair. *Ing. Investig*, 39(3):20–26, 2019.

[20] H. Chen and B. W. Spencer. Peridynamic bond-associated correspondence model: Stability and convergence properties. *International journal for numerical methods in engineering*, 117(6):713–727, 2019.

[21] Q. Chen, X. Zhang, and B. Zhu. Design of buckling-induced mechanical metamaterials for energy absorption using topology optimization. *Structural and multidisciplinary optimization*, 58(4):1395–1410, 2018.

[22] Y. Chen and C. A. Schuh. Analytical homogenization method for periodic composite materials. *Physical review. B*, 79(9), 2009.

[23] A. K. Chopra. *Dynamics of structures : theory and applications to earthquake engineering.* Pearson Education, Harlow, 4th ed., international ed. edition, 2014.

[24] K. Davami, M. Mohsenizadeh, M. Munther, T. Palma, A. Beheshti, and K. Momeni. Dynamic energy absorption characteristics of additively-manufactured shape-recovering lattice structures. *Materials Research Express*, 6(4):45302, 2019.

[25] F. Devries, H. Dumontet, G. Duvaut, and F. Lene. Homogenization and damage for composite structures. *Int. J. Numer. Meth. Engng*, 27(2):285–298, 1989.

[26] J. D. Eshelby. The determination of the elastic field of an ellipsoidal inclusion, and related problems. *Proceedings of the Royal Society of London. Series A, Mathematical and Physical Sciences*, 241(1226):376–396, 1957.

[27] F. Feyel and J. L. Chaboche. Fe2 multiscale approach for modelling the elastoviscoplastic behaviour of long fibre sic/ti composite materials. *Computer methods in applied mechanics and engineering*, 183(3-4):309–330, 2000.

[28] J. Fish, Q. Yu, and K. Shek. Computational damage mechanics for composite materials based on mathematical homogenization. *International Journal for Numerical Methods in Engineering*, 45(11):1657–1679, 1999.

[29] D. P. Flanagan and T. Belytschko. A uniform strain hexahedron and quadrilateral with orthogonal hourglass control. *International Journal for Numerical Methods in Engineering*, 17(5):679–706, 1981.

[30] M. G. D. Geers, V. G. Kouznetsova, and W. A. M. Brekelmans. Multi-scale computational homogenization: Trends and challenges. *Journal of Computational and Applied Mathematics*, 234(7):2175–2182, 2010.

[31] I. M. Gitman. *Representative Volumes and Multi-scale Modelling of Quasi-brittle Materials.* Thesis, Delft University of Technology, 2006.

[32] I. M. Gitman, H. Askes, and L. J. Sluys. Representative volume: Existence

and size determination. *Engineering Fracture Mechanics*, 74(16):2518–2534, 2007.

[33] S. Gourdin, L. Marcin, M. Podgorski, M. Cherif, and L. Carroz. Effective elastic properties and residual stresses in directionally solidified eutectic al2o3/yag/zro2 ceramics estimated by finite element analysis. *Journal of materials science*, 52(24):13736–13747, 2017.

[34] V. V. Gozhenko, A. K. Amert, and K. W. Whites. Homogenization of periodic metamaterials by field averaging over unit cell boundaries: use and limitations. *New Journal of Physics*, 15(4):043030, apr 2013.

[35] A. Grama. *Introduction to parallel computing.* Addison-Wesley, Harlow, 2nd ed. edition, 2003.

[36] J. N. Grima and R. Caruana-Gauci. Mechanical metamaterials: Materials that push back. *Nature materials*, 11(7):565–566, 2012.

[37] R. Gümrük, R. A. W. Mines, and S. Karadeniz. Determination of strain rate sensitivity of micro-struts manufactured using the selective laser melting method. *Journal of materials engineering and performance*, 27(3):1016–1032, 2018.

[38] F. Habib, P. Iovenitti, S. Masood, M. Nikzad, and D. Ruan. Design and evaluation of 3d printed polymeric cellular materials for dynamic energy absorption. *International journal of advanced manufacturing technology*, 103(5):2347–2361, 2019.

[39] J. O. Hallquist. *LS-DYNA Theory Manual.* Livermore Software Technology Corporation (LSTC), Livermore, 2016.

[40] Z. Hashin. The elastic moduli of heterogeneous materials. *Journal of applied mechanics*, 29(1):143–150, 1962.

[41] Z. Hashin. Analysis of Composite Materials—A Survey. *Journal of Applied Mechanics*, 50(3):481–505, 09 1983.

[42] Z. Hashin and S. Shtrikman. A variational approach to the theory of the elastic behaviour of multiphase materials. *Journal of the mechanics and physics of solids*, 11(2):127–140, 1963.

[43] J. Hetherington and H. Askes. Penalty methods for time domain computational dynamics based on positive and negative inertia. *Computers & structures*, 87(23):1474–1482, 2009.

[44] J. Hetherington, A. Rodríguez-Ferran, and H. Askes. A new bipenalty formulation for ensuring time step stability in time domain computational dynamics. *International journal for numerical methods in engineering*, 90(3):269–286, 2012.

[45] J. Hetherington, A. Rodríguez-Ferran, and H. Askes. The bipenalty method for arbitrary multipoint constraints. *International journal for numerical methods in engineering*, 93(5):465–482, 2013.

[46] T. A. M. Hewage, K. L. Alderson, A. Alderson, and F. Scarpa. Double-negative mechanical metamaterials displaying simultaneous negative stiffness and negative poisson's ratio properties. *Advanced materials (Weinheim)*, 28(46):10323–10332, 2016.

[47] R. Hill. Elastic properties of reinforced solids: Some theoretical principles. *Journal of the mechanics and physics of solids*, 11(5):357–372, 1963.

[48] R. Hill. On macroscopic effects of heterogeneity in elastoplastic media at finite strain. *Mathematical Proceedings of the Cambridge Philosophical Society*, 95(3):481–494, 1984.

[49] S. A. N. M. Hossain and I. Tsukerman. Non-asymptotic homogenization of

3-d periodic structures. *Physics Letters A*, 398:127278, 2021.

[50] J. Hua, H. Lei, C. F. Gao, X. Guo, and D. Fang. Parameters analysis and optimization of a typical multistable mechanical metamaterial. *Extreme Mechanics Letters*, 35:100640, 2020.

[51] T. J. R. Hughes. *The finite element method : linear static and dynamic finite element analysis*. Dover, Mineola, N.Y., rev. ed. edition, 2000.

[52] M. I. Hussein, M. J. Leamy, and M. Ruzzene. Dynamics of Phononic Materials and Structures: Historical Origins, Recent Progress, and Future Outlook. *Applied Mechanics Reviews*, 66(4), 05 2014.

[53] S. Ilanko. Existence of natural frequencies of systems with artificial restraints and their convergence in asymptotic modelling. *Journal of sound and vibration*, 255(5):883–898, 2002.

[54] S. Ilanko. Introducing the use of positive and negative inertial functions in asymptotic modelling. *Proceedings of The Royal Society A*, 461(2060):2545–2562, 2005.

[55] M. Jamshidinia, F. Kong, and R. Kovacevic. The numerical modeling of fatigue properties of a biocompatible dental implant produced by electron beam melting (ebm). In *International Solid Freeform Fabrication Symposium*. University of Texas at Austin, 2013.

[56] S. Janbaz, K. Narooei, T. van Manen, and A. A. Zadpoor. Strain rate-dependent mechanical metamaterials. *Science advances*, 6(25):eaba0616–eaba0616, 2020.

[57] T. Kanit, S. Forest, I. Galliet, V. Mounoury, and D. Jeulin. Determination of the size of the representative volume element for random composites: statistical and numerical approach. *International Journal of Solids and*

Structures, 40(13):3647–3679, 2003.

[58] D. M. Kochmann, J. B. Hopkins, and L. Valdevit. Multiscale modeling and optimization of the mechanics of hierarchical metamaterials. *Mrs Bulletin*, 44(10):773–781, 2019.

[59] B. Koohbor, S. Ravindran, and Kidane A. Experimental determination of representative volume element (rve) size in woven composites. *Optics and Lasers in Engineering*, 90:59–71, 2017.

[60] V. G. Kouznetsova, W. A. M. Brekelmans, and F. P. T. Baaijens. An approach to micro-macro modeling of heterogeneous materials. *Computational mechanics*, 27(1):37–48, 2001.

[61] R. S. Kshetrimayum. A brief intro to metamaterials. *IEEE potentials*, 23(5):44–46, 2004.

[62] S. Lee, F. Barthelat, J. W. Hutchinson, and H. D. Espinosa. Dynamic failure of metallic pyramidal truss core materials – experiments and modeling. *International journal of plasticity*, 22(11):2118–2145, 2006.

[63] Y. M. Li, M. P. Hoang, B. Abbes, F. Abbes, and Y. Q. Guo. Analytical homogenization for stretch and bending of honeycomb sandwich plates with skin and height effects. *Composite Structures*, 120:406–416, 2015.

[64] X. Lijun and S. Weidong. Additively-manufactured functionally graded ti-6al-4v lattice structures with high strength under static and dynamic loading: Experiments. *International journal of impact engineering*, 111:255–272, 2018.

[65] C. Liu and C. Reina. Variational coarse-graining procedure for dynamic homogenization. *Journal of the Mechanics and Physics of Solids*, 104:187–206, 2017.

[66] C. Liu and C. Reina. Dynamic homogenization of resonant elastic metamaterials with space/time modulation. *Computational mechanics*, 64(1):147–161, 2018.

[67] Y. Liu, J. Yuan, L. Dong, and F. Huang. Radiation characteristics of a reflector antenna under shock wave loading. *International journal of nonlinear sciences and numerical simulation*, 13(1):75–79, 2012.

[68] Z. Liu, X. Zhang, Y. Mao, Y. Y. Zhu, Z. Yang, C. T. Chan, and P. Sheng. Locally resonant sonic materials. *Science*, 289(5485):1734–1736, 2000.

[69] J. Luo, D. W. Shu, B. J. Shi, Q. Y. Ng, R. Zambri, and J. H. Lau. Study of the shock response of the hdd with ansys-lsdyna. *Journal of magnetism and magnetic materials*, 303(2):e57–e61, 2006.

[70] George Thomas Mase, George E. Mase, and Ronald E. Smelser. *Continuum mechanics for engineers.* CRC series in computational mechanics and applied analysis. CRC Press, an imprint of Taylor and Francis, Boca Raton, FL, third edition. edition, 2009.

[71] I. Maskery, A. O. Aremu, L. Parry, R. D. Wildman, C. J. Tuck, and I. A. Ashcroft. Effective design and simulation of surface-based lattice structures featuring volume fraction and cell type grading. *Materials & design*, 155:220–232, 2018.

[72] C. Miehe, J. Schröder, and J. Schotte. Computational homogenization analysis in finite plasticity simulation of texture development in polycrystalline materials. *Computer methods in applied mechanics and engineering*, 171(3):387–418, 1999.

[73] S. M. Mirkhalaf, P. F. M. Andrade, and R. Simoes. Determination of the size of the representative volume element (rve) for the simulation of

heterogeneous polymers at finite strains. *Finite Elements in Analysis and Design*, 119:30–44, 2016.

[74] A. Molinari and S. Mercier. Micromechanical modelling of porous materials under dynamic loading. *Journal of the Mechanics and Physics of Solids*, 49(7):1497–1516, 2001.

[75] H. Nassar, Q. C. He, and N. Auffray. Willis elastodynamic homogenization theory revisited for periodic media. *Journal of the Mechanics and Physics of Solids*, 77:158–178, 2015.

[76] V. P. Nguyen, O. L. Valls, M. Stroeven, and L. J. Sluys. On the existence of representative volumes for softening quasi-brittle materials – a failure zone averaging scheme. *Computer Methods in Applied Mechanics and Engineering*, 199(45):3028–3038, 2010.

[77] Z. G. Nicolaou and A. E. Motter. Mechanical metamaterials with negative compressibility transitions. *Nature materials*, 11(7):608–613, 2012.

[78] J. A. Oliveira, J. Pinho-da Cruz, and Teixeira-Dias F. Asymptotic homogenisation in linear elasticity. part ii: Finite element procedures and multiscale applications. *Computational Materials Science*, 45(4):1081–1096, 2009.

[79] S. L. Omairey, P. D. Dunning, and S. Sriramula. Development of an abaqus plugin tool for periodic rve homogenisation. *Engineering with computers*, 35(2):567–577, 2018.

[80] Z. Ozdemir, E. Hernandez-Nava, A. Tyas, J. A. Warren, S. D. Fay, R. Goodall, I. Todd, and H. Askes. Energy absorption in lattice structures in dynamics: Experiments. *International journal of impact engineering*, 89:49–61, 2016.

[81] Z. Ozdemir, A. Tyas, R. Goodall, and H. Askes. Energy absorption in lattice structures in dynamics: Nonlinear fe simulations. *International journal of impact engineering*, 102:1–15, 2017.

[82] P. Pacheco. *An Introduction to Parallel Programming*. Morgan Kaufmann Publishers Inc., San Francisco, CA, USA, 1st edition, 2011.

[83] C. Pelissou, J. Baccou, Y. Monerie, and F. Perales. Determination of the size of the representative volume element for random quasi-brittle composites. *International Journal of Solids and Structures*, 46(14):2842–2855, 2009.

[84] K. Pham, V. G. Kouznetsova, and M. G. D. Geers. Transient computational homogenization for heterogeneous materials under dynamic excitation. *Journal of the Mechanics and Physics of Solids*, 61(11):2125–2146, 2013.

[85] J. Pinho-da Cruz, J. A. Oliveira, and F. Teixeira-Dias. Asymptotic homogenisation in linear elasticity. part i: Mathematical formulation and finite element modelling. *Computational Materials Science*, 45(4):1073–1080, 2009.

[86] S. E. Rigby, A. Tyas, T. Bennett, S. D. Clarke, and S. D. Fay. The negative phase of the blast load. *International journal of protective structures*, 5(1):1–19, 2014.

[87] D. Roca, O. Lloberas-Valls, J. Cante, and J. Oliver. A computational multiscale homogenization framework accounting for inertial effects: Application to acoustic metamaterials modelling. *Computer methods in applied mechanics and engineering*, 330:415–446, 2018.

[88] M. Sahli, C. K. Malek, and J. C. Gelin. 3d modelling and simulation

of the filling of cavities by viscoelastic polymer in roll embossing process. *International Journal of Material Forming*, 2(Suppl 1):725–728, 2009.

[89] F. Scarpa, L. G. Ciffo, and J. R. Yates. Dynamic properties of high structural integrity auxetic open cell foam. *Smart materials and structures*, 13(1):49–56, 2004.

[90] A. Sciegaj, P. Grassl, F. Larsson, K. Runesson, and K. Lundgren. Upscaling of three-dimensional reinforced concrete representative volume elements to effective beam and plate models. *International journal of solids and structures*, 202:835–853, 2020.

[91] Q. H. Shah. Impact resistance of a rectangular polycarbonate armor plate subjected to single and multiple impacts. *International journal of impact engineering*, 36(9):1128–1135, 2009.

[92] C. Sharpe, C. C. Seepersad, S. Watts, and D. Tortorelli. Design of mechanical metamaterials via constrained bayesian optimization. volume Volume 2A: 44th Design Automation Conference of *International Design Engineering Technical Conferences and Computers and Information in Engineering Conference*. The American Society of Mechanical Engineers, 08 2018.

[93] C. F. Sieck, A. Alù, and M. R. Haberman. Dynamic homogenization of acoustic metamaterials with coupled field response. *Physics Procedia*, 70:275–278, 2015. Proceedings of the 2015 ICU International Congress on Ultrasonics, Metz, France.

[94] P. Siegkas, D. J. Sharp, and M. Ghajari. The traumatic brain injury mitigation effects of a new viscoelastic add-on liner. *Sci Rep*, 9(1):3471–3471, 2019.

[95] R. J. M. Smit, W. A. M. Brekelmans, and H. E. H. Meijer. Prediction

of the mechanical behavior of nonlinear heterogeneous systems by multi-level finite element modeling. *Computer methods in applied mechanics and engineering*, 155(1):181–192, 1998.

[96] M. Smith, W. J. Cantwell, Z. Guan, S. Tsopanos, M. D. Theobald, G. N. Nurick, and G. S. Langdon. The quasi-static and blast response of steel lattice structures. *The journal of sandwich structures & materials*, 13(4):479–501, 2011.

[97] J. U. Surjadi, L. Gao, H. Du, X. Li, X. Xiong, N. X. Fang, and Y. Lu. Mechanical metamaterials and their engineering applications. *Advanced engineering materials*, 21(3):1800864–n/a, 2019.

[98] D. J. Sypeck and H. N. G. Wadley. Multifunctional microtruss laminates: Textile synthesis and properties. *J. Mater. Res*, 16(3):890–897, 2001.

[99] T. Tancogne-Dejean, M. Diamantopoulou, M. B. Gorji, C. Bonatti, and D. Mohr. 3d plate-lattices: An emerging class of low-density metamaterial exhibiting optimal isotropic stiffness. *Advanced Materials*, 30(45), 2018.

[100] K. Terada and N. Kikuchi. Nonlinear homogenization method for practical applications. *American Society of Mechanical Engineers, Applied Mechanics Division, AMD*, 212:1–16, 1995.

[101] A. Toledano and H. Murakami. A high-order mixture model for periodic particulate composites. *International journal of solids and structures*, 23(7):989–1002, 1987.

[102] O. van der Sluis, P. J. G. Schreurs, W. A. M. Brekelmans, and H. E. H. Meijer. Overall behaviour of heterogeneous elastoviscoplastic materials: effect of microstructural modelling. *Mechanics of materials*, 32(8):449–462, 2000.

[103] O. van der Sluis, P. J. G. Schreurs, and H. E. H. Meijer. Homogenisation of structured elastoviscoplastic solids at finite strains. *Mechanics of materials*, 33(9):499–522, 2001.

[104] Flugge W. *Viscoelasticity.* Springer-Verlag, Berlin ; New York, 2nd rev. ed. edition, 1975.

[105] G. Wang. An efficient analytical homogenization technique for mechanical-hygrothermal responses of unidirectional composites with applications to optimization and multiscale analyses. *Chinese Journal of Aeronautics*, 32(2):382–395, 2019.

[106] C. Willberg, S. Duczek, J. M. Vivar-Perez, and Z. A. B. Ahmad. Simulation methods for guided wave-based structural health monitoring: A review. *Applied mechanics reviews*, 67(1), 2015.

[107] R. E. Winter, M. Cotton, E. J. Harris, D. E. Eakins, and G. McShane. High resolution simulations of energy absorption in dynamically loaded cellular structures. *Shock waves*, 27(2):221–236, 2017.

[108] S. Yan, J. Deng, C. Bae, S. Kalnaus, and X. Xiao. Orthotropic viscoelastic modeling of polymeric battery separator. *J. Electrochem. Soc*, 167(9):90530, 2020.

[109] H. Yang, B. E. Abali, D. Timofeev, and W. H. Müller. Determination of metamaterial parameters by means of a homogenization approach based on asymptotic analysis. *Continuum mechanics and thermodynamics*, 32(5):1251–1270, 2019.

[110] H. Yang and W. H. Müller. Size effects of mechanical metamaterials: a computational study based on a second-order asymptotic homogenization method. *Archive of applied mechanics (1991)*, 91(3):1037–1053, 2020.

[111] W. Yu. An introduction to micromechanics. *Applied mechanics and materials*, 828:3–24, 2016.

[112] X. Yu, J. Zhou, H. Liang, Z. Jiang, and L. Wu. Mechanical metamaterials associated with stiffness, rigidity and compressibility: A brief review. *Progress in materials science*, 94:114–173, 2018.

[113] Y. Zheng, Y. Wang, X. Lu, Z. Liao, and J. Qu. Evolutionary topology optimization for mechanical metamaterials with auxetic property. *International journal of mechanical sciences*, 179:105638, 2020.

[114] F. Zhu, G. Lu, D. Ruan, and Z. Wang. Plastic deformation, failure and energy absorption of sandwich structures with metallic cellular cores. *International journal of protective structures*, 1(4):507–541, 2010.

Appendix A

Script samples

A.1 Periodic boundary conditions function

```
%periodic boundary conditions
up=nod(ynod==+Lx/2);        % Support Nodes
Do=nod(ynod==-Lx/2);
[length(S),length(D),length(up),length(Do)]
S=sortrows(([S,ynod(S)]),2);
D=sortrows(([D,ynod(D)]),2);
up=sortrows(([up,xnod(up)]),2);
Do=sortrows(([Do,xnod(Do)]),2);
fid4 = fopen('Periodic_BC.k','wt');
sn=0;
for ix=[2:size(S)-1];
    sn=sn+1;
    cn=string(sn);
    cm=string(D(length(D)));
    c1=string(D(ix));
    c2=string(S(ix));
    fprintf(fid4,'*CONSTRAINED_MULTIPLE_GLOBAL\n');
    fprintf(fid4,cn);
    fprintf(fid4,'\n3\n');
    fprintf(fid4,cm);
    fprintf(fid4,',1,-1.00\n');
    fprintf(fid4,c1);
    fprintf(fid4,',1,+1.00\n');
    fprintf(fid4,c2);
    fprintf(fid4,',1,-1.00\n');
    sn=sn+1;
    cn=string(sn);
    fprintf(fid4,'*CONSTRAINED_MULTIPLE_GLOBAL\n');
    fprintf(fid4,cn);
    fprintf(fid4,'\n2\n');
    fprintf(fid4,c1);
    fprintf(fid4,',2,+1.00\n');
    fprintf(fid4,c2);
    fprintf(fid4,',2,-1.00\n');
end
for iy=[2:size(up)-1];
    sn=sn+1;
    cn=string(sn);
    cy1=string(up(iy));
    cy2=string(Do(iy));
    fprintf(fid4,'*CONSTRAINED_MULTIPLE_GLOBAL\n');
    fprintf(fid4,cn);
    fprintf(fid4,'\n2\n');
    fprintf(fid4,cy1);
    fprintf(fid4,',1,+1.00\n');
    fprintf(fid4,cy2);
    fprintf(fid4,',1,-1.00\n');
    sn=sn+1;
    cn=string(sn);
    fprintf(fid4,'*CONSTRAINED_MULTIPLE_GLOBAL\n');
    fprintf(fid4,cn);
    fprintf(fid4,'\n2\n');
    fprintf(fid4,cy1);
    fprintf(fid4,',2,+1.00\n');
    fprintf(fid4,cy2);
    fprintf(fid4,',2,-1.00\n');
end
fprintf(fid4, '*END');
fclose(fid4);
```

A.2 Abaqus python script

```
# Elepse size
x1=0.28906
y1=0.28906
x2=-0.096354
y2=0.096354
#
from abaqus import *
from abaqusConstants import *
import __main__
import section
import regionToolset
import displayGroupMdbToolset as dgm
import part
import material
import assembly
import step
import interaction
import load
import mesh
import optimization
import job
import sketch
import visualization
import xyPlot
import displayGroupOdbToolset as dgo
import connectorBehavior
s1 = ...
    mdb.models['Model-1'].ConstrainedSketch(name='__profile__', ...
    sheetSize=5.0)
g, v, d, c = s1.geometry, s1.vertices, s1.dimensions, ...
    s1.constraints
s1.setPrimaryObject(option=STANDALONE)
s1.rectangle(point1=(0.5, 0.5), point2=(-0.5, -0.5))
s1.EllipseByCenterPerimeter(center=(0.0, 0.0), ...
    axisPoint1=(x1, y1),
     axisPoint2=(x2, y2))
p = mdb.models['Model-1'].Part(name='Part-1', ...
    dimensionality=THREE_D,
     type=DEFORMABLE_BODY)
p = mdb.models['Model-1'].parts['Part-1']
p.BaseShell(sketch=s1)
s1.unsetPrimaryObject()
p = mdb.models['Model-1'].parts['Part-1']
session.viewports['Viewport: 1'].setValues(displayedObject=p)
del mdb.models['Model-1'].sketches['__profile__']
a = mdb.models['Model-1'].rootAssembly
session.viewports['Viewport: 1'].setValues(displayedObject=a)
a = mdb.models['Model-1'].rootAssembly
a.DatumCsysByDefault(CARTESIAN)
p = mdb.models['Model-1'].parts['Part-1']
a.Instance(name='Part-1-1', part=p, dependent=ON)
p = mdb.models['Model-1'].parts['Part-1']
session.viewports['Viewport: 1'].setValues(displayedObject=p)
a = mdb.models['Model-1'].rootAssembly
session.viewports['Viewport: 1'].setValues(displayedObject=a)
session.viewports['Viewport: ...
    1'].assemblyDisplay.setValues(loads=ON, bcs=ON,
     predefinedFields=ON, connectors=ON)
session.viewports['Viewport: ...
    1'].assemblyDisplay.setValues(mesh=ON, loads=OFF,
     bcs=OFF, predefinedFields=OFF, connectors=OFF)
session.viewports['Viewport: ...
    1'].assemblyDisplay.meshOptions.setValues(
     meshTechnique=ON)
p = mdb.models['Model-1'].parts['Part-1']
session.viewports['Viewport: 1'].setValues(displayedObject=p)
session.viewports['Viewport: 1'].partDisplay.setValues(mesh=ON)
session.viewports['Viewport: ...
    1'].partDisplay.meshOptions.setValues(
     meshTechnique=ON)
session.viewports['Viewport: ...
    1'].partDisplay.geometryOptions.setValues(
     referenceRepresentation=OFF)
p = mdb.models['Model-1'].parts['Part-1']
e = p.edges
pickedEdges = e.getSequenceFromMask(mask=('[#4 ]', ), )
p.seedEdgeBySize(edges=pickedEdges, size=0.02, ...
    deviationFactor=0.01,
     constraint=FIXED)
p = mdb.models['Model-1'].parts['Part-1']
e = p.edges
pickedEdges = e.getSequenceFromMask(mask=('[#8 ]', ), )
p.seedEdgeBySize(edges=pickedEdges, size=0.02, ...
    deviationFactor=0.1,
     constraint=FIXED)
p = mdb.models['Model-1'].parts['Part-1']
e = p.edges
pickedEdges = e.getSequenceFromMask(mask=('[#10 ]', ), )
```

```
p.seedEdgeBySize(edges=pickedEdges, size=0.02, ...
    deviationFactor=0.1,
     constraint=FIXED)
p = mdb.models['Model-1'].parts['Part-1']
e = p.edges
pickedEdges = e.getSequenceFromMask(mask=('[#2 ]', ), )
p.seedEdgeBySize(edges=pickedEdges, size=0.02, ...
    deviationFactor=0.1,
     constraint=FIXED)
p = mdb.models['Model-1'].parts['Part-1']
e = p.edges
pickedEdges = e.getSequenceFromMask(mask=('[#1 ]', ), )
p.seedEdgeBySize(edges=pickedEdges, size=0.02, ...
    deviationFactor=0.1)
p = mdb.models['Model-1'].parts['Part-1']
e = p.edges
pickedEdges = e.getSequenceFromMask(mask=('[#1 ]', ), )
p.seedEdgeBySize(edges=pickedEdges, size=0.02, ...
    deviationFactor=0.01)
p = mdb.models['Model-1'].parts['Part-1']
f = p.faces
pickedRegions = f.getSequenceFromMask(mask=('[#1 ]', ), )
p.setMeshControls(regions=pickedRegions, elemShape=QUAD, ...
    algorithm=MEDIAL_AXIS)
p = mdb.models['Model-1'].parts['Part-1']
p.generateMesh()
a = mdb.models['Model-1'].rootAssembly
a.regenerate()
a = mdb.models['Model-1'].rootAssembly
session.viewports['Viewport: 1'].setValues(displayedObject=a)
session.viewports['Viewport: ...
    1'].assemblyDisplay.setValues(mesh=OFF)
session.viewports['Viewport: ...
    1'].assemblyDisplay.meshOptions.setValues(
    meshTechnique=OFF)
mdb.Job(name='Job-1', model='Model-1', description='', ...
    type=ANALYSIS,
    atTime=None, waitMinutes=0, waitHours=0, queue=None, ...
        memory=90,
    memoryUnits=PERCENTAGE, getMemoryFromAnalysis=True,
    explicitPrecision=SINGLE, nodalOutputPrecision=SINGLE, ...
        echoPrint=OFF,
    modelPrint=OFF, contactPrint=OFF, historyPrint=OFF, ...
        userSubroutine='',
    scratch='', resultsFormat=ODB, ...
        parallelizationMethodExplicit=DOMAIN,
    numDomains=1, activateLoadBalancing=False, ...
        multiprocessingMode=DEFAULT,
    numCpus=1, numGPUs=0)
mdb.jobs['Job-1'].writeInput(consistencyChecking=OFF)
```

A.3 LS-DYNA input file

```
*KEYWORD
*TITLE
0-plastic
*CONTROL_TERMINATION
20,
*CONTROL_IMPLICIT_SOLUTION

*CONTROL_IMPLICIT_SOLVER

*CONTROL_IMPLICIT_AUTO
0,,,,,
*CONTROL_IMPLICIT_DYNAMICS

1,

*CONTROL_TIMESTEP

1E-2,0.9,,,,200,


*DATABASE_EXTENT_BINARY

,,,1,1,1,,,

,,,,

*DATABASE_BINARY_D3PLOT

1E-3,

*DATABASE_NODFOR

1E-3,

*DATABASE_NODOUT

1E-2,

*DATABASE_BNDOUT

1E-2,

*DATABASE_SPCFORC

1E-3,

*DATABASE_GLSTAT

1E-2,

*DATABASE_MATSUM

1E-2,

*DATABASE_NODAL_FORCE_GROUP

1,

*DATABASE_ELOUT

1E-2,

*DATABASE_HISTORY_SHELL_SET

1,
*MAT_ELASTIC

1, 0.780E+2, 6E+3,0

*MAT_006

2, 0.780E+2, 2.0E+3,3E+3,0E+3,10

*SECTION_SHELL

1,-16

1,1,1,1

*SECTION_SHELL

2,-16

1,1,1,1

*PART


1,1,1

*PART


2,2,2

*BOUNDARY_SPC_SET

2, ,1,0,0,0,0,0,

$1, ,1,0,0,0,0,0,

3, ,0,1,0,0,0,0,

4, ,0,1,0,0,0,0,

*DEFINE_CURVE

200,

0.0,0.00001

100.0,0.00001

*DEFINE_CURVE

100,

0.0,0.001
```

```
100.0,0.001

100.05,0

*DEFINE_CURVE

102,

0.0,1

30.0,1

30.01,0

*DEFINE_CURVE

103,

0.0,0.5

30.0,0.5

30.01,0

$*BOUNDARY_PRESCRIBED_MOTION_SET

$1, 1, 2, 100,,,1E-3,,

*LOAD_NODE_SET

6,1,102,

5,1,103,

$*LOAD_NODE_SET

$3,1,103,

*INCLUDE

nodes

*INCLUDE

4elementshell.k

*INCLUDE

4nodesmesh.k

*INCLUDE

shellset

*END
```

A.4 Parallel computing script

```
% For running relaxation test with single viscous inclusion
clear all; close all; clc;
lsdirec='C:\Users\ismai\Documents\dyna\ ...
ls-dyna_smp_s_R101_winx64_ifort131 i=mainFile.k ...
    memory=500000000 NCPU=2';
PathLS=['C:\Program Files\LSTC\LS-PrePost ...
    4.6\lsprepost4.6_x64.exe'];
aspect=[1:0.5:3];
Area=[0.1:0.025:0.175];
theta=[0.000000001:pi()/20:pi()/2+0.0000001];
cd1=cd;
mkdir(cd,'results');
dir=fullfile(cd,'results');
for i=[1:length(aspect)];
        if i>1;
            pause(500);
        end
    for j=[1:length(Area)];
        for k=[1:length(theta)];
            clearvars -except dir i j k asp A th dir lsdirec ...
                PathLS aspect Area theta cd1
            asp=(aspect(i)); A=(Area(j)); th=(theta(k));
            Abaqus_composite(asp,A,th,dir)
            cd(cd1);
            ls_com_Relax(lsdirec,PathLS,asp,A,th,dir);
            batch('Run')
            cd(cd1);
            pause(0.5);
        end
    end
end
```

A.5 Analytical solution of dynamic problem (spring)

```
function [Dis,Vel] = ElasticD(M,k,displacement,velocity,P,dt,T)
u_0=displacement;
du_0=velocity;
syms u(t)
Du = diff(u,t);
D2u = diff(u,t,2);
ode = (M)*diff(u,t,2)+k*u == P;
cond1 = u(0) == u_0;
cond2 = Du(0) == du_0;
conds = [cond1 cond2];
uSol(t) = dsolve(ode,conds);
%formulation of equation of motion and equation of velocity:
u=uSol;
velocity=diff(u);
time=[0.0:dt:T];
%solving for motion and velocity for the time domain:
for i=1:length(time);
    t0=time(i);
    D=subs(u,t,t0);
    Dis(i)=double(D);
end
for i=1:length(time);
    t0=time(i);
    VV=subs(velocity,t,t0);
    Vel(i)=double(VV);
end
end
```

A.6 Analytical solution of dynamic problem (Maxwell)

```
function [Dis,Vel] = MaxwellD(M,k,c,P,dt,T,UC, DUC, DUC2)
syms uc(t)
ode = (M*c/k)*diff(uc,t,3)+(M)*diff(uc,t,2)+(c)*diff(uc,t) == P;
cond1 = uc(0) == UC;
cond2 = Duc(0) == DUC;
cond3 = D2uc(0) == DUC2;
conds = [cond1 cond2 cond3];
ucSol(t) = dsolve(ode,conds);
uk=diff(ucSol)*c/k;
%formulation of equation of motion and equation of velocity:
u=uk+ucSol;
velocity=diff(u);
time=[0.0:dt:T];
%solving for motion and velocity for the time domain:
for i=1:length(time);
    t0=time(i);
    D=subs(u,t,t0);
    Dis(i)=double(D);
end
for i=1:length(time);
    t0=time(i);
    VV=subs(velocity,t,t0);
    Vel(i)=double(VV);
end
end
```

A.7 Analytical solution of dynamic problem (SSM)

```
function [Dis,Vel] = SSMD(M,k1,k2,c,P,dt,T,UC, DUC, DUC2)
syms uc(t)
ode=(M*c/k2)*diff(uc,t,3)+(M)*diff(uc,t,2)...
```

```
    +(c+(c*k1/k2))*diff(uc,t)+(k1)*uc==P;
cond1 = uc(0) == UC;
cond2 = Duc(0) == DUC;
cond3 = D2uc(0) == DUC2;
conds = [cond1 cond2 cond3];
ucSol(t) = dsolve(ode,conds);
uk=diff(ucSol)*c/k2;
%formulation of equation of motion and equation of velocity:
u=uk+ucSol;
velocity=diff(u);
time=[0.0:dt:T];
%solving for motion and velocity for the time domain:
for i=1:length(time);
    t0=time(i);
    D=subs(u,t,t0);
    Dis(i)=double(D);
end
for i=1:length(time);
    t0=time(i);
    VV=subs(velocity,t,t0);
    Vel(i)=double(VV);
end
end
```

Appendix B

Homogenised properties equations constants

Table B.1: Elastic modulus equation constant (x_0) values for different Aspect ratio and area combinations for all types of RVEs

Area	Aspect Ratio				
	1.00	1.50	2.00	2.50	3.00
0.100	0.000	0.052	0.091	0.124	0.153
0.125	0.000	0.060	0.105	0.142	0.175
0.150	0.000	0.067	0.117	0.159	0.196
0.175	0.000	0.073	0.128	0.174	0.215

Table B.2: Elastic modulus equation constant (C) values for different Aspect ratio and area combinations for all types of RVEs

Area	Aspect Ratio				
	1.00	1.50	2.00	2.50	3.00
0.100	0.766	0.757	0.739	0.719	0.699
0.125	0.723	0.713	0.693	0.671	0.649
0.150	0.683	0.672	0.651	0.627	0.602
0.175	0.647	0.635	0.612	0.586	0.560

Table B.3: Dynamic viscosity equation constant (x_0) values for different Aspect ratio and area combinations for RVEs with viscoelastic matrix and void inclusion

Area	Aspect Ratio				
	1.00	1.50	2.00	2.50	3.00
0.100	0.000	0.092	0.160	0.215	0.262
0.125	0.000	0.105	0.182	0.244	0.296
0.150	0.000	0.116	0.200	0.268	0.326
0.175	0.000	0.125	0.216	0.290	0.354

Table B.4: Dynamic viscosity equation constant (C) values for different Aspect ratio and area combinations for RVEs with viscoelastic matrix and void inclusion

Area	Aspect Ratio				
	1.00	1.50	2.00	2.50	3.00
0.100	1.371	1.346	1.299	1.248	1.197
0.125	1.278	1.251	1.200	1.145	1.091
0.150	1.194	1.165	1.112	1.055	0.999
0.175	1.116	1.087	1.032	0.973	0.915

Table B.5: Dynamic viscosity equation constant (x_0) values for different Aspect ratio and area combinations for RVEs with elastic matrix and viscoelastic inclusion

Area	Aspect Ratio				
	1.00	1.50	2.00	2.50	3.00
0.100	0.000	-0.431	-0.818	-1.207	-1.608
0.125	0.000	-0.479	-0.903	-1.325	-1.756
0.150	0.000	-0.517	-0.971	-1.420	-1.879
0.175	0.000	-0.547	-1.027	-1.500	-1.986

Table B.6: Dynamic viscosity equation constant (C) values for different Aspect ratio and area combinations for RVEs with elastic matrix and viscoelastic inclusion

Area	Aspect Ratio				
	1.00	1.50	2.00	2.50	3.00
0.100	0.830	0.943	1.169	1.449	1.760
0.125	0.954	1.075	1.317	1.613	1.941
0.150	1.058	1.185	1.438	1.747	2.086
0.175	1.149	1.279	1.540	1.857	2.207

Appendix C

Normalised results

C.1 Linear Elastic

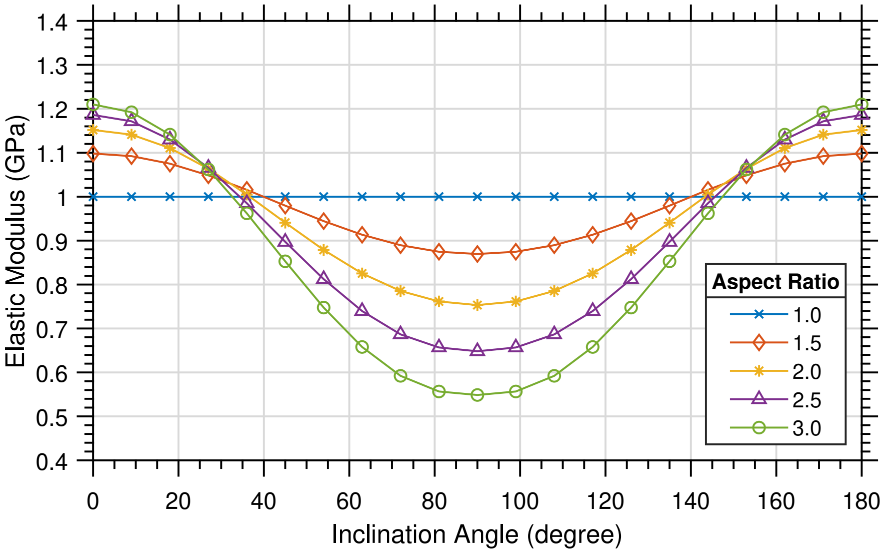

Figure C.1: Variation of homogenised elastic modulus $\bar{E}$ with the inclination angle θ for elastic unit cell(A_r=0.175 mm^2)

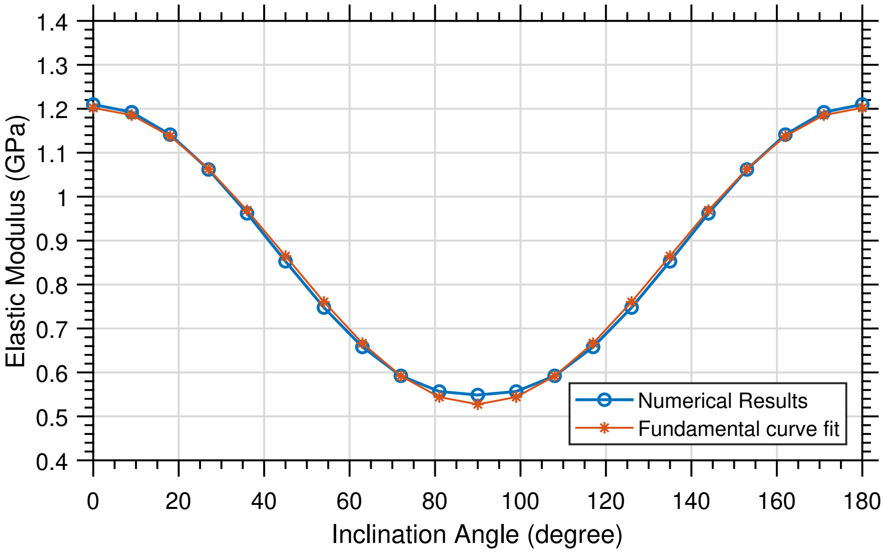

Figure C.2: Variation of homogenised elastic modulus $\bar{E}$ with the inclination angle θ for elastic unit cell (A_r=0.175 mm^2 and AsR=3)

C.2 Maxwell viscoelastic

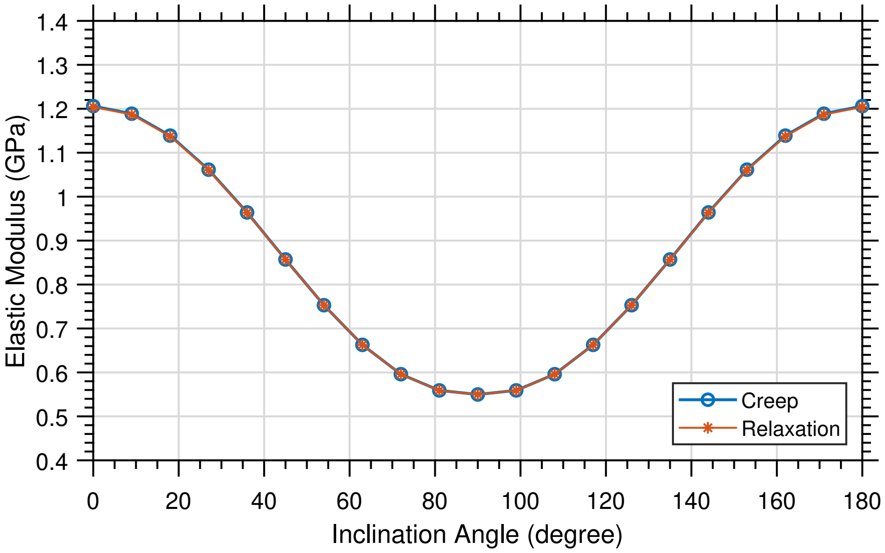

Figure C.3: Variation of homogenised elastic modulus $\bar{E}$ with the inclination angle θ for viscoelastic unit cell (A_r=0.175 mm^2 and AsR=3)

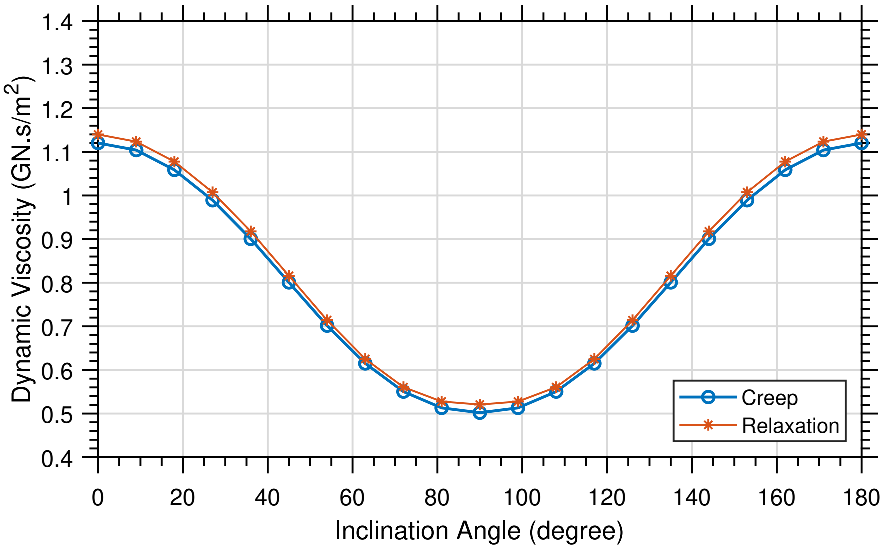

Figure C.4: Variation of homogenised dynamic viscosity $\bar{\eta}$ with the inclination angle θ for viscoelastic unit cell (A_r=0.175 mm^2 and AsR=3)

C.3 Composite

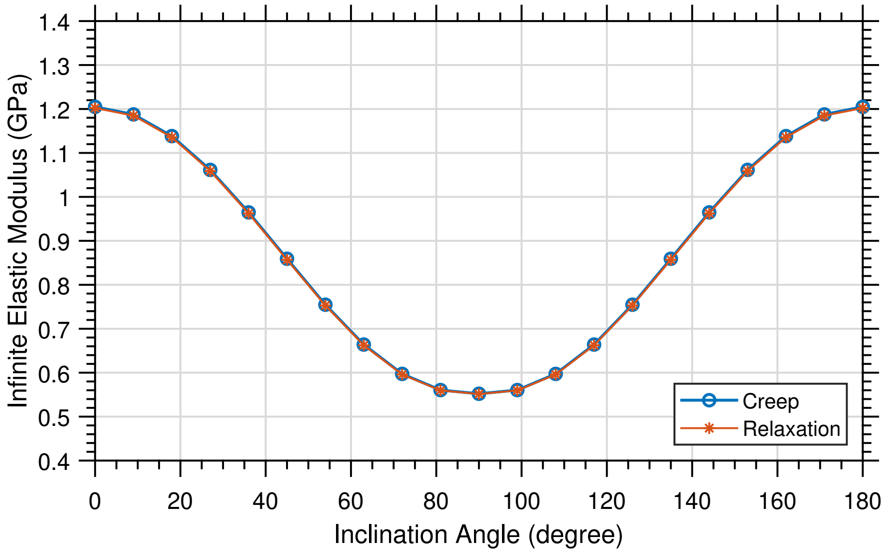

Figure C.5: Variation of infinite homogenised elastic modulus $\bar{E}$ with the inclination angle θ for a composite unit cell (A_r=0.175 mm^2 and AsR=3)

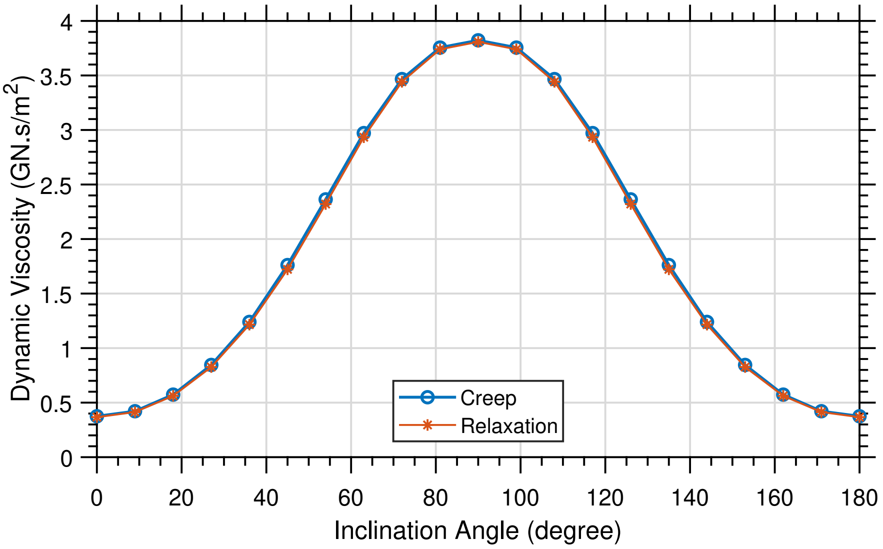

Figure C.6: Variation of homogenised dynamic viscosity $\bar{\eta}$ with the inclination angle θ for a composite unit cell (A_r=0.175 mm^2 and AsR=3)

Appendix D

Further Dynamics Results

D.1 Linear elastic RVE with viscoelastic inclusion inclined at $\theta = 0°$

The following figures (D.1 and D.2) present the displacement and velocity, respectively, due to a constant sudden load.

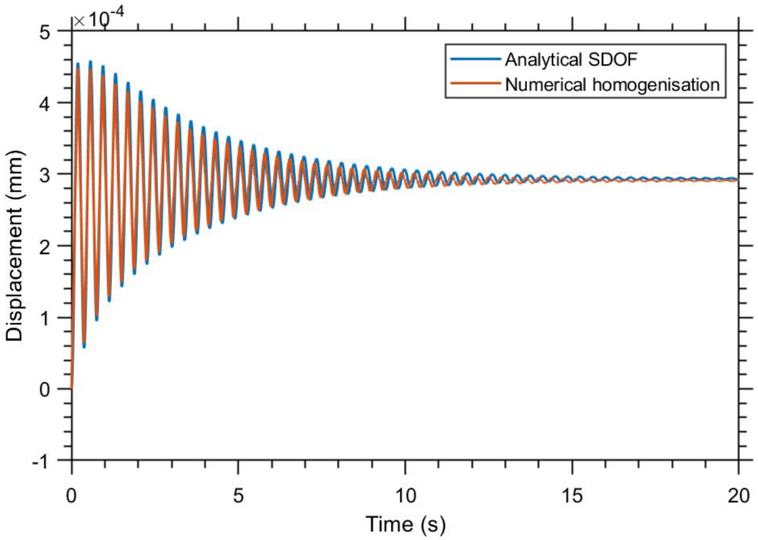

Figure D.1: Displacement vs time due to a sudden constant load applied on an elastic RVE with viscoelastic inclusion (A_r=0.175 mm^2, ASP=3 and $\theta = 0°$).

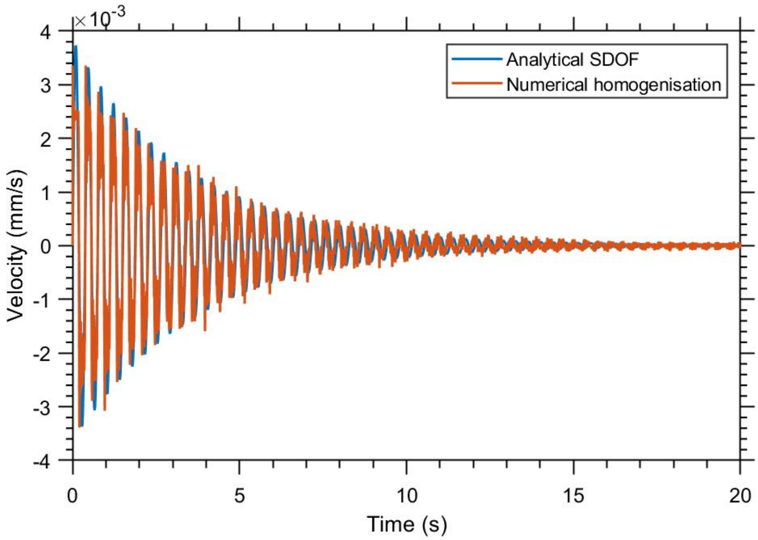

Figure D.2: Velocity vs time due to a sudden constant load applied on an elastic RVE with viscoelastic inclusion (A_r=0.175 mm^2, ASP=3 and $\theta = 0°$)

The following figures (D.3 and D.4) present the displacement and velocity, respectively, due to a pulse load.

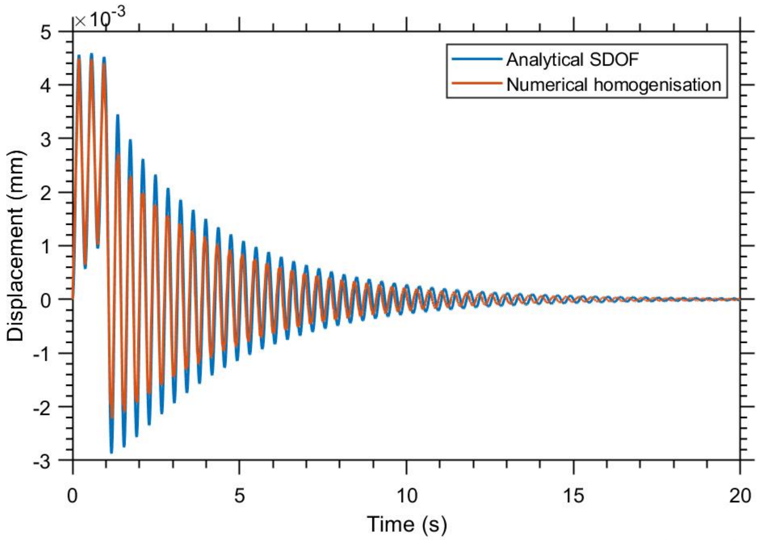

Figure D.3: Displacement vs time due to an impulsive load applied on an elastic RVE with viscoelastic inclusion (A_r=0.175 mm^2, ASP=3 and $\theta = 0°$)

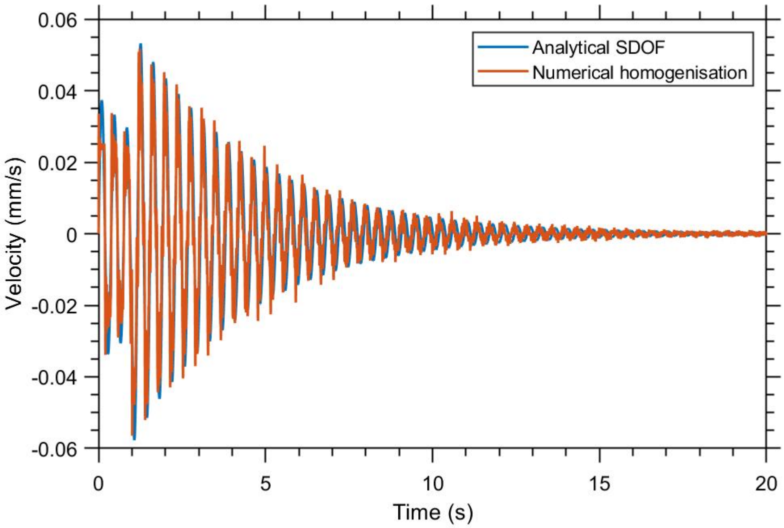

Figure D.4: Velocity vs time due to an impulsive load applied on an elastic RVE with viscoelastic inclusion (A_r=0.175 mm^2, ASP=3 and $\theta = 0°$)

D.2 Linear elastic RVE with viscoelastic inclusion inclined at $\theta = 90°$

The following figures (D.5 and D.6) present the displacement and velocity, respectively, due to a constant sudden load.

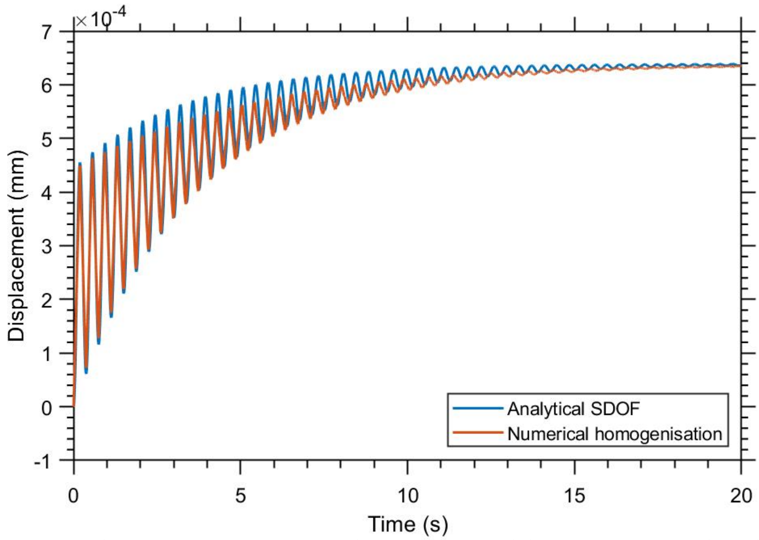

Figure D.5: Displacement vs time due to a sudden constant load applied on an elastic RVE with viscoelastic inclusion (A_r=0.175 mm^2, ASP=3 and $\theta = 90°$).

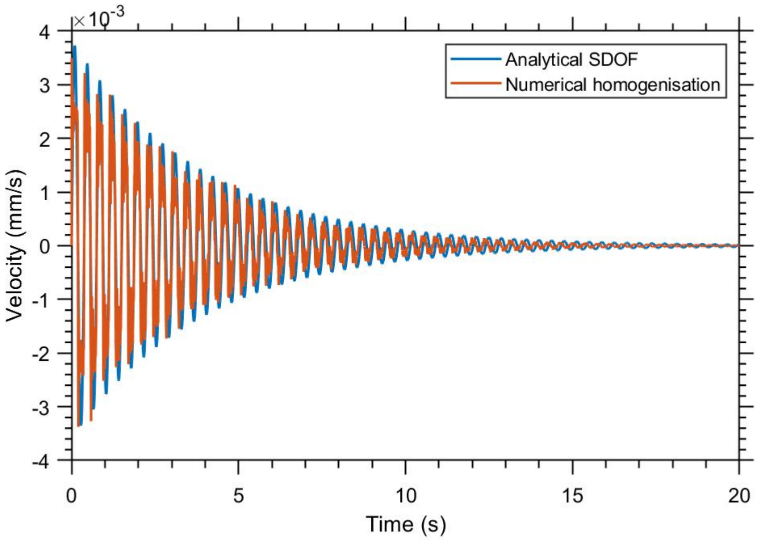

Figure D.6: Velocity vs time due to a sudden constant load applied on an elastic RVE with viscoelastic inclusion (A_r=0.175 mm^2, ASP=3 and $\theta = 90°$)

The following figures (D.7 and D.8) present the displacement and velocity, respectively, due to a pulse load.

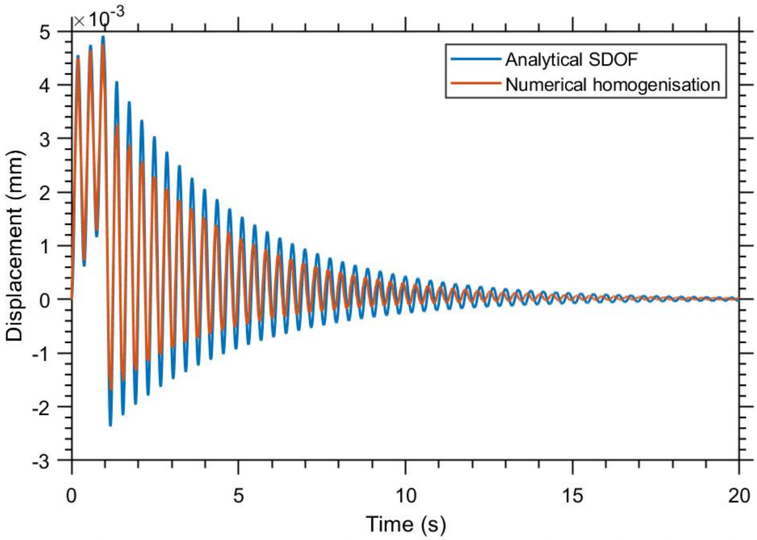

Figure D.7: Displacement vs time due to an impulsive load applied on an elastic RVE with viscoelastic inclusion (A_r=0.175 mm^2, ASP=3 and $\theta = 90°$)

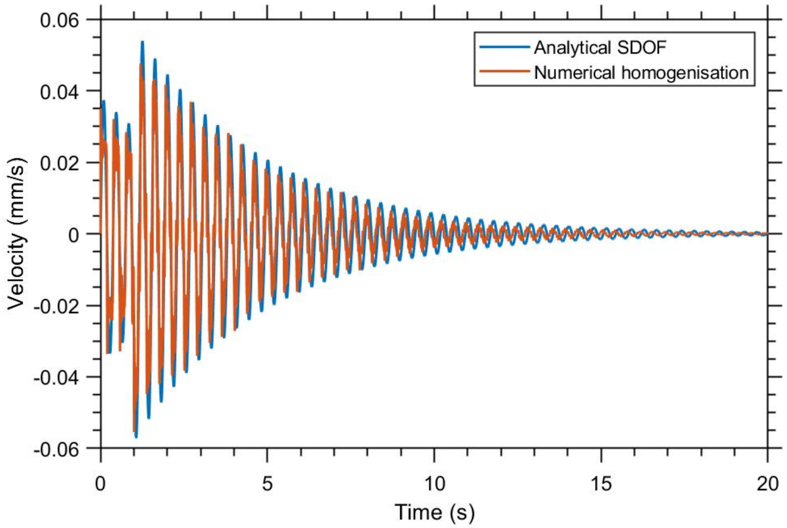

Figure D.8: Velocity vs time due to an impulsive load applied on an elastic RVE with viscoelastic inclusion (A_r=0.175 mm^2, ASP=3 and $\theta = 90°$)

D.3 Maxwell viscoelastic RVE, space homogenised stress and strain

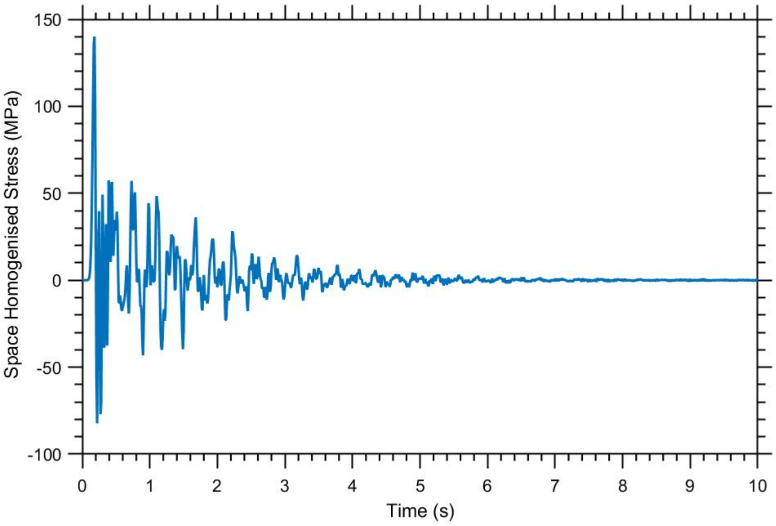

Figure D.9: Space homogenised stress

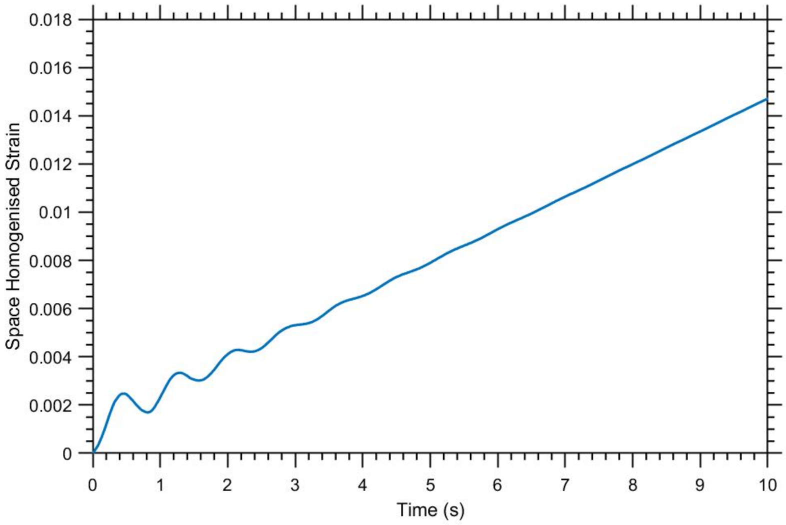

Figure D.10: Space homogenised strain